UNIVERSITAT POLITÈCNICA DE CATALUNYA
INSTITUTO TECNOLÓGICO DE BUENOS AIRES

DOCTORAT EN AUTOMÀTICA, ROBÒTICA I VISIÒ
DOCTORADO EN INGENIERÍA

Doctoral Thesis

MATHEMATICAL MODELLING AND ADVANCED CONTROL DESIGN APPLIED TO HIGH-PRESSURE ELECTROLYZERS FOR HYDROGEN PRODUCTION

Martín Rafael David

Advisors:
Carlos Ocampo Martínez, PhD
Ricardo Sánchez Peña, PhD

July 2021

Universitat Politècnica de Catalunya (UPC)
Departament d'Enginyeria de Sistemes, Automàtica i Informàtica Industrial
Doctoral Program:
Automatic Control, Robotics and Computer Vision

Instituto Tecnológico de Buenos Aires (ITBA)
Departamento de Ingeniería Mecánica
Doctoral Program:
Engineering

This PhD thesis was completed at:

Institut de Robòtica i Informàtica Industrial, CSIC-UPC, and Instituto Tecnológico de Buenos Aires

Advisors:
Carlos Ocampo-Martínez, PhD[1]
Ricardo Sánchez Peña, PhD[2]

[1] Advisor at Universitat Politècnica de Catalunya and co-advisor at Instituto Tecnológico de Buenos Aires

[2] Advisor at Instituto Tecnológico de Buenos Aires and co-advisor at Universitat Politècnica de Catalunya

Firstly to God,
to Juan Pedro and
the one who is coming,
to Milagros,
to my parents.

Acknowledgements

At the end of every journey, it is good to observe the route to rescue the best experiences and, above all, to recognize the people with whom it was shared and to thank for having crossed them.

First, I want to especially thank my thesis supervisors, Prof. Ricardo Sánchez-Peña and Prof. Carlos Ocampo-Martínez, who have been those who accompanied me from beginning to end with extreme patience and a critical eye, always seeking to obtain my best performance. They have been a source of academic knowledge but they have also known how to guide and advise me on everyday issues.

Second, I am grateful to have met Prof. Hernán Álvarez Díaz and Dr. Fernando Bianchi with whom I shared part of my research and from whom I learned many things. They have been extremely open to sharing their knowledge and offering their time.

Third, I want to recognize the entire Energy group of the Instituto Tecnológico de Buenos Aires (ITBA, Argentina). Very especially to Prof. Ricardo Lauretta who was the one who introduced me to this exciting topic of hydrogen and renewable energy. It has been many hours invested in talking about topics as varied as physics to parenthood. Then, I want to thank Prof. Sebastián D'Hers who was the one who suggested that I start this journey.

Fourth, I want to remember those colleagues with whom I have shared from studies and discussions to mutual emotional pushes. Having met with Marcela Moscoso Vázquez, Marcos Bamonte, Ricard Bordalba, Carlos García and Lorena Díaz has been one of the greatest discoveries on this journey.

Fifth, I want to thank the entities that have financially supported this trip. To the Consejo Nacional de Investigaciones Científicas y Técnicas (CONICET, Argentina) for the grant awarded, and to the Ministerio de Economía, Industria y Competitividad and the Consejo Superior de Investigaciones Científicas (CSIC, Spain) for the grant from the Enhancing Mobility between Latin America program, Carabbean and the European Union in Health and Environment (EMHE) that allowed me to carry out stays at the Polytechnic University of Catalonia (UPC).

Finally, I would like to recognize those people who without knowing anything about alkaline electrolysis were those most interested in learning about the technology, I am talking about my family. To my parents in the first place since, needless to say, without them I would not be here. They have raised me in the culture of effort and dedication and have supported me in every step that I have taken until today (and those that I continue to take). And second to my wife Milagros and my children Juan Pedro and the one who is coming. She is the main companion of the entire journey called life and the support in every adventure undertaken. And they are the spark that clears discouragement and relieves tension.

To all of them, I will be eternally grateful. And I will try to be for others, what they have been and are for me.

Martín Rafael David
Barcelona, 2021

Abstract

This thesis is mainly dedicated to the study of high pressure alkaline electrolysis. Alkaline electrolysis is a well established technology and is commercially available. However, the operation at high pressure for dispensing compressors was not fully investigated. Moreover, there is a lack of dynamic models and publications related to control strategies. Therefore, this thesis contributes especially in the modelling and control of high pressure alkaline electrolyzers in order to improve purity of produced gases.

The thesis is framed within a general idea about the renewed concern for the care of the environment, which involves reducing greenhouse gas emissions without sacrificing modern comforts. Widespread proposal focuses on energy produced from renewable sources and its subsequent storage and transportation based on hydrogen. Currently, this gas applies to the chemical industry and its production is based on fossil fuels. The introduction of this energy vector requires the development of environmental-friendly methods for obtaining it. Existing techniques are presented and the main focus is made on electrolysis, a mature procedure. In turn, some developed proposals as previous steps to the hydrogen economy are presented. Moreover, some lines of research to improve electrolysis technology are commented.

Afterwards, a phenomenological-based semiphysical model for a self-pressurized alkaline electrolyzer is proposed. The model, based on mass and energy balances, represents the dynamic behavior of hydrogen and oxygen production using electrolysis. The model allows to anticipate operational variables as dynamic responses in the concentrations of the electrolytic cell, and variations in both, level and pressure, at the gas separation chambers due to the change in electric current. The model parameters have been adjusted based on experimental measurements taken from an available prototype and through a suitable identification process. Simulation results replicate the current dynamic response of the experimental self-pressurized electrolyzer assembly. This model proves to be useful in the improvement of the control of gas production rate in this kind of assemblies, both as a validated simulation platform and as a source of reduced order models for model-based control design.

Later, this thesis presents two control strategies that mitigate the cross contamination of H_2 and O_2 in a high-pressure alkaline electrolyzer, which consequently increases the supplied purity of the gases: one based on a decoupled PI scheme and the other based on optimal control tools. In order to reduce the diffusion of gases through the membrane, the controllers establish the opening of two outlet valves based on the pressure of the system and the difference in liquid level between both separation chambers. Therefore, two multiple input - multiple output controllers are designed. For this purpose, the high-fidelity model previously mentioned was simplified in order to obtain a control-oriented model. The proposed controllers were evaluated in simulation using the high-fidelity nonlinear model in a wide operating range, which resulted in less than 1% impurity of gases. In addition, tests were carried out in the prototype electrolyzer where the operation of the PI and $\mathcal{H}_\infty$ controls were verified, obtaining even better results, with a maximum contamination of 0.2%.

Keywords: Hydrogen, alkaline electrolysis, high pressure alkaline electrolyzer, phenomenological-based semiphysical model, gas contamination, multivariable control, $\mathcal{H}_\infty$ optimal control

Resumen

Esta tesis está dedicada principalmente al estudio de la electrólisis alcalina de alta presión. La electrólisis alcalina es una tecnología bien establecida y está disponible comercialmente. Sin embargo, la operación a alta presión para dispensar el uso de compresores no ha sido investigada completamente. Además, hay una falta de modelos dinámicos y publicaciones relacionadas con las estrategias de control. Por tanto, esta tesis contribuye especialmente en el modelado y control de electrolizadores alcalinos de alta presión para mejorar la pureza de los gases producidos.

La tesis se enmarca dentro de una idea general sobre la renovada preocupación por el cuidado del medio ambiente, que pasa por reducir las emisiones de gases de efecto invernadero sin sacrificar las comodidades modernas. La propuesta generalizada se centra en la energía producida a partir de fuentes renovables y su posterior almacenamiento y transporte a base de hidrógeno. Actualmente, este gas se utiliza en la industria química y su producción se basa en combustibles fósiles. La introducción de este vector energético requiere el desarrollo de métodos amigables con el medio ambiente para su obtención. Se presentan las técnicas existentes y se hace hincapié en la electrólisis, un procedimiento maduro. A su vez, se presentan algunas propuestas desarrolladas como pasos previos a la economía del hidrógeno. Además, se comentan algunas líneas de investigación para mejorar la tecnología de electrólisis.

Posteriormente, se propone un modelo semifísico de base fenomenológica para un electrolizador alcalino autopresurizado. El modelo, basado en balances de masa y energía, representa el comportamiento dinámico de la producción de hidrógeno y oxígeno mediante electrólisis. El modelo permite anticipar variables operativas como respuestas dinámicas en las concentraciones de la celda electrolítica y variaciones tanto de nivel como de presión en las cámaras de separación de gases debido al cambio de corriente eléctrica. Los parámetros del modelo se han ajustado en base a medidas experimentales tomadas de un prototipo disponible y mediante un proceso de identificación adecuado. Los resultados de la simulación replican la respuesta dinámica actual del conjunto electrolizador autopresurizado experimental. Este modelo demuestra ser útil en la mejora del control de la tasa de producción de gas en este tipo de montajes, tanto como plataforma de simulación validada como fuente de modelos de orden reducido para el diseño de control basado en modelos.

Después, esta tesis presenta dos estrategias de control que mitigan la contaminación cruzada de H_2 y O_2 en un electrolizador alcalino de alta presión, lo que consecuentemente aumenta la pureza suministrada de los gases: una basada en un esquema de PI desacoplado y otra basada en herramientas de control óptimo. Para reducir la difusión de gases a través de la membrana, los controladores establecen la apertura de dos válvulas de salida en función de la presión del sistema y la diferencia de nivel de líquido entre ambas cámaras de separación. Por lo tanto, se diseñan dos controladores de múltiples entradas y múltiples salidas. Para ello, se simplificó el modelo de alta fidelidad anteriormente mencionado para obtener un modelo orientado al control. Los controladores propuestos se evaluaron en simulación utilizando el modelo no lineal de alta fidelidad en un amplio rango operativo, lo que resultó en menos de 1 % de impureza de gases. Además, se realizaron ensayos en el electrolizador prototipo donde se constató el funcionamiento de los controles PI y $\mathcal{H}_\infty$, obteniendo inclusive mejores resultados, con una contaminación máxima de 0,2 %.

Palabras clave: Hidrógeno, electrólisis alcalina, electrolizador alcalino de alta presión, modelo semifísico de base fenomenológica, contaminación de gases, control

multivariable, control óptimo $\mathcal{H}_\infty$

Resum

Aquesta tesi es dedica principalment a l'estudi de l'electròlisi alcalina d'alta pressió. L'electròlisi alcalina és una tecnologia ben establerta i està disponible comercialment. Tanmateix, no s'ha investigat completament el funcionament a alta pressió per a la distribució de compressors. A més, falten models dinàmics i publicacions relacionades amb les estratègies de control. Per tant, aquesta tesi contribueix especialment en el modelatge i control d'electrolitzadors alcalins d'alta pressió per tal de millorar la puresa dels gasos produïts.

La tesi s'emmarca dins d'una idea general sobre la renovada preocupació per la cura del medi ambient, que consisteix a reduir les emissions de gasos d'efecte hivernacle sense sacrificar les comoditats modernes. Una proposta generalitzada es centra en l'energia produïda a partir de fonts renovables i el seu posterior emmagatzematge i transport basat en hidrogen. Actualment, aquest gas s'aplica a la indústria química i la seva producció es basa en combustibles fòssils. La introducció d'aquest vector energètic requereix el desenvolupament de mètodes respectuosos amb el medi ambient per obtenir-lo. Es presenten les tècniques existents i es centra principalment en l'electròlisi, un procediment madur. Al seu torn, es presenten algunes propostes desenvolupades com a passos previs a l'economia de l'hidrogen. A més, es comenten algunes línies de recerca per millorar la tecnologia d'electròlisi.

Posteriorment, es proposa un model semifísic de base fenomenològica per a un electrolitzador alcalí auto-pressuritzat. El model, basat en els balanços de massa i energia, representa el comportament dinàmic de la producció d'hidrogen i oxigen mitjançant electròlisi. El model permet anticipar variables operatives com a respostes dinàmiques en les concentracions de la cèl·lula electrolítica i variacions en el nivell i la pressió de les cambres de separació de gas a causa del canvi de corrent elèctric. Els paràmetres del model s'han ajustat en funció de mesures experimentals obtingudes en d'un prototip disponible i mitjançant un procés d'identificació adequat. Els resultats de la simulació repliquen la resposta dinàmica actual del conjunt experimental d'electrolitzador auto-pressuritzat. Aquest model demostra ser útil per millorar el control de la taxa de producció de gas en aquest tipus d'assemblatges, tant com a plataforma de simulació validada com a font de models d'ordre reduït per al disseny de control basat en models.

Posteriorment, aquesta tesi presenta dues estratègies de control que mitiguen la contaminació creuada de H_2 i O_2 en un electrolitzador alcalí d'alta pressió, que en conseqüència augmenta la puresa subministrada dels gasos: una basada en un esquema de PI desacoblat i l'altra basada en un esquema de control òptim. Per tal de reduir la difusió de gasos a través de la membrana, els controladors estableixen l'obertura de dues vàlvules de sortida en funció de la pressió del sistema i de la diferència de nivell de líquid entre les dues cambres de separació. Per tant, es dissenyen dos controladors d'entrada i sortida múltiple. Amb aquest propòsit, el model d'alta fidelitat esmentat anteriorment s'ha simplificat per obtenir un model orientat al control. Els controladors proposats han estat avaluats en simulació mitjançant el model no lineal d'alta fidelitat en un ampli rang operatiu, el qual ha resultat en una impuresa de gasos inferior a 1%. A més, es van realitzar proves experimentals amb l'electrolitzador prototip on es va constatar el funcionament dels controls PI i $\mathcal{H}_\infty$, obtenint encara millors resultats, amb una contaminació màxima de 0.2%.

Paraules clau: hidrogen, electròlisi alcalina, electrolitzador alcalí d'alta pressió, model semifísic de base fenomenològica, contaminació de gasos, control multivariable, control òptim $\mathcal{H}_\infty$

Contents

List of Figures

List of Tables

Part I

Preliminaries

Chapter 1

Introduction

1.1 Motivation

The world economy is constantly expanding. There are two influencing factors related to that expansion: the population growth and progress in personal comfort. Both factors affect the current fossil economy by increasing consumption and generating greater amount of greenhouse gases (GHG). The International Energy Agency (IEA) [93] informs world energy consumption in 2018 of 9.938 Mtoe (1.1×10^5 TWh). That fact represents a growth of 17.59% and 88.90% over the past ten (2008) and forty (1978) years, respectively. Besides, CO_2 emissions in 2018 were 33153 MTon, compared to 29166 MTon in 2008 (13.67% increment) and 17361 MTon in 1978 (90.96% increment) . It is accepted that this scenario needs to change as evidenced by the generation of global impact studies and environmental protection policies [70, 124]. Moreover, the fact that fossil fuels are neither renewable nor evenly distributed across the globe leads to geopolitical conflicts and unequal situations.

Around the world, proposed solutions focus on the production of renewable energy. However, the share of renewable energies has not grown significantly (from 12.7% in 1975 to 13.5% in 2015). Besides costs issues, the global experience indicates that advances are needed to solve technical problems related to energy fluctuations produced in renewable sources. To achieve high integration of renewable energy, it is necessary to have the ability to accumulate the excess of energy to be consumed at a time when consumption exceeds production. Figure 1.1 shows the variety of available technologies for energy storage. While some technologies such as supercapacitors or flywheels are used to store a reduced amount of power (up to 10MW) for a short time (up to an hour) and redeliver it quickly, for the case raised, it is necessary to use other technologies such as

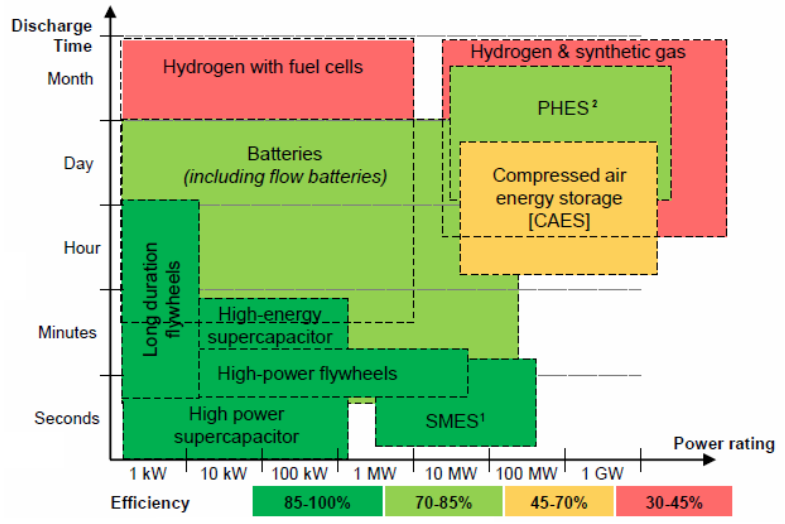

Figure 1.1: Current energy storage methods (taken from [167]). [1]SMES: Superconducting Magnetic Energy Storage, [2]PHES: Pumped Hydro Energy Storage.

Compressed Air Energy Storage (CAES), Pumped Hydro Energy Storage (PHES) or hydrogen.

So far, the most common way to store large amounts of energy is PHES. The biggest disadvantage of this technology is related to its requirements on specific geographical features for installation and political conditions. It is here that among the methods of energy storage, hydrogen production currently takes relevance for its energy density, high energy capacity and transportability [126, 167].

Moreover, in the same direction, there is the concern about pollution in the transportation sector. Along with the development of electric vehicles, the hydrogen appears as an interesting energy vector. Both technologies, electric and H_2-based vehicles, share the benefit of eliminating urban pollution and, depending on the original source, reducing or eliminating pollution in the whole process [178]. The union of these two sectors, electricity and transport, generates what is disclosed as *hydrogen economy*. The *hydrogen economy* is stated as an integral solution for the problem of producing, storing and supplying energy including all final uses while succeeding in GHG mitigation.

The industrial use of hydrogen dates from almost a century ago with a wide consumption in the chemical and oil industries (89% of consumption share) [32]. However, progress must be achieved in various issues in order to accomplish competitiveness of these technologies and develop this economic concept. Issues such as the efficiency and cost of production, storage and

transport, are concepts that several companies, research centers and governments are developing.

The motivation of this thesis will be to investigate the most developed and accepted hydrogen production clean method, which is also the most easily interconnected with renewable energies: alkaline electrolysis. Given that prior to this work, experience with this technology at high pressure has been gained, this thesis will seek to invest that knowledge in the development of physical models that allow to have a deep understanding of the processes that occur there. In this way, as will be seen in Chapter 3, information will be provided to a gap in the state of the art: complete models that mainly come from phenomenology and less empirical adjustments. The ultimate goal of this development will be to implement advanced control strategies based on the model obtained and make comparisons between them.

1.2 Research questions

The research objectives of this work are guided by the following questions:

(Q1) What is the current state of hydrogen production according to the extended idea of using it as an energy vector?

(Q2) How developed is the modelling and control of alkaline electrolysis since this technology is long established?

(Q3) How to describe the complete operation of alkaline electrolyzers involving all processes and auxiliary systems?

(Q4) How to design a model capable of describing the main operating variables of the electrolyzer, especially gas concentrations?

(Q5) Is it possible to design better control strategies in order to improve performance (i.e., purity of output gases) in high-pressure operation?

This thesis focuses on the quest to improve alkaline electrolysis operation in order to be able to produce high-quality gases safely at higher pressures. This is: to design control strategies adaptable to different operating states of pressure, temperature and current for the alkaline self-pressurized electrolyzer prototype previously developed. Therefore, the last question is the most important, while the others serve as a clear path in order to develop and answer the *research question* (Q5).

1.3 Thesis outline

This thesis is divided into four parts:

I) Preliminaries,

II) System description,

III) Control, and

IV) Concluding remarks.

The road map of the current thesis is presented in Figure 1.2. It can be seen the interconnection between different chapters and the suggested order of reading. Each part mentioned above is divided into chapters which are summarized as follows:

Chapter 2: State of the art of hydrogen production

This chapter introduces the concept of the hydrogen economy and evaluates the different options of hydrogen production, answering the *research question* (Q1). The hydrogen production by electrolysis is emphasized as it is the method applied in this thesis. The chapter is based on the following publication:

- David, M., Ocampo-Martínez, C., Sánchez-Peña, R. (2019). Advances in alkaline water electrolyzers: A review. *Journal of Energy Storage* (Q2, IF 3.762), 23, 392-403. 113 citations.
  https://doi.org/10.1016/j.est.2019.03.001.
- David, M. and Ocampo-Martínez, C. Current status of water electrolysis for energy storage. In *Comprehensive renewable energy, 2nd edition.* Elsevier Ltd, 2021. (early access).
  https://doi.org/10.1016/B978-0-12-819727-1.00039-X.

Chapter 3: Literature review on modelling and control

In this chapter, a literature review is developed about the main contribution of this thesis: the modelling of alkaline electrolysis and control strategies in order to improve the purity of produced gases. A lack of dynamic models and advanced control strategies has been found, which answers the *research question* (Q2). This chapter is partially based on the following papers:

- David, M., Álvarez, H., Ocampo-Martínez, C., Sánchez-Peña, R. (2020). Dynamic modelling of alkaline self-pressurized electrolyzers: a phenomenological-based semiphysical approach. *International Journal of Hydrogen Energy* (Q1, IF 4.939), 45(43), 22394-22407. 4 citations.
  https://doi.org/10.1016/j.ijhydene.2020.06.038.

- David, M., Bianchi, F., Ocampo-Martínez, C., Sánchez-Peña, R. (2021). Model-based control design for H_2 purity regulation in high-pressure alkaline electrolyzers. *Journal of the Franklin Institute* (Q1, IF 4.036), 358, 4373–4392. https://doi.org/10.1016/j.jfranklin.2021.04.005.

Chapter 4: High pressure alkaline electrolyzer

The high-pressure alkaline electrolyzer prototype considered in this thesis is presented and described in this chapter. This chapter answers the *research question* (Q3) and it is partially based on the following publications:

- David, M., Álvarez, H., Ocampo-Martínez, C., Sánchez-Peña, R. (2019). Phenomenological based Model of Hydrogen production using an Alkaline self-pressurized Electrolyzer. *18th European Control Conference (ECC)*, 4344–4349.

- David, M., Álvarez, H., Ocampo-Martínez, C., Sánchez-Peña, R. (2020). Dynamic modelling of alkaline self-pressurized electrolyzers: a phenomenological-based semiphysical approach. *International Journal of Hydrogen Energy*, 45(43), 22394-22407.

Chapter 5: Phenomenological-based semiphysical model

This chapter explains the phenomenological-based semiphysical modelling approach along with the presentation of the model developed. This chapter answers the *research question* (Q4). Moreover, this chapter is based on:

- David, M., Álvarez, H., Ocampo-Martínez, C., Sánchez-Peña, R. (2019). Phenomenological based Model of Hydrogen production using an Alkaline self-pressurized Electrolyzer. *18th European Control Conference (ECC)*, 4344–4349.

- David, M., Álvarez, H., Ocampo-Martínez, C., Sánchez-Peña, R. (2020). Dynamic modelling of alkaline self-pressurized electrolyzers: a phenomenological-based semiphysical approach. *International Journal of Hydrogen Energy*, 45(43), 22394-22407.

Chapter 6: Control-oriented model description

After the construction and validation of a simulation-oriented model, in this chapter a model adapted to control is presented. This chapter introduces the answer to *research question* (Q5) and it is based on:

- David, M., Bianchi, F., Ocampo-Martínez, C., Sánchez-Peña, R. (2021). H_2 purity control of high-pressure alkaline electrolyzers. *16th IFAC Symposium on Advanced Control of Chemical Processes (ADCHEM)*, 54, 109–114.
  https://doi.org/10.1016/j.ifacol.2021.08.227

- David, M., Bianchi, F., Ocampo-Martínez, C., Sánchez-Peña, R. (2021). Model-based control design for H_2 purity regulation in high-pressure alkaline electrolyzers. *Journal of the Franklin Institute*, 358(8), 4373.4392.

Chapter 7: Design and simulation of control strategies

This chapter introduces the control strategies and shows simulations of the plant, using the phenomenological-based semiphysical model designed in Chapter 5, in closed loop. This chapter partially answers the *research question* (Q5). Also, this chapter is based on the following publications:

- David, M., Bianchi, F., Ocampo-Martínez, C., Sánchez-Peña, R. (2021). H_2 purity control of high-pressure alkaline electrolyzers. *16th IFAC Symposium on Advanced Control of Chemical Processes (ADCHEM)*, 54, 109–114.

- David, M., Bianchi, F., Ocampo-Martínez, C., Sánchez-Peña, R. (2021). Model-based control design for H_2 purity regulation in high-pressure alkaline electrolyzers. *Journal of the Franklin Institute*, 358(8), 4373–4392.

Chapter 8: Experimental results from electrolyzer prototype

Both experimental setup and results are presented in this chapter in order to compare simulations with real data. Both control strategies, the PI and $\mathcal{H}_\infty$ controllers, were implemented and tested in the electrolyzer prototype. These outcomes become the validation and the final answer to the *research questions* (Q4) and (Q5). This chapter is based on the following publication:

- David, M., Bianchi, F., Ocampo-Martínez, C., Sánchez-Peña, R. (2021). Experimental implementation of model-based control strategies for the increment of H_2 purity in high-pressure alkaline electrolyzers (in preparation).

Chapter 9: Contributions and concluding remarks

Finally, last remarks are presented with the most outstanding results of this thesis. The contributions made throughout this thesis are condensed in this chapter. Moreover, the research questions are answered and possible future research is proposed.

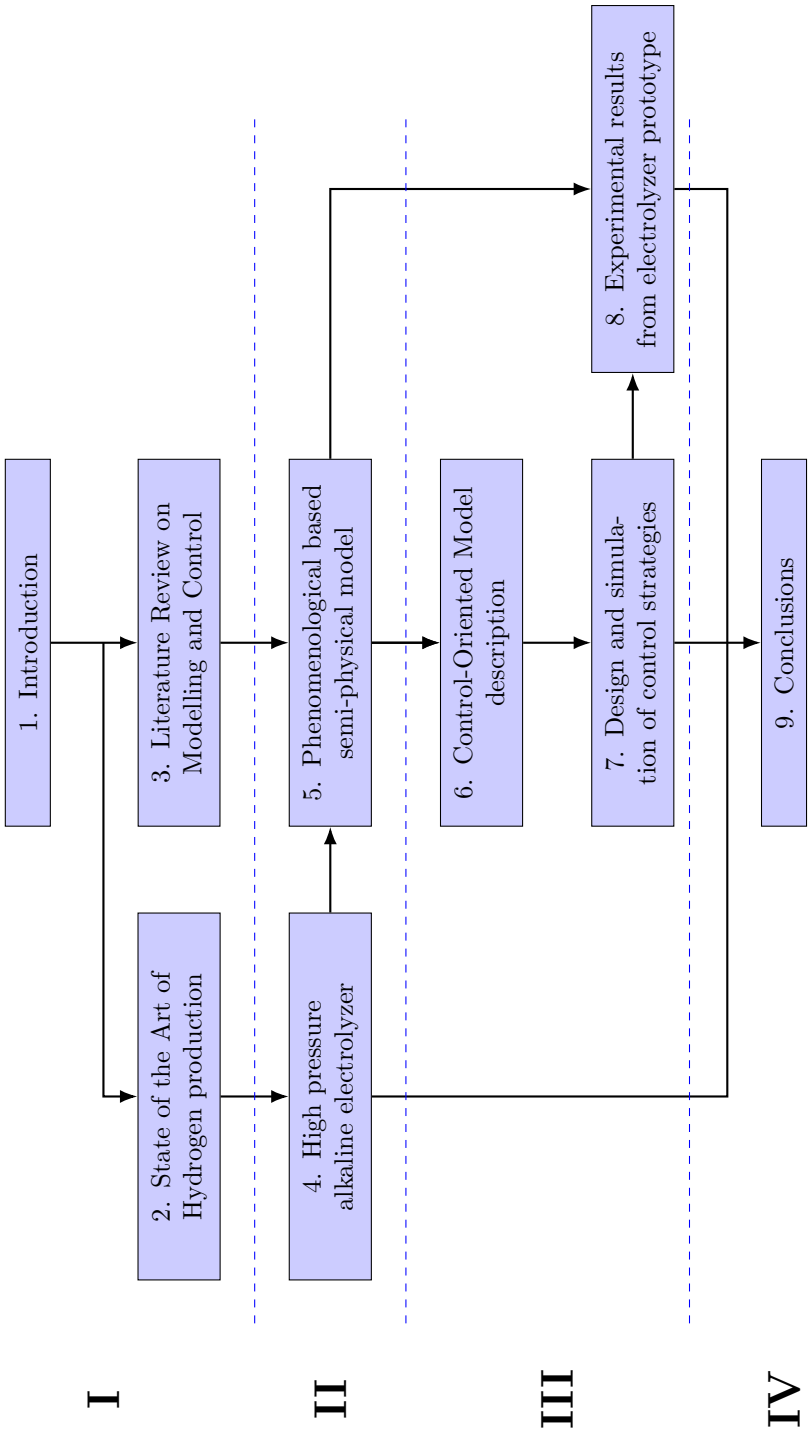

Figure 1.2: Road map of the thesis. Arrows indicate *read-before* relations.

Chapter 2

State of the art of hydrogen production

2.1 Hydrogen economy perspective

Several reviews can be found that present the different technologies related to the use of hydrogen. Abdalla et al [3] published a review of hydrogen technologies making a detailed explanation and comparison of current storage methods. Zhang et al [217] present a brief and well-organized compendium of production, storage and electricity generation technologies. Dutta [52] summarizes development models for the hydrogen economy in various countries along with an explanation of hydrogen production, storage and utilization. Mazloomi and Gomes [129] discuss the economic aspects of centralized and distributed production. In addition, they present the risks inherent in the production, storage and distribution stages, proposing possible risk-reduction techniques.

At the same time, there are studies such as [58] that detail the steps to be followed in order to reach a mature *hydrogen economy*. Among those steps there are the Power-to-Gas [63, 173], the use of fossil hydrogen to power vehicles [7, 19, 91, 139] and the integration of electrolyzers with renewable energies in microgrids [13, 64]. All these developments bring hydrogen technologies taking into account the necessary economic issues in order for it to be sustainable over time. To do this, it will be necessary that companies, governments and research centers cooperate together in this direction [19].

This chapter provides an overview of the hydrogen production technologies, specifically emphasizing production from alkaline electrolysis. Mueller-Langer et al [138] in their techno-economic assessment assure that natural gas steam reforming, coal and biomass gasification and

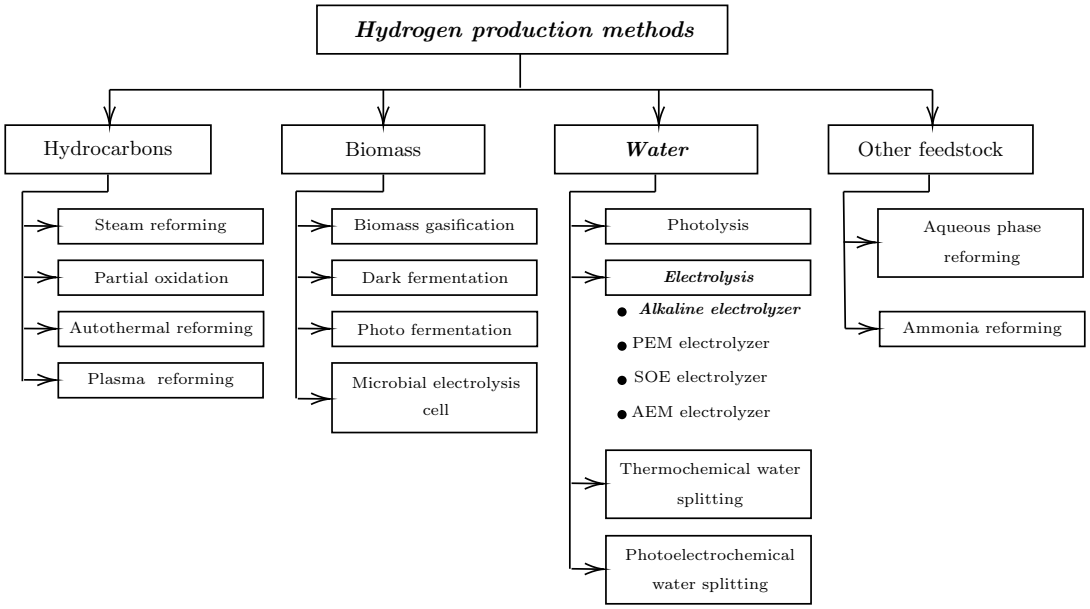

Figure 2.1: Taxonomy of hydrogen production with emphasis in the objective of the present thesis (in boldface).

water electrolysis will play a significant role in the short and medium term. Besides, electrolysis occupies until today a dominant position as it is the only technology that can use directly the power surplus from renewable and fluctuating energies like wind mills or solar panels [217] so it has a concrete perspective on the use of this type of energy as the axis of the hydrogen economy. Among CO_2-neutral H_2 production, electrolysis highlight because it produces high purity hydrogen and it has an infrastructure already developed being a well-established technology [141, 198]. In the same direction, alkaline electrolysis is a mature and reliable technology which stands out from other types of electrolysis based on cost and simplicity [174].

2.2 Hydrogen production technologies

Figure 2.1 shows the different methods of hydrogen production presented in this section. It highlights the approach outlined in this chapter [46], explaining its organization.

There are several methods of hydrogen production with different stages of development. Currently, its production is mainly based on the reforming of fossil fuels (78%) and coal gasification (18%). From the pending 4% of alternate resources, the main technology is the electrolysis of water as a byproduct from chlor-alkali process [108, 140]. Despite the current use of hydrogen

Table 2.1: Summary of methods for obtaining H_2 (adapted from [83])

Technology	Energy source	Feedstock	Efficiency (%)	Maturity	Reference
Steam reforming	Thermal	Hydrocarbons	70-85 [a]	Commercial	[133]
Partial oxidation	Thermal	Hydrocarbons	60-75 [a]	Commercial	[133]
Autothermal reforming	Thermal	Hydrocarbons	60-75 [a]	Near term	[133]
Plasma reforming	Electric	Hydrocarbons	9-85 [b]	Long term	[149]
Aqueous phase reforming	Thermal	Carbohydrates	35-55 [a]	Mid term	[159]
Ammonia reforming	Thermal	Ammonia	NA [c]	Near term	-
Biomass gasification	Thermal	Biomass	35-50 [a]	Commercial	[1, 142, 188]
Photolysis	Solar	Water	0.5 [d]	Long term	[106]
Dark fermentation	Biochemical	Biomass	60-80 [e]	Long term	[1, 100]
Photo fermentation	Solar	Biomass	0.1 [f]	Long term	[1, 188]
Microbial electrolysis cell	Electric	Biomass	78 [g]	Long term	[27]
Alkaline electrolyzer	Electric	Water	50-60 [h]	Commercial	[188, 196]
PEM electrolyzer	Electric	Water	55-70 [h]	Commercial	[47, 188, 196]
Solid oxide electrolysis cell	Electric+Thermal	Water	40-60 [i]	Mid term	[142]
Thermochemical water splitting	Thermal	Water	NA [c]	Long term	-
Photoelectrochemical water splitting	Solar	Water	12.4 [d]	Long term	[195, 196]

[a] Thermal efficiency, based on the Higher Heating Values (HHV)
[b] Based on efficiency equation from [27]
[c] Not available
[d] Solar to hydrogen via water splitting and does not include hydrogen purification
[e] Percent of 4 mol H_2 per mole glucose theoretical maximum
[f] Solar to hydrogen via organic materials and does not include hydrogen purification
[g] Overall energy efficiency including the applied voltage and energy in the substrate. Hydrogen purification not included
[h] Lower heating value of hydrogen produced divided by the electrical energy to the electrolysis cell
[i] High-temperature electrolysis efficiency is dependent on the temperature the electrolyzer operates at and the efficiency of the thermal energy source. If thermal energy input is ignored, efficiencies up to 90% have been reported [142].

produced by the last process, this technology will not be considered in the analysis because in the long term and taking into account the amount of hydrogen necessary, it would not be sustainable due to the chlorine produced at the same time.

In addition to the named technologies, in Table 2.1 it can be seen the selection offered by Holladay et al. [83] covering industrial methods and those which are being developed.

Some of the parameters used to compare different methods of hydrogen production are efficiency, cost and environmental consequences. Efficiency, overall, compares the energy provided by the one obtained as the Lower Heating Value (LHV) of H_2 produced, whose ranges are listed in Table 2.1.

Moreover, the economic cost has the difficulty of analyzing mature technologies such as the steam methane reforming (SMR) with newly developed methods on a laboratory scale as photolysis. In turn, the technologies that rely on fossil fuels have different costs in case carbon capture and storage (CCS) approaches are considered or not. For instance, Parthasarathy and Narayanan [148] present SMR and coal gasification as the cheapest options (0.75 U\$Skg^{-1} and 0.92 U\$Skg^{-1} of H_2 produced, both without CO_2 capture) while electrolysis, considering the

Table 2.2: Cost of hydrogen production methods (from [85])

Process	Cost of H_2 (U$S kg^{-1})
Natural gas reforming	1.03
Natural gas reforming + CCS	1.22
Natural gas reforming + PSA + CCS [a]	1.56
Coal gasification	0.96
Coal gasification + CCS	1.03
Wind electrolysis [b]	6.64
Biomass gasification	4.63
Biomass pyrolisis	3.80
Nuclear thermal splitting of water	1.63
Gasoline (for comparison purposes)	0.93

[a] Current central H_2 production from Natural Gas with Pressure Swing Adsortion (PSA) used for H_2 purification up to 99.6% [74]

[b] Electrolysis using electricity generated by wind turbines

production of electricity with nuclear energy, costs between 2.56 USkg^{-1}$ and 2.97 USkg^{-1}$.

Besides, Hosseini et al [85] present a cost comparison between some production methods as can be seen in Table 2.2. Production from fossil fuels was shown to be cheaper, even if CCS were required. Levene et al [115] consider that electricity costs have a great influence on the price of hydrogen produced by electrolysis, so it is concluded that the cost of electricity must be four times lower than the current price to have a competitive solution using solar and wind energy.

Concerning the environmental consequences, there are two commonly used rates. Bhandari et al indicate that most of the studies analyzed are concentrated in the Global Warming Potential (GWP) and some in the Acidification Potential (AP) [24]. These potentials measure the equivalent mass of CO_2 and SO_2 emitted per kilogram of H_2 generated, respectively. Figures 2.2 and 2.3 show the comparison of these rates for electrolysis from various renewable energy sources along with other methods of obtaining hydrogen. Marks above the bars in the graph highlights the different GWP values extracted by Bhandari et al from their sources [24]. It must be emphasized that these studies are based on Life Cycle Assessment (LCA), which comprises the construction, operation and end of cycle of each technology. It can be seen that electrolysis together with renewable sources produces less pollution than widely used technologies, even in cases of considering CCS. Although thermal decomposition has better results, it still needs to be developed. Besides, biomass gasification is slightly more polluting than electrolysis but it is a technology that also receives interest today.

Based on the previous study, Dincer and Acar [48] present an analysis comparing various technologies based on sustainability and costs. It is necessary to clarify that for the calculation of the environmental impact of electrolysis, these authors took the average value of all sources of

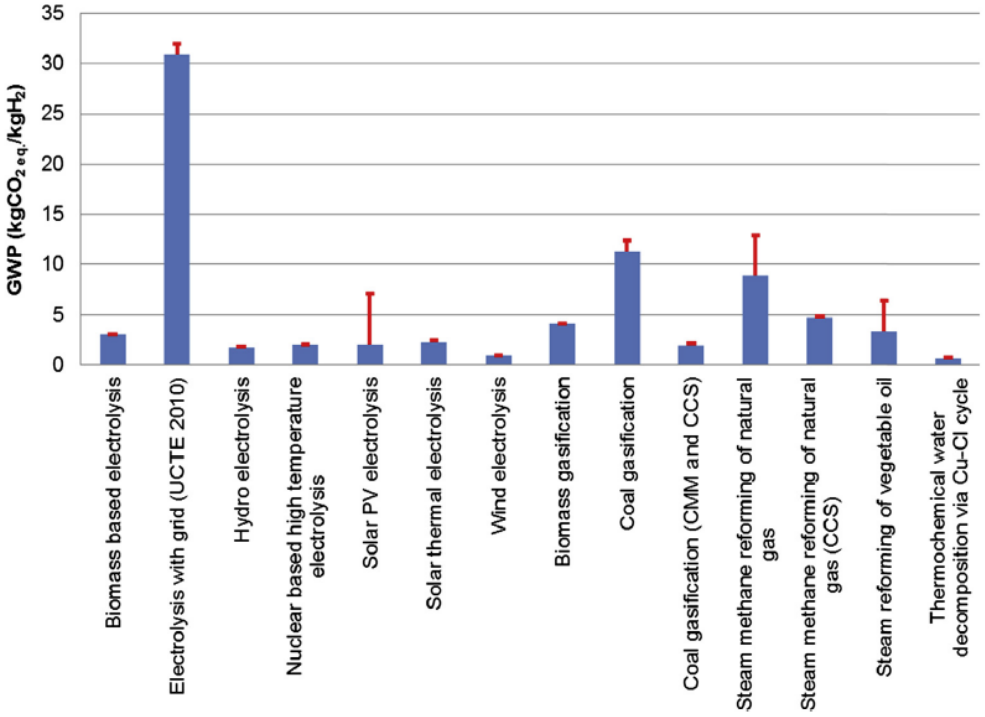

Figure 2.2: GWP for various H_2 production technologies (taken from [24]).

electricity, including the grid. Therefore, due to the fact that the electricity network has higher polluting emissions, the GWP value of electrolysis appears as a non ecofriendly method. This is not the case when electrolysis is combined with renewable sources, as will be considered in this work.

While the electrolysis was the first commercial method of obtaining hydrogen [24], other methods such as SMR have taken its place and are today the processes used at industrial level because of their better efficiency and costs. However, facing the new optical of environment care and GHG emissions mitigation, electrolysis takes back relevance and the research is aimed at improving those two aspects.

Moreover, there are various methods of producing hydrogen which are ecofriendly and competitive. Currently, there is a strong research on the use of biomass, which is accepted as the substitute for the use of fossil resources [85]. However, these technologies require different levels of development and scalability testing, but promise to be competitive [141]. Among them, it is worth mentioning the case of microbial electrolysis, since it can achieve a high efficiency in the production of hydrogen and is considered versatile in terms of the various alternatives of

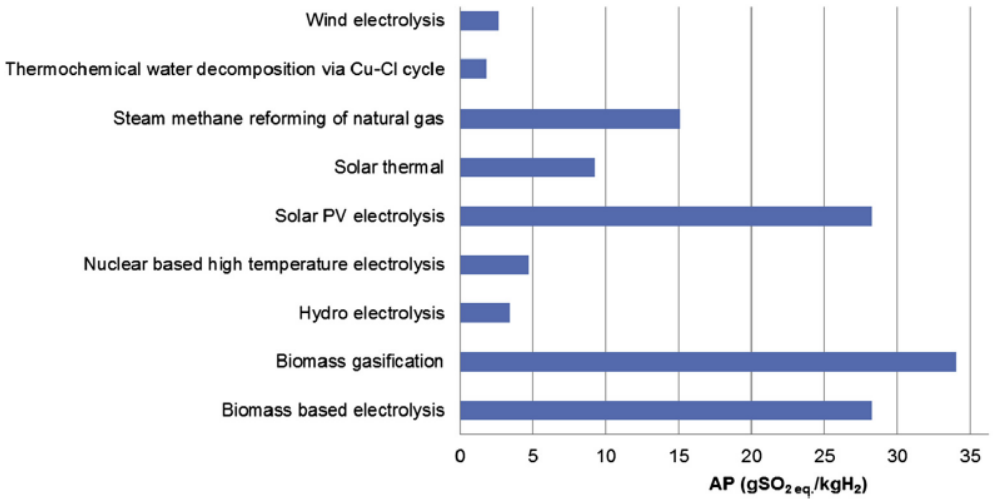

Figure 2.3: AP for various H_2 production technologies (taken from [24]).

application [219].

As stated in § 1.1, electrolysis has the ability to take direct advantage of the surplus electricity from renewable energy sources that is a fundamental step in the development of the hydrogen economy. So the next sections will focus on this technology.

2.3 Water electrolysis

Electrolysis is the method through which the water molecule is separated into hydrogen and oxygen by applying an electric current [24]. Although there are different methods, which are introduced below, they share the same global reaction

$$H_2O\,(l) \longrightarrow H_2(g) + \frac{1}{2}\,O_2(g).$$

2.3.1 Alkaline water electrolysis (AWE)

Alkaline water electrolysis (AWE) is the most mature and simplest method. The largest electrolyzers are of this type and have the greatest commercial reach [48]. The cell consists of a pair of electrodes separated by a diaphragm that is filled with an alkaline solution, typically potassium hydroxide in a concentration between 25 to 30%. Water is split at the cathode in order to form H_2 and release hydroxide anions (OH^-) that cross through the diaphragm and combine to form O_2 at the anode. This is represented by the following half-reactions, known as Hydrogen

and Oxygen Evolution Reactions (HER/OER), respectively:

$$2\,H_2O\,(l) + 2\,e^- \longrightarrow H_2(g) + 2\,OH^-(aq),$$
$$2\,OH^-(aq) \longrightarrow \frac{1}{2}\,O_2(g) + 2\,e^- + H_2O.$$

Commonly, there is an either natural or forced convection through the system which separates the produced gases from the solution. In commercial electrolyzers, the temperature is below 80ºC and they are designed for a pressure of up to 30 bar despite the fact that some lines of research are oriented to increase it.

2.3.2 Proton exchange membrane water electrolysis (PEMWE)

In the 1960s, Proton Exchange Membrane water electrolyzer (PEMWE) was designed to produce oxygen for life support in space or underwater [137]. Instead of an alkali atmosphere, here the electrolysis occurs in an acidic one. Furthermore, the cell is immersed in pure water and the acidic nature is provided by a polymeric membrane which allows the protons (H^+) exchange. On the sides of the so-called Proton Exchange Membrane (PEM), there are both electrodes. This package is named as Membrane Electrode Assembly (MEA). Water oxidizes forming O_2 at the anode and releasing protons which pass through PEM and are reduced to form H_2 at the cathode according to the following reactions [28]:

$$H_2O\,(l) \longrightarrow \frac{1}{2}\,O_2(g) + 2\,H^+(aq) + 2\,e^-,$$
$$2\,H^+(aq) + 2\,e^- \longrightarrow H_2(g).$$

Operating temperature and pressure are similar to alkaline partners. In addition, this method has the advantage to be capable of having different pressure at both sides of the PEM which is not possible for alkaline ones. The materials used remain the same as in their origin: platinum based catalysts for the cathode, iridium based catalysts for the anode and solid perfluorated sulfonic acids for the membrane [28]. The costs related to these materials are the main drawback of this technology.

2.3.3 Solid oxide water electrolysis (SOWE)

The two above methods are named as Low Temperature Electrolysis (LTE). This third option, known as Solid oxide water electrolyzer (SOWE), is also called as High Temperature Electrolyzer

(HTE) to distinguish it from the previous ones. In this sense, HTE differs by performing electrolysis of water vapour at temperatures around 1000ºC. Its structure is similar to the previous methods. Porous electrodes are separated by a dense electrolyte that benefits the transport of $O_2{}^-$ ions. The reactions occurring at the cathode and anode are as follows:

$$\mathrm{H_2O\,(g) + 2\,e^-} \longrightarrow \mathrm{H_2(g) + O^{2-}},$$
$$\mathrm{O^{2-}} \longrightarrow \frac{1}{2}\,\mathrm{O_2(g) + 2\,e^-}.$$

In addition to SOWE, other solid oxide electrolyzers reduce H_2O and/or CO_2 in the cathode. In such cases, synthesis gas (syngas) is produced. Characteristic high temperature results in higher efficciencies and allows waste heat to be used instead of part of the required electricity [16, 105]. In spite of this competitive feature, they have durability issues because of the harsh atmosphere and are still in a research and development stage. The materials commonly used are Ni-based cermet for the cathode, La-Sr-Mn- and La-Sr-Co-Fe-based materials for the anode and yttrium stabilized zirconia (YSZ) for the electrolyte [222]. Wang et al [209], in a recent review, summarize the most important degradation mechanisms and describe emerging mitigation strategies . The key question is how to reduce the anodic overpotential, which could be achieve by using active nanoparticles, developing new materials and enhancing gas transport [34].

2.3.4 Anion exchange membrane water electrolysis (AEMWE)

As a way of combining the advantages of both LTE methods, the technology known as the Anion Exchange Membrane water electrolysis (AEMWE) appears. Its scheme is similar to a PEM cell but the membrane carries OH^-. In that sense, the same reactions occur as the traditional alkaline electrolyzer [213]. As was stated, AEM method brings together some advantages compared to previous LTE technologies [11, 206]:

1. Compared to PEMWE, there is no carbonates precipitation because of the absence of metal cations.
2. In contrast to AWE, it has lower ohmic losses due to thinner membranes.
3. The membrane is cheaper than the PEM.
4. In comparison to AWE, AEMWE has less critical installation and simpler operation due to the absence of a concentrated solution of KOH.

Table 2.3: Typical specifications of electrolizers (taken from [48] and updated with information from [26])

Specification	Units	Alkaline	PEM	SOE
Technology maturity		Widespread commercialization	Commercialization	Research & Development
Cell pressure	bar	<30	<30	<30
Current density	A cm^{-2}	<0.45	1.0-3.0 [a]	0.3-1.0
Cell voltage	V	1.8-2.4	1.8-2.2	0.95-1.3
Voltage efficiency	%	62-82	67-82	81-86
Cell area	m^2	3-3.6	<0.13	<0.06
Hydrogen production per stack [b]	Nm^3 h^{-1}	<1400	<400	<10
Stack lifetime	kh	55-120	60-100	8-20 [c]
System lifetime	year	20-30	10-20	-
Hydrogen purity	%	>99.8	99.999	-
Cold start-up time	min	15	<15	>60

[a] Typical commercial values, although laboratory experiments with a current density up to 20 A cm^{-2} are reported [117].
[b] According to a recent market survey
[c] High uncertainity due to pre-commercial status of SOE

Moreover, AEMWE does not require platinum-group-metal (PGM) catalysts like PEMWE because of the alkaline atmosphere. Alternatively, cheaper transition-metal catalysts have been tested resulting in correct performances [54, 111, 150, 191]. Another advantage over AWE under study is its ability to produce gases with higher purity while increasing system pressure [94].

A mathematical model validated with experimental data shows an improvement in performance at higher current densities and with thicker membranes [11]. Similar to what happens with SOWE, all these advantages have a main drawback which is AEM durability because its chemically instability [22, 147, 202, 206].

2.4 Comparison of electrolytic methods

The three main methods of electrolysis have various features and different stages of development, as can be seen in Table 2.3.

Because of its long tradition, alkaline electrolyzers are nowadays sold in greater numbers, although PEM models are competing with them. As can be seen in Table 2.3, the latter have important advantages over the former in relation to a higher current density, a greater operating range and a higher purity [28]. On the other hand, the biggest disadvantage of PEM electrolysers lies in the durability of the components [61] and in the higher costs associated with titanium-based contact elements, such as bipolar plates and current collectors, and the high iridium charge of the electrocatalyst for Oxygen Evolution Reaction (OER) in MEA [62]. Because of this, the

greatest efforts in the latter are devoted to the search for new materials. In spite of greater efficiency, SOE electrolyzers are still being developed for commercialization so this technology will not be deeply analyzed. Its efficiency closed to 100% (in practice it can reach values of 90%) generates interest in the developments related to the improvement of durability and costs [69]. Despite these efforts, the SOE electrolysers are far from reaching commercialization status [17].

In the research carried out by Felgenhauer and Hamacher [55] to BMW, different companies and models of alkaline and PEM electrolyzers are compared until the first half of 2014. In Table 2.4, it can be seen some technical data of electrolyzers from nine companies: CETH2/Areva H2Gen, Hydrotechnik, Hydrogenics, ITM Power, McPhy Energy, NEL, Next Hydrogen, PERIC and Siemens.

For large-scale systems, there are configurations commercially available formed by several stacks allowing greater production than the ones listed in Table 2.3. Another advantage of this type of configuration is the possibility to have a wider range of operation.

Although it is not explicit in the table, Felgenhauer and Hamacher say that efficiency is between 52% and 62% for alkaline electrolyzers and 57-64% for PEM systems, at the beginning of life (BOL) and 10 bar outlet pressure. Taking into account that the average of the efficiency degradation of the models analyzed by Felgenhauer and Hamacher is double for the PEM type (1.57%) than for the alkaline ones (0.78%), the former difference becomes less important, leading to an even situation throughout the life of the system.

In the study mentioned, an economic evaluation of these systems is performed and better outcomes for the case of higher alkali production are obtained. In Figure 2.4, investment cost and the cost of annual operation and maintenance per produced power of hydrogen (LHV) are observed. Moreover, the best cases (AEL25+), which represent Alkaline Electroyzers with a generation capacity over 25 $kg_{H_2}h^{-1}$, are shadowed.

Being the technologies in commercial state, Schalenbach et al [172] make a comparison between the alkaline electrolysis cells and the PEM cells together with a review of the challenges of both.

In Figure 2.5, it can be seen schemes of both cells with a similar configuration. The most important difference lies in the nature of the separator that divides the half-cells of H_2 and O_2 production: in the case of the alkaline electrolyzers, this is a porous diaphragm that allows the free circulation of the hydroxyls present in the alkaline solution, generally potassium hydroxide

Table 2.4: Technical data of commercial electrolyzers (taken from [55])

System	Generation capacity (kgH_2/hour)	Efficiency degradation (%/year)	Maximum output pressure (bar)	Stack lifetime (hour)
Alkalines				
A06	5.9	1.50	10	55000
A10	9.9	1.50	10	55000
A25	25.0	1.00	1	78840
A27A	27.0	0.50	13	87600
A27B	27.0	0.25	10	96000
A31	31.4	0.10	13	50000
A36	36.0	1.00	30	87600
A44	43.7	1.00	1	78840
A45	45.0	0.25	10	96000
A50	50.0	1.00	1	78840
A54	54.0	0.50	13	87600
PEM				
P09	9.0	1.17	30	70080
P11	12.0	2.50	14	100000
P21	21.2	0.50	35	80000
P22	21.6	2.50	14	100000
P47	47.0	1.17	30	70080

(KOH), which floods the cell [49], while in the PEM cells, it is a solid polymeric electrolyte (SPE) that provides the necessary protons for the process [28].

Behind the separator, there are electrodes whose surface is covered with electro-catalysts that allow the reaction. These electrodes must be porous to allow the circulation of water, produced gases, electrons and ions [169]. In the case of the PEM cells and due to their acidity, only the platinum-group metals (PGM) have been tested commercially for being stable and having an acceptable ionic activity as electro-catalysts. However, the advances that have been made in the use of electro-catalysts with a transition metal base are promising. Such is the case of the transition metals of the first row (Mn, Fe, Co, Ni, Cu) as calchogenides, phosphides, nitrides and carbides [118, 194]. In addition, the electrochemical properties of transition metal carbides (WC, Mo_2C, TaC, NbC) have been tested for HER at medium temperatures (200-400 ^oC) obtaining a proper activity although a demonstration is still needed under realistic conditions [134].

That is why the electrodes are commercially made with an SPE base coated with platinum at the cathode and iridium at the anode. On the other hand, as the KOH solution provides the anions, the electrodes can be made as a metallic mesh, usually Ni. Moreover, stable catalysts made of Ni, Co and Fe are much more abundant and cheaper than their PGM pairs [172].

Since the Ni electrodes allow a proper electrical conduction and have sufficient mechanical resistance, it is not necessary to use collectors in the alkaline electrolyzers, therefore the electrodes

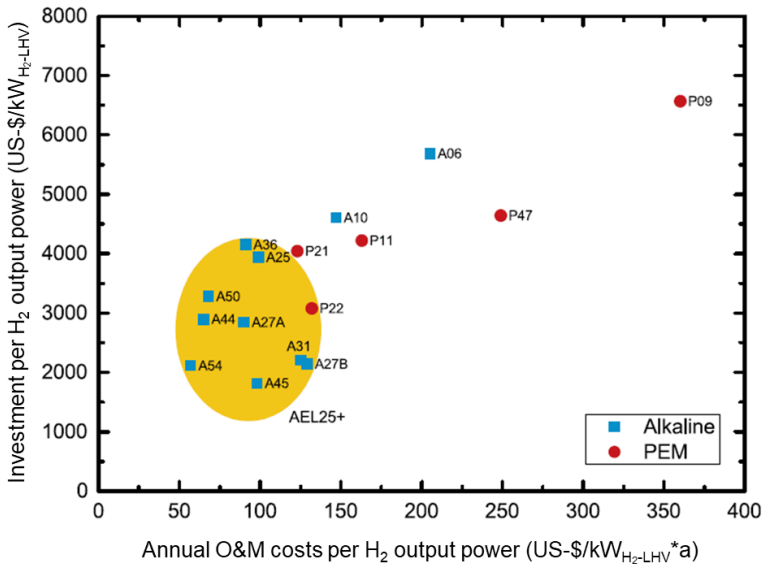

Figure 2.4: Investment cost and cost of operation and maintenance by produced power of H_2 (taken from [55]). The best cases (AEL25+), that represent Alkaline Electroyzers with a generation capacity over 25 $kg_{H_2} h^{-1}$, are highlighted.

are connected directly to the bipolar plate. On the contrary, the electrodes of the PEM cell require the support of the collectors to ensure the conductivity and structural stability.

The problems of durability [56] in the PEM cells lie in the replacement of protons by other cations losing conductivity [190], the loss of dimensional properties under temperature and pressure [103], the degradation by the formation of HF [30] and the ohmic losses by the oxidation of Ti present in the collectors and bipolar plates [154]. In contrast, alkaline electrolyzers are intrinsically more durable but it is important to be careful with the Ni disolution when the cell potential falls below 1.23V, so it would be necessary to maintain a stand-by power that would hinder direct and isolated interconnection with renewable energies.

The study concludes that, for large-scale industrial water electrolysis, liquid alkaline electrolyzers seem to be more suitable because they are not limited to the use of precious and scarce metals. In turn, due to the different corrosion mechanisms in acidic and alkaline media, the latter show greater durability. Finally, the alkaline electrolyte is chemically stable and interchangeable, while the SPEs are vulnerable to the loss of conductivity due to impurities, chemical decomposition and thermomechanical deformation. As presented by the companies in Table 2.4, a tie situation can be observed in terms of the stack durability and a minor difference from the

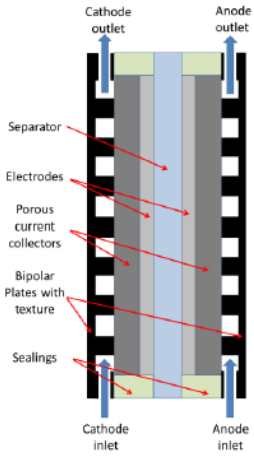

Figure 2.5: Schematic of an electrolytic cell (taken from [172]).

summary presented in Table 2.3. This is not in accordance with what was stated before but it could be justified by the efficiency degradation which was pointed out by Felgenhauer and Hamacher [55].

Before presenting current developments in the following section, the main issues which need improvement in each technology are summarize next. Firstly, the challenges for PEM cells are:

- Designing more durable chemically and thermomechanically SPE membranes.
- Detecting substitutes for Ir as suitable catalysts.
- Counteracting the degradation of anodic collector bipolar plates due to the corrosion and low conductivity of passive layers.
- Improving purity by lowering diffusivity in the solid phase of membranes.

On the contrary, for alkaline cells:

- Optimizing porous electrodes in order to assure the effective emptying of the bubbles and, consequently, reduce the ohmic drop.
- Improving alloys catalysts based on Ni, Fe and Co.
- Preventing in Ni cathode the formation of hydride and the hydrogen embrittlement.
- Enhancing purity by decreasing pores diameters of separators.

2.5 Current developments

Ogawa et al analyze the citations about electrolysis made in recent years [143]. It was found that the number of publications associated with this technology is rising. Among other areas, catalysts for both technologies, AWE and PEMWE, are attracting more interest. It is clear that the developing advances in various fields are still receiving attention, despite the fact that electrolysis is a widely known technology. Some of these lines of research are presented below [45].

2.5.1 Alkaline water electrolysis

In recent decades, advances have been made in this type of electrolyzers called as advanced alkaline electrolyzers. The most important points of development are [198]:

- Zero-gap configuration. It consists of minimizing the distance between electrodes to reduce the ohmic losses.
- New materials for the diaphragm. Previously made of asbestos, the use of inorganic membranes is investigated. Some are based on antimony polyacid impregnated with polymers [201], on porous composite composed of a polysulfone matrix and ZrO_2 (Zirfon) [203], or on polyphenil sulfide (Ryton) [153].
- Temperature increase. The temperature is increased to promote electrolytic conductivity and improve reaction kinetics at the electrodes.
- Electrocatalytic materials. Such materials are developed to reduce overpotentials at the electrodes.

High temperature and pressure electrolysis

The electrolyzers are currently designed for stationary operation. In turn, there are electrolyzers that produce gases at atmospheric pressure or up to 30 bar. So compression stages are required for storage at high-pressure levels. Against this, the opinions are divided between those who propose to design electrolizers that produce directly the gases with greater pressure [145, 224] and those who assure that this is a loss of efficiency [158].

Table 2.5: Development perspectives of selected parameters in alkaline electrolysis technology (taken from [224])

Specification	Symbol	Unit	State of the art	Short-term Development	Middle-term Development
Temperature	ϑ		70-80	80-90	>90
Pressure	p	bar	30	>60	>100
Current density	i	kA/m^2	3-4	6-8	>10
Cell voltage	U	V	1.9-2.3	1.8-2.1	1.7-2.0
Voltage efficiency	Φ	%	64-78	70-82	74-87
Spec. energy use, sys	Ψ_{sys}	kWh/Nm^3	4.6-6.8	4.5-6.4	4.4-5.9
Part load capacity	θ	%	25	<15	<10
Operating life	τ	h	<90000	>100000	>120000
System durability	Π	y	<25	30	>30

In the last group are Roy et al [158] who consider in their analysis the energy consumption in the auxiliary equipment and the loss of gas during the operation to conclude that atmospheric electrolyzers are more efficient compared to electrolyzers operating at pressures up to 700 bar. The percentage of increase in energy consumed reaches 16.66% at 700 bar, according to the calculations of the authors. At the same time, they consider that corrosion, hydrogen embrittlement, operation complexity, dynamic response and costs, make pressurized electrolyzers less favorable.

On the contrary, the first group claim that the energy needed to compress the gases grows more than the theoretical energy of dissociation of water. There are even projects that try to demonstrate with pilot plants the realizability of such a solution, as the case of Brandenburg University of Technology Cottbus [224]. In the presentation of the project, they define the perspectives on the technology of alkaline electrolysis, as shown in Table 2.5.

Allebrod et al [8] assure to have succeeded in improving the efficiency of alkaline systems with an operating state of 240 and 37 bar. In turn, they propose a new design with electrolyte inside a porous structure allowing current densities up to 2 Acm^{-2} and voltages not exceeding 1.75 V (typical value in commercial equipment). On the other hand, in the cost analysis competitive prices are obtained by not using precious metals.

Ganley [65] also experimented with electrolytic cells of high pressure and temperature (up to 87 bar and 400). The results were promising given that the applied voltage is drastically reduced. However, the author raises objections about these results due to the possible mixture of products and corrosion of the electrodes that could have distorted the aforementioned values. Having said that, it is necessary to design new experiments that allow to explain the observed phenomena.

In conclusion, it is theoretically possible to increase the efficiency of the system by increasing the pressure and temperature but there are still technical issues to be solved, among which cross-contamination of gases and materials stability stands out, respectively.

Overpotentials reduction

Several authors has described the working principle of AWE. Based on thermodynamics and heat transfer concepts, Ulleberg [197] presented a model dependent on the imposed current in order to obtain the voltage of the stack, the flow rate of the gases produced and the thermal equilibrium of the system. The validation of this model was carried out with data collected at the PHOEBUS plant in Jülich, where experiments using solar energy to produce and store hydrogen are performed [21].

Moreover, Ursúa and Sanchis [199] began from the same thermodynamic basis and defined the ideal voltage in the dissociation of water in order to develop an electrical model of the overpotentials. The final model has terms identical to those suggested by Ulleberg, which are

$$v_e = N_s(V_{rev} + v_{act} + v_{ohm}), \tag{2.1}$$

where v_e is the voltage applied to the stack, N_s is the cells number with a series configuration, v_{act} is the activation overpotential and v_{ohm} is the overpotential due to ohmic losses.

The first overpotential, v_{act}, occurs due to the polarization of the electrodes when the electrolyte ions aproximates to the electrodes surface, which is called double layer effect. Roy, in her doctoral thesis Roy [157], suggests a way to calculate the second overpotential taking into account the materials conductivity in the electrical current path and the existence of gas bubbles in the chemical solution. Therefore, this overpotential involves both electrical and ionic conductivities.

A model to analyze the effects on the ohmic overpotential of different materials properties was proposed by Zourhi and Lee. The causes of this ohmic overpotential, which means efficiency losses, are, in order of importance:

1. The presence of hydrogen bubbles on the surface of the electrode
2. The ionic resistivity of the electrolyte
3. The presence of oxygen bubbles
4. Electrodes distance

5. Membrane (or diaphragm) resistivity

Construction costs can be reduced by increasing the electrical current density. To do this, it is required to minimize overpotentials in order to avoid efficiency losses. Therefore, this particular issue currently attracts the highest interest. In particular, much research concentrates on catalysts, electrode materials and their structres. This topic will be covered in § 2.5.1.

Furthermore, a particular way to lower ohmic overpotentials is the utilization of an intermediate electrode which causes the reduction and oxidation of water to occur in different processes and not simultaneously. As an example, Choi et al present a three electrodes cell immersed in an alkaline environment: *i)* metal hydride (MH, negative), *ii)* manganese dioxide (MnO_2, intermediate) and *iii)* nickel hydroxide ($Ni(OH)_2$, positive). This proposal arises from the experience on the incorporation of a third electrode in the thermochemical cycle of water splitting [31, 189]. The common reactions of each half-cell are

$$\text{OER:} \qquad 2\,MnO_2 + H_2O \longrightarrow 2\,MnOOH + \frac{1}{2}\,O_2,$$

$$\text{HER:} \qquad 2\,MnOOH \longrightarrow 2\,MnO_2 + H_2.$$

Two goals are achieved by having an intermediate solid electrode which splits the reactions: *a)* greater purity due to the gases are produced in successive steps, and *b)* lower ohmic overpotential, because of a thinner separator. In this case, cell potential below 1.6V was reached at 60, making this option a probably more efficient way of producing hydrogen with higher purity.

Impact of electric input fluctuation

The study of the response to variable input currents is of great interest given the attention caused by the interconnection of electrolyzers with renewable energies. The more direct the connection between them, the higher efficiency can be achieved in the storage of energy in the form of hydrogen. While there are certain investigations that study the response of electrolyzers to the change in the power supply such as a complete interruption or an impulse [130, 176, 181, 200], there is not much information about it [131].

Dobó and Palotás [50, 51] developed a series of experiments to characterize the response of an alkaline electrolysis cell to fluctuations in voltage and current. The electrolytic cell consisted of a closed container filled with 30 wt. % potassium hydroxide solution with flat plate stainless steel electrodes.

In the first case, the cell was fed with a sinusoidal voltage signal with amplitude a and frequency f mounted on a direct voltage U_{DC}. With an amplitude between 0 and 2V, a frequency between 1Hz and 5000Hz and a direct voltage between 1.4V and 2.8V, 6512 experiments lasting 15s were carried out. In each case, the electric power delivered and the gases produced were calculated, the second ones as a function of the pressure change in the cell. The results obtained show that at greater amplitude a and frequency f, the efficiency of the cell decreases. In turn, U_{DC} values are found in which the efficiency is maximum (around 2.2V). Efficiency is defined as

$$\eta = 100Q \left[\frac{V_m P}{U^0 F} \left(\frac{1}{z_{H_2}} + \frac{1}{z_{O_2}} \right) \right]^{-1},$$

where Q is the measured flow of gases produced, V_m is the molar volume of the ideal gases for normal conditions, U^0 is the theoretical decomposition voltage of water, F is the Faraday constant and z is the charge number. A degradation of efficiency is obtained with respect to that corresponding to the DC operation of up to 20%. However, there are work zones in which the efficiency drops due to the fluctuation in the input (<2%) can be considered negligible. It is concluded that it is possible to accept fluctuation in the tension but it is recommended to soften the ripple to obtain better results.

In the second case, the cell was fed with several current waveforms (sine, triangle, sawtooth and square) characterized by the direct current I_{DC}, the root mean square (rms) value I_{rms} and the frequency f. In turn, a ripple factor r is defined as the relationship between the rms value of the I_{rms} alternating component and the continuous I_{DC} value, thus comparing the different waveforms.

More than 4600 experiments were carried out in a range of 1 to 10000 Hz in frequency, 1 to 5 kA m^{-2} of direct current and 0 A m^{-2} to I_{DC}. From the results it can be concluded that the increase in direct current generates a decrease in efficiency. Besides, there is an efficiency decrease with higher ripple factor (e.g. for f = 1kHz and I_{DC} = 4kA m^{-2}, the efficiency decreases by 16 % when the ripple factor goes from r = 0% to r = 100%). This is because the production of gases could be considered as directly related to I_{DC} and the alternating component only raises the power demanded for the same I_{DC}. In spite of having a smaller participation, a frequency increase can improve efficiency (e.g., for I_{DC} = 2kA m^{-2} and r =100%, the efficiency is 48.5% for the continuous case and is 50% for f = 10kHz).

Table 2.6: Oxygen overpotential of different electrode materials [taken from [216]]

Composition formula	Method	T (^{o}C)	Electrolyte	C (mol dm^{-3})	j (Am^{-2})	η_{oxygen} (mV)	Ref.
Ni+Spinel type Co_3O_4	Thermo-decomposition	25	KOH	1	1000	235 ± 7	[186]
Ni+La doped Co_3O_4	Thermo-decomposition	25	KOH	1	1000	224 ± 8	[186]
MnOx modified Au	Electro-deposition	25	KOH	0.5	100	300	[53]
Li10% doped Co_3O_4	Spray pyrolysis	RT	KOH	1	10	550	[75]
Ni	N/A	90	KOH	50 wt%	1000	300	[212]
$La_{0.5}Sr_{0.5}CoO_3$	Spray-stiner	90	KOH	50 wt%	1000	250	[212]
$Ni_{0.2}Co_{0.8}LaO_3$	Plasma jet projection	90	KOH	50 wt%	1000	270	[212]

Table 2.7: Hydrogen overpotential of different electrode materials [taken from [216]]

Composition formula	Method	T (^{o}C)	Electrolyte	C (mol dm^{-3})	j (Am^{-2})	$\eta_{hydrogen}$ (mV)	Ref.
Ni-Fe-Mo-Zn	Co-deposition	80	KOH	6	1350	83	[39]
Ni-S-Co	Electro-deposition	80	NaOH	28 wt%	1500	70	[77]
Ni50%-Zn	Electro-deposition	N/A	NaOH	6.25	1000	168	[179]
$MnNi_{3.6}Co_{0.75}Mn_{0.4}Al_{0.27}$	Arc melting	70	KOH	30 wt%	1000	39	[87]
Ti_2Ni	Arc melting	70	KOH	30 wt%	1000	16	[88]
Ni50%Al	Melting	25	NaOH	1	1000	114	[123]
Ni75%Mo25%	Co-deposition	80	KOH	6	3000	185	[152]
Ni80%Fe18%	Co-deposition	80	KOH	6	3000	270	[152]
Ni73%W25%	Co-deposition	80	KOH	6	3000	280	[152]
Ni60%Zn40%	Co-deposition	80	KOH	6	3000	225	[152]
Ni90%Cr10%	Co-deposition	80	KOH	6	3000	445	[152]

Electrode materials

The electrodes are usually made of nickel because of its stability. However, it is necessary to counteract the deactivation mechanism. Some solutions are the iron coating [128] or vanadium disolution [4].

On the other hand, the use of electro-catalysts allows, in addition to stabilizing the electrodes, to reduce the ohmic overpotential. Zeng and Zhang [216] present some examples of anode (Table 2.6) and cathode (Table 2.7) materials used in commercial electrolyzers.

In turn, there are those who claim that, for the estimated global capacity of electrolyzers, it will be necessary to dispense with noble metals [2]. Therefore, there are experiences using stainless steel electrodes seeking to improve their electrical efficiency [107]. Besides, Cruden et al [40] compare electrodes based on Nickel with Molybdenum-Resorcinol-Formaldehyde (Mo RF) and other Ni-C-Pt-made electrodes. It is concluded that the proposed Ni-Mo RF can be a replacement for the existing Ni-C-Pt electrodes, the latter being more expensive.

As stated previously, the study of catalysts is receiving increasing interest. As stated by Sapountzi et al [164], the worldwide development of hydrogen production by electrolysis is limited by the search for stable, active and abundant electro-catalysts that allow intermittent conditions.

Moreover, the use of nanostructures is being investigated in order to obtain greater efficiencies

Table 2.8: Main electrocatalyst materials and their current development (taken from [164])

Material	Activity	Stability	Status
Raney Ni	Sufficient activity	Deactivation after intermittent operation	Commercially used
Ni–Co, Ni–Fe	High activity, which can be further improved upon alloying with rare earths	Better stability than Raney Ni, but still not optimal	Laboratory applications
$NiFe_2O_4$	Very high activity	Long term stability	Applied in lab-scale electrolysis with polymeric membrane
Ni–Mo	Very high activity	Long term stability	Pyrophoric material: inappropriate for commercialization
(Ni,Co)–W	High activity	Unknown	Laboratory applications
Co_2Si	Very high activity	Unknown	Laboratory applications
Ni_3N	High activity	Unknown	Laboratory applications

Table 2.9: Comparison of works using nanostructures to obtain higher electrolysis efficciencies

Material	Nanostructure	HER/OER [a]	Activity	Stability	Ref
CoP	Nanosheet@microwire array on Nickel foam	OER	High activity (296mv @100mA)	At least 65h	[95]
$NiWO_4$	Nanowire on Ti mesh	Both	Good activity (101mV for HER and 322mV for OER @20mA)	—	[96]
$CoTe_2-MnTe_2$	Hybrid nanowire on Ti mesh	OER	Sufficient activity (310mV @50mA)	At least 60h	[211]
$Fe-NiCr_2O_4/NF$	Fe doped nanoparticles film	OER	Good activity (228mV @20mA and 318mV @500mA)	At least 60h	[221]
CoP_3	Nanowire array	HER	Sufficient activity (76mV @10mA)	At least 60h	[97]
CoP	Nanosheet on carbon cloth	Both	High activity (52mV for HER and 300mV for OER @10mA)	—	[122]
$PtCo-Co/TiM$	Ultrafine alloy decorated nanowire	HER	Superior to Pt-based electrocatalysts (70mV @46.5mA)	At least 50h	[210]

[a] Tested in Hydrogen or Oxygen Evolution Reaction

or reduce the amount of required precious metals. The deposition of Pd and Ru [151], the incorporation of NiO into a Ni-P matrix [180], the use of Ni nanoparticles on carbon nanotubes [132] and the development of RuO_2-NiO nanorod arrays on a Ni foam substrate [218] are some examples of this. Table 2.9 presents the most recent developments in the implementation of nanostructures, demonstrating the diversity of materials and forms which are used. The list is not exhaustive due to the large dispersion that exists.

Gas-purity dependence

To study the change on the volumetric concentration of H_2 in O_2, a set of experiments were carried out by Haug et al. A zero-gap alkaline electrolyzer was tested which concluded in the following tendencies in the operating characteristics:

- A decrease in the electrolyte recirculation flow rate generates less impurities.
- An increase in the electrolyte concentration reduces the hydrogen content in oxygen.
- A rise in the temperature of the electrolyte allows less impurities.

It should be noted that these trends are also related to other characteristics, such as materials properties or ohmic overpotentials.

Another idea investigated is to know the change of the impurities with three configurations of the circuit. The first and traditional one is the mixing of the electrolyte recirculation circuits to the cell and the interconnection of both gas separators (mixed). The second one is the independence of recirculations and gas separators, while the third one keeps the recirculation circuits separated but allows the interconnection of the gas separators (partly separated). It is observed that there is an improvement in the purity when passing to separate recirculation circuits while it is not considerable when the gas separators are independent. However, the separation of the recirculation circuits does not allow the equalization of KOH concentrations necessary for the suitable performance of the cell. That is why two solutions that improve the purity are proposed:

- Partly separated method at low current densities (when impurities are higher) and change to mixed method when higher current densities are reached.
- Period cycling of the order of half an hour between the methods partly separated and mixed to achieve an improvement in the purity with respect to the traditional method.

Enhanced separators

Nowadays, Zirfon PERL is widely used as separator in commercial alkaline water electrolyzers. This material is composed of 85 wt.% zirconia oxide nanoparticles and 15 wt.% polysulfone (PSU). It has acceptable stability in KOH solution up to 80^oC, high bubble point pressure (up to 2 bar) and low area resistance (less than 0.3 Ω cm^{-2}). Other composites as PSU-based [6], sulphonated poly-ether-ether-ketone (SPEEK) [99] and barite/PSU separators have been studied [204].

The main challenge of AWE is the interconnection with fluctuating renewable sources because of its minimal partial load (typically between 10% and 40%) [146]. By decreasing the current density, the hydrogen anolyte concentration is increased due to dissolved H_2 crossover through separator. This effect is magnified with high pressure. Therefore, improving the material of the separators will help to enhance the performance, purity and pressure of alkaline electrolyzers.

Lately, In Lee et al have synthesized ZrO_2/PSU separators with different proportions of zirconia oxide and compared them taking into account ionic resistance, bubble point pressure

and H_2 permeability [92]. They conclude that separator with 75% of ZrO_2 has better results due to the small pore size achieved (70 nm): high bubble point pressure (3.8 bar, vs 2.5 bar of Zirfon), low permeability of H_2 (4.2×10^{-12} mol bar $^{-1}$ s^{-1} cm^{-1}, vs 20 $\times10^{-12}$ mol bar $^{-1}$ s^{-1} cm^{-1}) and low ionic resistance (0.3 Ω cm^{-2}, similar to Zirfon).

2.5.2 PEM water electrolysis

As stated in this technology description, in § 2.3, its most important drawbacks are durability and costs. Current collectors/separator plates and the MEA represent 48% and 24% of the total cost of the cell, respectively [37]. Therefore, a lot of effort is being put into the development of compounds and structures at the nanoscale to obtain better performance with minimal cost. This topic along with the other most important lines of research are described below.

electro-catalysts and collectors materials

Current collectors and bipolar plates are crucial in the PEM cell configuration. They electrically connect the electrodes and at the same time serve as a mechanical support. Moreover, the incoming water passes through them to react around the catalysts and the outgoing produced gases must be properly evacuated. Thereofore their material is expected to have suitable electrical conductivity and correct mechanical and corrosion resistance due to the acidic atmosphere and the presence of O_2. Titanium turns out to be the relative-cheapest material that is stable and form an acceptable semiconducting oxide. Nevertheless, its passivation layer generally grows, increasing electrical resistance (i.e., decreasing performance) [172]. So, in anode side, precious metal coatings and alloys were tested [60]. In spite of preventing corrosion, costs are increased. Therefore, a significant challenge is found in developing an optimal relationship between economy and performance. About geometry, porous Ti current collectors are preferred but grids, meshes and felts are used also. Other materials such as graphite and stainless steel have been tested, but with poorer electrochemical performance [104, 114]. Typically, current collectors have a porosity of 20-50%, pore size of 5-30μm and particle size of 25-250μm [5].

As was described previously, in the cathode, electro-catalysts based on platinum-group metal (PGM) are typically used for the HER. On the contrary, for the OER, at the anode, RuO_2 and IrO_2 are present. Due to the expected requirement for mass production of green H_2, tons of noble metals will be needed. For example, according to Carmo et al [29], an estimated scenario in Germany with an installed capacity of 28GW will need 39 Tons and 12 Tons of Ir and Pt,

respectively, for the current technology. So, because of sustainability, the investigation interest in this topic is constantly increasing (e.g., from approximately 100 reports on OER and HER in 2007 to more than 2000 in 2017 [12]). Table 2.10 presents a historical summary of the different uses of electro-catalysts in PEMWE made by Shiva Kumar and Himabindu [182].

Table 2.10: Historical electro-catalysts in PEMWE (taken from [182])

Catalyst		Loading (mg cm^{-2})		Membrane	Temperature	Voltage at	Ref.
Anode	Cathode	Anode	Cathode		(°C)	1 A cm^{-2}	
Ir−Black	40% Pt/GNF	2.0	0.8	Nafion-115	90	1.67	[71]
Ir−Black	40% Pt/XC-72	2.0	0.8	Nafion-115	90	1.70	[71]
Ir−Black	Pt40/Vulcan®XC-72	2.4	0.7	Nafion-115	90	1.66	[72]
Ir−Black	Pd40/Vulcan®XC-72	2.4	0.7	Nafion-115	90	1.70	[72]
Ir−Black	Pt-black	2.0	0.8	Nafion-117	90	1.71	[73]
IrO_2	Pt-black	2.0	2.5	Nafion-115	80	1.60	[220]
RuO_2	40% Pt/C	10	0.4	Nafion-115	–	1.88	[125]
RuO_2	30% Pt/C	3.0	0.5	Nafion-112	80	1.65	[187]
RuO_2	30% Pt/C	1.5	0.5	Nafion-1035	80	1.63	[35]
IrO_2	30% Pt/C	1.5	0.5	Nafion-1035	80	1.67	[35]
IrO_2	60% Pt/C	3.0	0.5	Nafion-115	80	1.58	[25]
IrO_2	30% Pt/C	2.5	0.5	Nafion-115	80	1.70	[214]
Ir−Black	Pt/CNT	2.4	–	Nafion-115	90	1.72	[136]
$Ru_{0.7}Ir_{0.3}O_2$	40% Pt/C	2.5	0.5	Nafion-117	80	1.70	[127]
IrO_2/SnO_2	40% Pt/C	1.5	0.5	Nafion-212	80	1.57	[121]
RuO_2/SnO_2	40% Pt/C	30	0.6	Nafion-115	80	1.72	[121]
RuO_2	40% Pt/C	3.0	0.6	Nafion-115	80	1.74	[121]
RuO_2	30%Pd/N-CNT	3.0	0.7	Nafion-115	80	1.84	[156]
RuO_2	30%Pd/P-CNPs	3.0	0.7	Nafion-115	80	2.00	[183]
RuO_2	30%Pd/PG	3.0	0.7	Nafion-115	80	1.95	[185]
RuO_2	30%Pd/PN-CNPs	3.0	0.7	Nafion-115	80	1.90	[184]
$Ru_{0.8}Pd_{0.2}O_2$	30% Pt/CB	3.0	0.7	Nafion-115	80	2.03	[102]
$Ir_{0.6}Ru_{0.4}O_2$	20% Pt/C	2.04	2.04	Nafion-115	80	1.56	[127]
RuO_2	46% Pt/C	1.0	0.2	Nafion-117	80	1.68	[15]
$Ru_{0.9}Ir_{0.1}O_2$	46% Pt/C	1.0	0.2	Nafion-117	80	1.75	[15]
$Ru_{0.7}Ir_{0.3}O_2$	46% Pt/C	1.6	0.2	Nafion-117	80	1.80	[15]
$Ru_{0.3}Ir_{0.7}O_2$	46% Pt/C	1.4	0.2	Nafion-117	80	1.74	[15]
IrO_2	46% Pt/C	1.2	0.2	Nafion-117	80	1.80	[15]

In the cathode, Pt has excellent HER activity and stability in acidic atmosphere. Currently, the catalyst is supported by a carbon structure that gives it proper electrical conductivity. Catalyst loading is normally between 0.5 and 1 mg cm^{-2}. However, many efforts are being made to decrease it. Giddey et al prepared Pt/C catalyst with Pt loading of up 0.4 mg cm^{-2} [67]. Nowadays, ultra-low loadings of PGMs are being demonstrated to have comparative performance to commercial PEMWE. Bernt et al have reduced Pt loading from 0.3 mg cm^{-2} to 0.025 mg cm^{-2} [23]. Moreover, some other materials were tested as catalysts. Hinnemann et al have studied the utilization of MoS_2 that results in an acceptable activity but with lower current densities (10 mA cm^{-2}) than Pt-catalysts [82]. A better performance was obtained by Corrales-Sánchez et al mixing MoS_2 with commercial conductive carbon, Vulcan®XC72, and achieving current densities of 0.3 A cm^{-2}, still below common cathodes [38]. Following this investigation, Sarno

et al synthesized RuS_2@MoS_2 catalyst which allow current densities up to 1.1 A cm^{-2} [166].

Pd, as other PGMs, has received renewed interest recently due to its abundance and performance comparable to Pt for diverse reactions [165]. Due to worse results in HER than using Pt, investigation is focused on special structures, like Pd carbon nanotubes (Pd/CNTs). Moreover, hetero atom doped carbon nanoparticles were studied for increasing electron conductivity [120]. Alternatively, free platinum cathodes were investigated by using earth abundant metals [20].

On the anode, RuO_2 and IrO_2 are widely used as catalyst. The former has a better performance while the latter is more stable to corrosion in acidic media. So the use of bimetallic oxide has been studied in order to take advantage of both properties [36, 119]. Furthermore, about the cost issue, many transition metals have been tested in order to reduce the amount of noble metal used. Alternatively, IrO_2 and RuO_2 were mixed with TiO_2 [78], SnO_2 [98], Ta_2O_5 [86], Nb_2O_5 [192], Sb_2O_5 [33], PbO_2 [215], MnO_2 [193], among others. And as has been analyzed for the cathode, again, nanostructures are tested to enhance performance and reduce the amount of catalyst, as the case of vertical nanotubes proposed by Ghadge et al [66].

Current density

As described before, commercial PEM electrolyzers operate with a maximum electrical current of 3 A cm^{-2}. Up to 20A cm^{-2} extension of this range is being evaluated, as in the case of [116]. The main reason is the possible reduction in cost of H_2 production. CAPEX is inversely proportional to current density while OPEX increases with current density. An analysis of their relationship concludes that the optimal point depends on the cost of electricity due to the strong dependence of OPEX on it [205]. Although nowadays the minimum cost is around 2.5 A cm^{-2}, the deployment of renewable energies would lower the price of electricity and, therefore, increase the optimal current density. However, operational issues such as heat dissipation and mass transport within the cell must be addressed. Electrolysis process have irreversibility due to current loses that generates heat. It is necessary to maintain the operating temperature in order to ensure thermal stability of the PEM and avoid thermal gradients. For that purpose, the water is recirculated. Moreover, increasing current density means more water consumed and more gases produced. Therefore, current collectors must be designed in order to allow correct transport of flows to and from the electrodes.

PEM degradation

As one of the disadvantages of this technology compared to alkaline electrolyzers, understanding degradation principles and finding the best operating conditions have gained a lot of interest lately. An extensive work on dynamic operation can be found in [155]. Cyclical operation could be beneficial as constant operation causes passivation of current collectors made of Ti [154], membrane thinning [57] and degradation of anode catalyst [113]. Frensch et al carried out a systematic study to compare PEMWE degradation on different dynamic operation modes and testing various working temperatures [59]. They conclude that operation at high temperatures (90^oC) increases efficiency but also enlarges fluoride emission rates and, consequently, membrane thinning. Therefore, a thinner membrane increases gas crossover. Moreover, the high temperature enlarges the passivation of Ti, so the original efficiency benefit could be cancelled out over time. On the other hand, fast cycle modes increase performance due to reduced ohmic resistance. Also, faster cycles enhance fluoride emission but no thinning of the membrane occurs.

Recycling catalyst

As was already mentioned, PEMWE needs expensive noble metals like Pt and Ir [160]. In addition to trying to reduce amount of material required, another line of research is the possibility of recycling the components of PEM cell. Carmo et al present a method to recover both Pt and Ir catalysts and membrane [29]. This approach consist in inserting the catalyst-coated membrane (CCM) into a recycle reactor where a solution of deionized water and alcohol is circulated on both sides of the membrane. This delamination takes less than 30 minutes, resulting in a nearly clean membrane which can be dried for reuse. The two separate solutions with the catalyst residues are then centrifuged to obtain solids that are also dried. Results are promissory because more than 90% of the catalysts were recycled. Moreover, the conservation of the membrane allows its reutilization. Although membrane can be reused, its performance is insufficient. In that case, it will be advisable to reprocess the Nafion chemistry.

2.6 Summary

The search for alternative methods of power generation and transport has developed the concept of hydrogen economy. While today hydrogen is obtained mainly from hydrocarbons, new technologies to achieve lower GHG emissions are being developed and consolidated. Here, the

different methods of hydrogen production were summarized with emphasis on the current status of alkaline electrolysis. Among hydrogen methods, electrolysis stands out for ease of connection to renewable energies, obtainable purity and their existing but nascent commercialization.

As presented in the current review, there are interesting alternative methods for the production of hydrogen with virtually zero emissions, among them highlighting the production from biomass and electrolysis. Its biggest disadvantage is the economic cost superior to industrial processes such as the SMR in both construction and operation. It can be seen that these three technologies will coexist in the medium term, waiting for the proportion of SMR to gradually decrease, generating two important niches to be filled by the other two methods: mass production of hydrogen for industry and mobility from biomass, and electrolysis as an energy buffer for renewable sources.

Within the area of electrolysis, a comparative analysis of the various existing technologies was carried out. Advantages and disadvantages of the two commercially available methods have been pointed out, observing opinions of authors in favor of one and against another indistinctly. Actually, both technologies have benefits that lead to their use in different situations: in the case of alkaline electrolyzers, more developed and tested, they are usable as large installations for the stabilization of electrical networks or directly connected to large wind or solar farms. On the other hand, for PEM electrolyzers, with better dynamics and gas quality, it is expected that they can be used as an intermediate energy buffer in industrial plants or at a residential level. In any case, the need to continue research lines to increase their efficiency and reduce their costs is highlighted. Among them is the study of materials for electrodes, electro-catalysts and separators. The other two technologies in development, the SOE and AEM electrolyzers, must overcome the durability barriers in order to compete with the previous ones in the medium to long term.

Current lines of research on alkaline electrolyzers were discussed as it is the ecofriendly-technology with the highest maturity so far. Nevertheless, it requires improvements to be competitive against the production of fossil hydrogen, which means lowering construction and operating costs. The former depends mainly on the materials of the electrodes, so simple or coated non-precious metals are proposed. The later are strongly linked to the efficiency of the system which implies reducing ohmic overpotentials and gases cross-linking of gases. For this purpose, there are several proposals that will need to be deeply discused and analysed to find the optimum point of operation of alkaline electrolyzers.

The public has to be aware of the importance of reducing the GHG emissions. The hydrogen economy and renewable energies are, until today, the best solution. The development of these technologies needs the coworking between politics, business and science.

This thesis focuses on the modelling and development of control strategies of alkaline electrolyzers. Therefore, the next chapter describes the advances in these topics.

Chapter 3

Literature review on modelling and control

3.1 Alkaline electrolysis models

While it is true that the principle of operation of alkaline cells has been described widely by several authors, most of them focused on the stationary regime and presented empirical analytical relationships from the adjustment of a specific electrolyzer. Most models focus only on the cell-stack description but not in the entire system [76, 80, 135]. Moreover, most of them describe the stationary regime and are built from empirical equations [10, 90, 197]. Recently, Sanchez et al [161] used a commercial software to model the entire system while the cell-stack is described by a semi-empirical approach. Another recent example of dynamic model is the one developed by Lee et al [109]. They present a three-dimensional transient numerical model for the alkaline cell considering the electrochemical reactions and transport processes inside a zero-gap configuration as mentioned in § 2.4. Next, the most important points of the existing models in the literature will be developed.

3.1.1 Electrochemical reactions

In 2003, Ulleberg [197] proposed a model based on thermodynamic concepts and heat transfer to obtain the voltage of the package, the gas flow produced and the thermal equilibrium of the system, all of them as a function of the imposed current. These results were validated at the PHOEBUS plant in Jülich, where photovoltaic cells, hydrogen production and storage tests were carried out [21].

In this chapter, the enthalpy (ΔH) and entropy (ΔS) change will be the difference between the enthalpy and entropy values of the reactant (H_2O) and the products (H_2 and O_2). The Gibbs energy change (ΔG) is expressed as

$$\Delta G = \Delta H - T\Delta S. \tag{3.1}$$

The electromotive force necessary to reversibly separate the water is given by Faraday's law as

$$U_{rev} = \frac{\Delta G}{zF}. \tag{3.2}$$

From (3.1), it can be seen that the Gibbs free energy includes the heat demand defined as $T\Delta S$ for a reversible process. In turn, the thermoneutral voltage assumes zero heat exchange, so it is related to the demand for ΔH as

$$U_{tn} = \frac{\Delta H}{zF}. \tag{3.3}$$

The voltage actually applied to the cell is in practice greater than the reversible voltage, precisely due to irreversibility. Ulleberg proposes certain terms in his model that add to U_{rev} as follows:

$$U = U_{rev} + (r_1 + r_2 T)I + s.\log\left[\left(t_1 + \frac{t_2}{T} + \frac{t_3}{T^2}\right)I + 1\right], \tag{3.4}$$

being the parameters r_j, s and t_k calculated based on experimental data, while T is the cell temperature and I the applied current. As explained later by Amores et al [10], the second term corresponds to ohmic overpotentials and the third to activation overpotentials. These authors, in addition to the dependence on current and temperature, add the influence of electrolyte concentration, C, and the distance between electrodes, d, thus proposing

$$U = U_{rev} + \left[(r_1 + p_1 + q_1) + r_2 T + p_2 C + p_3 C^2 + q_2 d\right] I + s.\log\left[\left(t_1 + \frac{t_2}{T} + \frac{t_3}{T^2}\right)I + 1\right]. \tag{3.5}$$

Moreover, Ursúa and Sanchis [199] start from the same thermodynamic theory to define the ideal dissociation voltage of water to build an electrical model of overvoltages. They propose an analytical calculation for U_{rev} dependent on temperature, pressure and concentration molar solution of Hydrogen Potassium oxide (KOH) as

$$U_{rev} = N_S\left\{U^0_{rev,T} + \frac{RT}{zF} ln\left[\frac{(p - p_{v,KOH})^{3/2}}{a_{H_2O,KOH}}\right]\right\}, \tag{3.6}$$

where N_S is the number of cells in series, $U^0_{rev,T}$ is the voltage of the reversible process for a given temperature, $p_{v,KOH}$ is the KOH vapour pressure and $a_{H_20,KOH}$ is the the aqueous activity of KOH. These variables can be obtained from empirical relationships in a validity range of temperature T, pressure p and molar concentration C between 0 and 250 ºC, 1 and 200 bar and 2 and 18 mol kg^{-1} [18, 112].

The electrical current that participates in the redox reactions is a function of the voltage which is obtained from the modification of the Tafel equation as

$$\begin{aligned} v_{act,a,E} &= N_S v \ln\left(\frac{1}{w} i_{act,a} + 1\right) \\ \therefore i_{act,a} &= w\left(e^{\frac{v_{act,a,E}}{N_S v}} - 1\right), \end{aligned} \tag{3.7}$$

$$\begin{aligned} v_{act,c,E} &= N_S x \ln\left(\frac{1}{y} i_{act,c} + 1\right) \\ \therefore i_{act,c} &= y\left(e^{\frac{v_{act,c,E}}{N_S x}} - 1\right), \end{aligned} \tag{3.8}$$

being the parameters v, w, x and y functions of the temperature as

$$\begin{aligned} v &= v_1 + v_2 T + v_3 T^2, \\ w &= w_1 + w_2 T + w_3 T^2, \\ x &= x_1 + x_2 T + x_3 T^2, \\ y &= y_1 + y_2 T + y_3 T^2. \end{aligned}$$

The final model of Ursúa and Sanchis, which is presented in its equivalent electrical form in Figure 3.1, has the same terms proposed by Ulleberg: the reversible process voltage, the ohmic resistance and the activation overpotential and shows a dynamic description of the changes in electric current.

The ohmic resistance is calculated from physical (area A) and state (temperature) parameters as

$$R_{ohm,E} = N_S \frac{r}{A}, \tag{3.9}$$

being r in turn calculated as

$$r = r_1 + r_2 T + r_3/T + r_4/T^2. \tag{3.10}$$

In his doctoral thesis, Roy [157] proposes the calculation of the voltage drop due to ohmic resistance as presented next:

$$U_{ohmic} = r_{final} i + U_{bubble}. \tag{3.11}$$

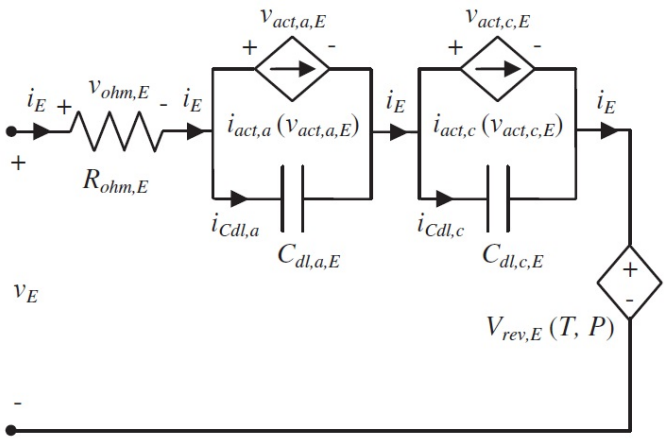

Figure 3.1: The electric model of the electrolytic cell (taken from [198]).

Table 3.1: Measurement of initial resistances of electrolytic cell components (taken from [157])

Components	Electrode area	Resistivity	Thickness	Number of units in a cell	Resistance
	$[m^2]$	$[\Omega m]$	$[m]$		$[\Omega]$
KOH layer	0.1	0.012	0.0001	2	2.4×10^{-5}
Electrodes	0.1	6.8×10^{-8}	0.001	2	13.6×10^{-10}
Current collector (wire plesh)	0.1	5×10^{-8}	0.003	2	3×10^{-9}
Bipolar plate	0.1	6.8×10^{-8}	0.002	1	13.6×10^{-10}
Gas separator (VITO)	0.1	$9 \times 10^{-6}\Omega m^2$	—	1	9×10^{-5}
Total initial resistance ($r_{initial}$)					$11.4 \times 10^{-5}\Omega$

The voltage drop due to the presence of bubbles (U_{bubble}) is discussed in the next section. Furthermore, the final resistance (r_{final}) arises from the adjustment on an experimental basis. This value depends on the construction design of the equipment and on the temperature as

$$r_{final} = r_{initial} - 4 \times 10^{-6} \ln(T - 273.15) + 4 \times 10^{-6} \ln(T^2), \tag{3.12}$$

where $r_{initial}$ arises from the measurement of the cell components as can be seen in Table 3.1 as an example of the electrolyzer used by Roy.

3.1.2 Effect of bubble generation

The presence of bubbles in the electrolytic cell decreases the real area of the electrolyte, increasing the resistance of the cell. Higher current density produces more gas and therefore greater resistance will be observed. In his doctoral thesis, Roy [157] proposes a method for estimating the effect of the presence of bubbles. As previously stated, the voltage drop due to the presence of bubbles (U_{bubble}) depends on the construction design of the equipment and on the electric

current, being in the case of Roy adjusted by the following equation:

$$U_{bubble} = 10^{-5}i - 4 \times 10^{-9}i^2 + 10^{-9}i^3. \tag{3.13}$$

Moreover, Milewski et al [135] adopt the correlation proposed by Bruggeman, which is [101]

$$\frac{\sigma_\epsilon}{\sigma_0} = (1-\epsilon)^{1.5}, \tag{3.14}$$

being σ_0 and σ_ϵ the electrical conductivities in the electrolyte free of bubbles and in the presence of bubbles, respectively. While ϵ is the fraction of bubbles in electrolyte estimated as

$$\epsilon = \frac{2}{3}\theta = 0.0153\left(\frac{i}{i_{lim}}\right)^{0.3}. \tag{3.15}$$

This estimate is suggested by Vogt et al [208] based on the results of studies by diverse authors for H_2 and O_2 bubbles in different electrolytes and with various electrode materials.

3.1.3 Gases production

As previously mentioned, the circulation of electric current through the package produces the separation of the water into H_2 and O_2 . But not all the current that circulates does so through the electrolyte because there are eddy currents. This phenomenon is described from the Faraday efficiency, η_F, or current efficiency that relates the amount of gas produced ($\dot{n}_{H_2}$) with the input current [197] as

$$\dot{n}_{H_2} = \eta_F \frac{N_{celdas} i}{zF}, \tag{3.16}$$

where z is the number of electrons exchanged in the process ($z = 2$) and F is the Faraday constant ($F = 96485.3365 \text{C.mol}^{-1}$). The Faraday efficiency η_F depends especially on the Temperature T at which the process occurs. Furthermore, the production of O_2 , $\dot{n}_{O_2}$, and H_2O at the anode, $\dot{n}_{H_2O,a}$ and the consumption of H_2O at the cathode, $\dot{n}_{H_2O,c}$, are obtained through the stoichiometric relationships

$$\dot{n}_{H_2} = 2\dot{n}_{O_2} = \dot{n}_{H_2O,a} = -\frac{1}{2}\dot{n}_{H_2O,c}.$$

It is recognized that this efficiency decreases along with the current density. However, there are various methods for calculating it. Hug [90] proposes

$$\eta_F = B_1 + B_2 e^{\frac{B_3 + B_4 T + B_5 T^2}{i/A}}, \tag{3.17}$$

where B_1 to B_5 to be determined empirically, and A is the area of the electrodes. In a similar way, Ulleberg raises

$$\eta_F = \frac{(i/A)^2}{f_1 + (i/A)^2} f_2, \tag{3.18}$$

being f_1 and f_2 constants determined empirically. Moreover, Havre et al [81], adjusting the parameters a_1 to a_7 with data from [89], formulated

$$\eta_F = a_1 e^{\left[\frac{a_2+a_3T+a_4T^2}{i/A} + \frac{a_5+a_6T+a_7T^2}{(i/A)^2}\right]}. \tag{3.19}$$

Finally, Roy defines the loss resistance r_L to be empirically adjusted from the voltage, current and gas produced data depending on the electrolyzer under consideration as

$$r_L(T) = r_L(348.15K) - 0.09(T - 348.15K). \tag{3.20}$$

The eddy currents i_L will then be calculated from ohm's law as

$$i_L = \frac{U_{stack}}{r_L}, \tag{3.21}$$

where U_{stack} is the cell package voltage applied. Thus, the Faraday efficiency is calculated directly as

$$\eta_F = 100 - i_{l,\%}. \tag{3.22}$$

3.1.4 Gas contamination

The main difficulty in the operation of an alkaline electrolyzer is the contamination of both streams, especially on the O_2 side. Generally, this concept is approached in the models as an empirical equation that relates contamination to the state of the system (e.g., current density, temperature, pressure). This way evidences the lack of dynamic analysis of purity. Empirical adjustments, as is the case of the work done by Hug et al. [90], can be found. This work is considered by Sánchez et al. [162] to perform a semi-empirical model for a 15kW electrolyzer. Moreover, in the Max Planck Institute for Iron Research there are studies on physical models of the gases diffusion and the properties of the membrane that separates half cells [168, 170]. However, a model integrating cell behaviors and transport phenomena taking place in the assembly as a whole has not been found so far in the literature. Moreover, there are studies that analyze the phenomenology of the contamination process as [172].

There are two driving forces for gas cross-permeation through the membrane. The first one is diffusion driven by differences in dissolved gas concentration between the two half cells [171]. This phenomenon can be modelled on the basis of Fick's law as

$$\Phi_{\mathrm{H_2-O_2},Fick} = D_{\mathrm{H_2}} \frac{C_{\mathrm{H_2},III} - C_{\mathrm{H_2},IV}}{z_{cell}}, \tag{3.23}$$

being $\Phi_{c\to a,Fick}$ the H_2 flux from cathode (c) to anode (a), $D_{\mathrm{H_2}}$ the diffusion coefficient of H_2 through the separator, $C_{\mathrm{H_2},x}$ the H_2 concentration in both half cells and z_{cell} the separator width. The presented equation corresponds to the H_2 diffusion, a similar equation can be described for the O_2.

The second cause of cross-contamination is the permeability of the electrolyte with dissolved gases due to differential pressure between both half cells. Based on Darcy's law, H_2 flux when cathodic pressure is higher than anodic one can be written as

$$\Phi_{\mathrm{H_2-O_2},Darcy} = \epsilon_{H2}^{Darcy} \frac{P_{III} - P_{IV}}{z_{cell}}, \tag{3.24}$$

where $\Phi_{c\to a,Darcy}$ is the H_2 flux from cathode to anode when cathodic pressure P_c is greater than anodic pressure P_a. The H_2 permeability ϵ_{H2}^{Darcy} depends on fluid properties and the concentration of dissolved H_2. In case anodic pressure is greater than the cathodic one, a similar equation can be obtained for the O_2 contamination flux. Clearly, only one flux occurs at a time.

To fill the gap, a phenomenological-based semiphysical model (PBSM) that feeds from previous modelling and gathered experience, and describes the phenomena that occur within the electrolyzer is proposed. The availability of this model will allow a more accurate idea of the dynamics and even set guidelines for design improvement in future prototypes. The phenomenological-based approach gives in addition the possibility of refinements of the model by the use of better formulations to calculate model parameters. This experimentally-validated model can also be used as a source for reduced models with a control-oriented purpose.

3.2 Review of control strategies for alkaline electrolyzers

Similar to what happen with modelling, after an exhaustive revision of the related literature and also from the conclusions reported by Olivier et al [144], the design of controllers to manage the operation of electrolyzers considering the issues mentioned previously seems not to be addressed yet in the literature. Therefore, the development of useful input-output models for control

design is an open research topic [144]. In general, control objectives are completely focused on the management of the electrolyzer as an electrical consumer and producer of H_2 connected to a grid [63, 207].

In the current thesis, the management of the outlet valves becomes of great interest. However, their control could be found mentioned only by Schug [175] in his description of a pilot plant and recently in the model presented by Sanchez et al [162]. Schug, in his work, described in detail an alkaline electrolyzer along with experimental results. Unfortunately, the control system is not detailed enough, but the connection of plant output with control action can be recognized in the simplified flow diagram presented. Also, Sanchez et al briefly explained the control scheme in which a back-pressure regulator maintains the system pressure while a set of solenoid valves controlled the level difference.

Given the lack of control strategies designed for such systems and, in particular, those strategies based on suitable and reliable models properly obtained for control tasks, the main contribution of this thesis is twofold. First, from a well-established nonlinear model considering the dynamics and the accurate phenomenology of the alkaline electrolyzers which was reported in [41, 42], a reduced order control-oriented model is obtained and properly validated by using the complete nonlinear model (which, in turn, is validated with real data). Second, by using the reduced model, an optimal controller is designed and the closed-loop performance of the system is evaluated based on the maximization of the hydrogen purity through the mitigation of the cross-contamination of gases into the chambers.

3.3 Summary

It can be concluded from the revision of the state of the art on the modelling and control of alkaline electrolysis that there is enough space to contribute to this issue. As will be discussed in Chapter 4, this contribution will take advantage of the experience gathered in recent years in the development and operation of high pressure alkaline electrolyzers.

Part II

Description and modelling of high-pressure alkaline electrolyzers

Chapter 4

High pressure alkaline electrolyzer

4.1 Background

The Instituto Tecnológico de Buenos Aires (ITBA) has been working on the alkaline electrolysis area, for H_2 and O_2 production, during more than a decade, specifically with regard to high pressure systems. Initially, the first electrolytic reaction tests were carried out in a closed single cell in which pressures of up to 950 bar were obtained (Figure 4.1). The so-called first generation was then tested for feasibility, being able to operate up to 700 bar. This systems were designed for intermittent operation (Figure 4.2a).

With the accumulated experience, two second-generation prototypes were developed for research projects. As the first prototypes of continuous production, they were designed for a widely used 30 bar operating pressure. The first one was installed at the Esperanza Base (Antarctica)

Figure 4.1: Closed single cell tested up to 950 bar.

(a) First generation

(b) Second generation. Antarctica

(c) Second generation. Universidad Nacional de Córdoba

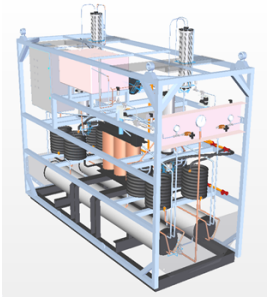

(d) Third generation. Pico Truncado

Figure 4.2: Electrolyzer prototypes developed by ITBA.

for the storage of wind energy used in the consumptions of the local laboratory (see Figure 4.2b). With a maximum H_2 production of 0.8 Nm^3h^{-1}, it has a specific design due to the low temperatures of the environment. The second prototype, which can be seen in Figure 4.2c, was delivered to Universidad Nacional de Córdoba to study the electrolyzer-wind generator interface.

The third generation is the electrolyzer developed for the experimental hydrogen plant in Pico Truncado, Santa Cruz (Figure 4.2d). This plant was a pioneer in the filling of CNG+H for automobiles. It was designed for a maximum pressure of 200 bar and a maximum H_2 production of 5 Nm^3h^{-1}.

Finally, gathering all lessons learned, an electrolyzer was designed to continue the developments at the university and to undergo future modifications. It is the so-called Electrolyzer of the Hydrogen Laboratory (EHL) that is currently used in this doctoral work (see Figure 4.3). The following section describes the high pressure electrolyzer designed and developed at the university.

Figure 4.3: Picture of the Electrolyzer of the Hydrogen Laboratory which is currently being studied for the present work.

4.2 System description

As previously mentioned, a proposed solution for energy storage is the combination of an electrolyzer, storage tanks and a fuel cell. In this way, the additional electrical energy is used to produce hydrogen that is stored in the tanks. When renewable energy sources are not able to meet the demand, the stored hydrogen is consumed by the fuel cell.

High-pressure alkaline electrolyzers can supply gases at a storage pressure, dispensing with the use of compressors. However, cross-contamination, i.e. the concentration of O_2 in the H_2 stream and vice versa, increases with pressure, then special attention is required in operation due to safety and quality issues.

In Figure 4.4 it can be seen the Electrolyzer of the Hydrogen Laboratory (EHL) schematic, that is composed by various subsystems that will be explained and detailed later:

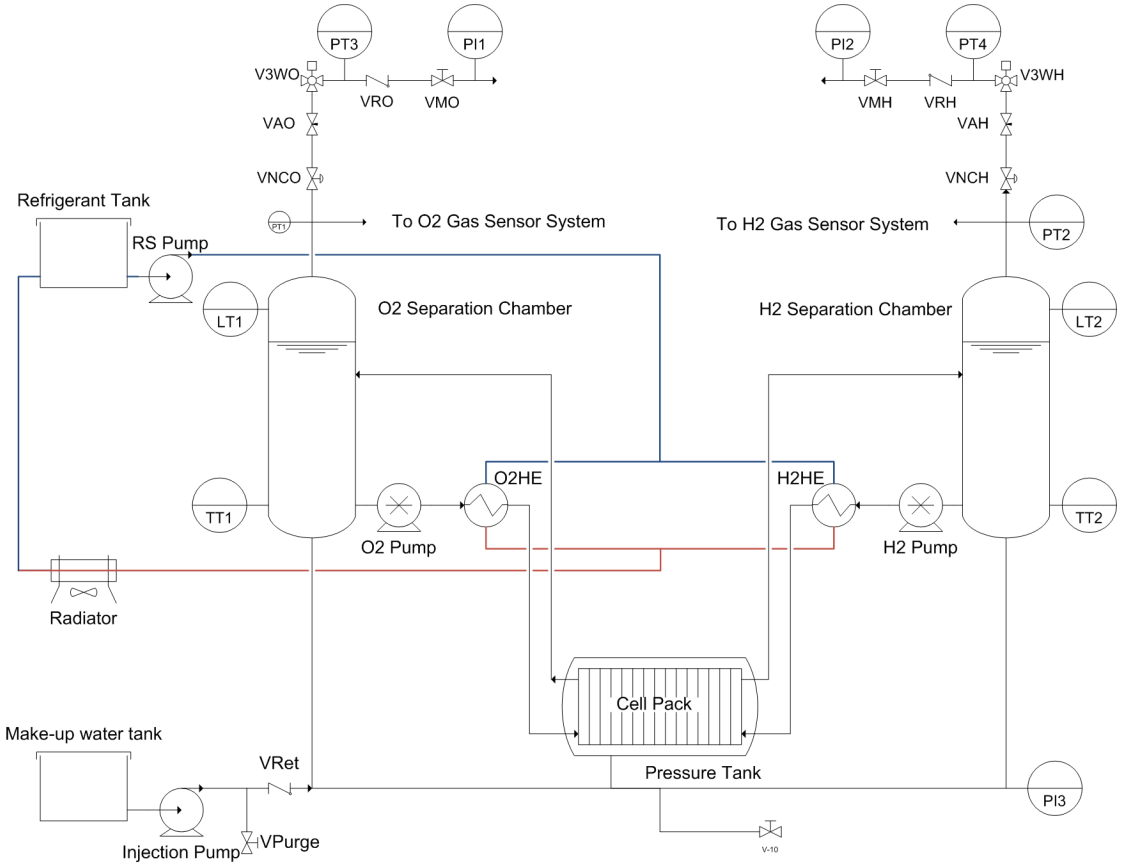

Figure 4.4: Process flow diagram of the Electrolyzer of the Hydrogen Laboratory (EHL). Indicators and transmitters are included without control loops.

- Pressure Tank (PT): contains the Cell Pack and serves to interconnect gas separation chambers.
- Cell Pack (CP): is the heart of the system, where electrolysis takes place.
- Separation chambers of H_2 and O_2 (SCH and SCO): in its upper part the gases produced accumulate, increasing the pressure of the equipment.
- Output Lines of H_2 and O_2 (OLH and OLO): the gas output is controlled from each SC to maintain the desired levels and pressure.
- Cooling System (CS): keeps the temperature of the equipment around the set value.
- Injection Pump (IP): replenishes water that is consumed during the operation.

4.2.1 Cell pack

The main part of the EHL is the Cell Pack (CP) consisting of fifteen individual electrolytic cells of alkaline type connected in series as can be seen in Figure 4.5, each of which is formed by two half cells: one producer of O_2 and another one of H_2. The electrolytic cell is separated into two hemicells by means of a membrane that prevents the mixing of the gases produced. This membrane is a material composed of a polymer (polysulfone) and a porous ceramic (Zirconia ZnO2), called Zirfon PERL. The characteristics sought in this membrane are:

- Porosity and high wettability (high ionic conductivity due to adequate circulation of OH^-)
- Small pores (low gas permeability)
- High electrical resistance (low eddy currents)
- Thin materials (low ohmic flow due to ionic conduction)
- High volumetric pore fraction (high ionic conductivity)
- Flexibility, mechanical stability and chemical durability

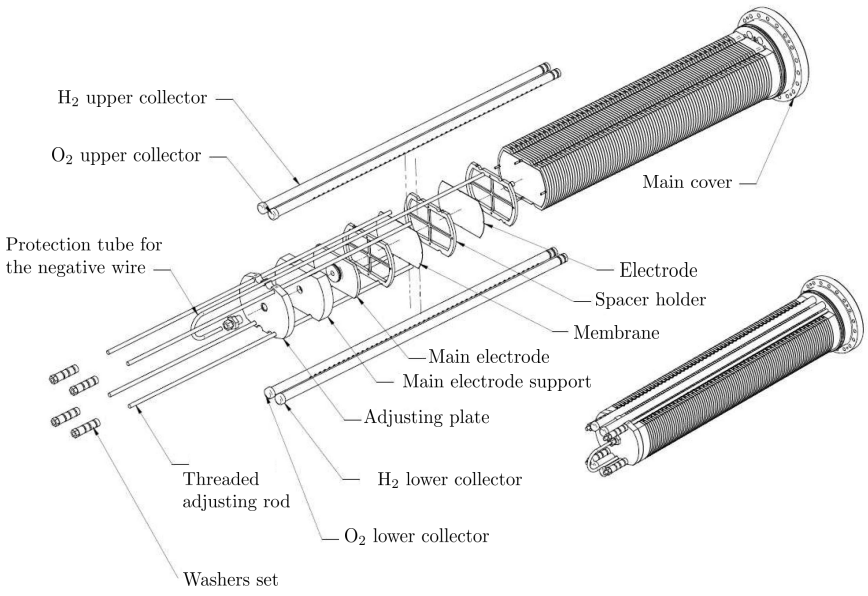

Figure 4.5: Cell Pack set exploded. Electrodes, membrane and spacer holders can be seen.

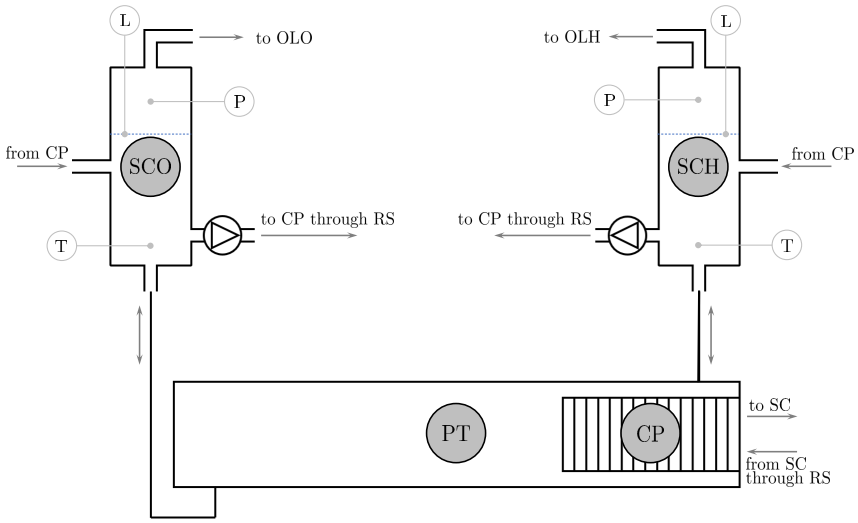

Figure 4.6: Set formed by the Separation chambers and the pressure tank.

The electrodes are nickel sheets that act as cathodes for one cell and anode for the next. The distance between cathode and anode is approximately 2 cm. The cell is flooded with a 30% Potassium Hydroxide (KOH) solution (where the highest ionic conductivity is obtained), which is the one that provides the necessary OH^- anions to facilitate the reaction. Finally, to extract the gases produced from the cell (to improve electrical efficiency and reduce cross contamination) it is necessary to recirculate the KOH solution. Therefore, it is entered at the bottom of the cell to drag the bubbles out at the top. In electrolyzers operating at low pressure, this process occurs by natural convection, while for higher pressures it is necessary to generate recirculation. The rate of ascent of bubbles is a variable that, as indicated previously, affects contamination and electrical efficiency.

4.2.2 Separation chambers and pressure tank

From the PC, two flows of KOH solution come out mixed with bubbles of H_2 and O_2 that are dumped in the SC to allow the bubbles break off and collect at the top (Figure 4.6). It is through this movement of the solution that the gas, dissolved and in bubbles, produced in the half cell, reaches the separation chamber where it leaves the solution.

In SC the gas produced in its upper part accumulates, thus increasing the total system pressure. The Output Lines (OLs) of gases are controlled by two motorized valves that allow to

define an operating pressure of the EHL.

As can be concluded from Figure 4.7, water is produced at the anode while at the cathode it is consumed, resulting in a final consumption balance of one mole of water for each mole of H_2 produced. Due to this, the concentration of solute (KOH) at the anode decreases and at the cathode increases, which generates an increase in electrical potential and the consequent decrease in electrical efficiency. For that reason, it is necessary that both circuits, presently independent, have some connection. This is achieved through the interconnection of the bottoms of the SC through the PT. This device, in addition to allowing the flow of water from the SCO to the SCH, allows for minimum mechanical stresses of the CP since the internal and external pressures are practically equal.

A pump (called Recirculation Pump) is installed in the lower part of the CS that drives the solution, already free of bubbles, towards the lower part of the PC, thus achieving the mentioned recirculation.

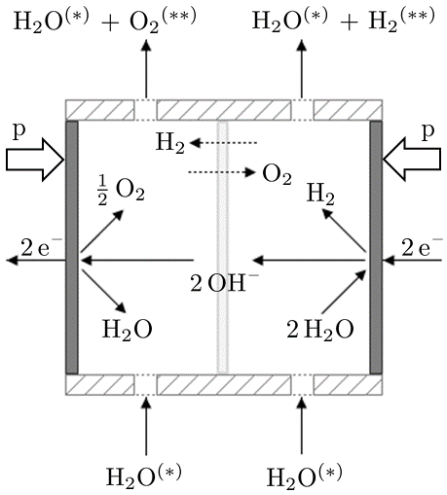

Figure 4.7: Scheme of the electrolytic cell with reactions. $H_2O^{(*)}$ represents KOH solution and $O_2{}^{(**)}$ and $H_2{}^{(**)}$ represent outputs that are contaminated with H_2 and O_2, respectively.

Dimensions of the piping and tanks are shown in Table 4.1. All connections between tanks and pipes are considered as sudden contractions and expansions with $\frac{d}{D} \to 0$, being d and D the smaller and larger diameters, respectively.

Table 4.1: Measured dimensions for piping sections and accessories

Accessory	Length [cm]	Diameter [cm]
Straight sections I[1]	312	1.58
Straight sections II[2]	244	1.58
Annulus	32	$D_{equiv} = 7.57$
Cell[3]	1.6	13.8
Separation chamber	60	8.2
Other accessories	-	1.58

[1] Identical circuit for the cathodic and anodic recirculation line (13 → 11 and 14 → 12). The numbering refers to Figure 5.1.
[2] Equalization line (7/8 → 8/7)
[3] Values for individual cell. Number of cells in the Package Cell $n_{cell} = 15$

4.2.3 Output lines

In order to maintain equalized levels and pressure around the working point, the exit of the gases through the upper part of the SCs is controlled through a motorized valve. After a normally closed safety solenoid valve there is the previously named motorized valve. This is a three-way valve allowing the opening to Vent or Tank. The first outlet is used for intermediate operations such as Pressurization and Depressurization, moments in which the quality of the gases produced (purity) is lower.

Prior to the safety valve, there is a connection to the gas purity measurement system. This takes a sample of the exhaust gases that pass through a pressure regulating valve to reach pressure values of less than 1 bar gauge required by the sensor. This device measures the amount of O_2 and H_2 present in the lines of H_2 and O_2, respectively.

4.2.4 Auxiliary systems

At the outlet of the Recirculation Pumps (RP) and prior to re-enter into the PC, there are two countercurrent tube-in-tube heat exchangers with distilled water cooled afterwards in a radiator with fan. This system operates intermittently based on a hysteresis-type control law that will be discussed in § 7.1.

Moreover, in the downstream pipe from the SCO to the PT, there is an inlet connected to a check valve that allows operating an Injection Pump (IP) to inject distilled water to replace that which is consumed in the reaction. This pump also operates intermittently when reaching a combination of levels in both SCs and interrupts against a given level value in either SC.

Table 4.2: Measured variables present in EHL.

Variable	Description	Sensor type	Expected range	Device range	Units
I	Electric current	Hall, Hass 100S	0–60	0–100	A
U	Voltage	Resistive divider	0–60	-90–90	V
T_{SCH}, T_{SCO}	Temperature	Pt100	20–60	-200–850	^{o}C
P_{SCH}, P_{SCO}, P_{OLH}, P_{OLO}	Pressure	Transmitter membrane SML	0–70	0–200	bar
L_{SCH}, L_{SCO}	Level	Capacitive sensor	0–90	0–90	mm
x_{H_2,O_2}	H_2 concentration in O_2 stream	CiTiceL T3HYE	0–10000	0–30000	ppm
x_{O_2,H_2}	O_2 concentration in H_2 stream	CiTiceL T7OX-V	0–1	0–25	%

Table 4.3: Current actuators in the EHL

Variable	Description	Actuator type	Range	Unit
u_{PWM} [1]	Power source modulation	IGBT	0-100	%
u_{PS}	Power source activation	SSR	0/1	ON/OFF
u_{RS} [2]	Refrigeration system	Relay	0/1	ON/OFF
u_{IP} [2]	Injection pump	Relay	0/1	ON/OFF
u_{RP}	Recirculation pump	-	-	l h^{-1}

[1] Despite not being part of the equipment, the power delivered to the EHL can be regulated with a duty cycle control for direct current supply.
[2] See § 7.1.

4.2.5 Variables

In Table 4.2 all the measurements currently carried out on the tested equipment are summarized, while in Table 4.3 the outputs or actions of the system are observed.

4.3 Summary

After several prototypes designed and tested, it is now intended to advance in the in-depth study of the processes that occur in the electrolyzer. As it was concluded from the state of the art, there is still much to understand about this technology. Therefore, by computing a dynamic integration model of the complete system will pursue two objectives. First, it provides a tool to improve the control strategy of the operation; and second, it adds decision elements to improve the design and development of new prototypes. In the next section, a phenomenological-based semiphysical model will be developed.

As mentioned above, the main objective of an alkaline electrolyzer is to separate water to form H_2 and O_2 by applying an electric current I. In this process, it is highly important to minimize the diffusion through the membrane caused by differences in both concentration and pressure. Up to 2% of H_2 in the O_2 stream is widely accepted as a limit, taking into account

that the lower explosive limit of H_2 is 4%. Additionally, H_2 and O_2 gases must be delivered at high pressures in order to avoid the use of compressors. Since gas purity decreases with higher pressures, it is expected to increase the possible operating pressure preventing contamination with a suitable control strategy.

Chapter 5

Phenomenological-based semiphysical model

5.1 Model development

In this chapter, the PBSM for a water electrolyser located in the ITBA Energy Laboratory is developed. Then the steps of the method to obtain an PBSM are followed, as reported in [9, 110].

5.1.1 Process description and model objective

As the first step in this method, the system along with its operation was described in Chapter 4. The following model gives information about flows, concentrations and pressures within the high-pressure alkaline electrolyzer by knowing the electrical input and control actions.

5.1.2 Modeling hypothesis

For this process no analogy should be resorted to, since all phenomena are known from the physico-chemical. The water in contact with the electrodes participates in the following two chemical reactions in the electrolytic cell (Figure 4.7), one at each electrode, driven by the electric current symbolized by the flow of electrons e^-:

$$\begin{aligned} &\text{Reaction 1:} \quad 2\,H_2O + 2\,e^- \longrightarrow H_2 + 2\,OH^-(aq), \\ &\text{Reaction 2:} \quad OH^-(aq) \longrightarrow \frac{1}{2}\,O_2 + 2\,e^- + H_2O. \end{aligned} \tag{5.1}$$

Each reaction occurs in a half cell, so there is no direct mixing of gases in that space. However, the membrane that separates the half cells is slightly permeable to gases, so that a first focus of

cross-contamination of gases appears. As the reactions produce gases and the aqueous solution has a limit capacity of solubilization of those gases, the solutions will be considered to leave each half cell at its limit of solubilization of the corresponding gas. Therefore, all the excess gas that produces the reaction on that limit of solubility, is transported in the liquid as small bubbles of that gas. In the separation chamber to which each solution passes, the separation of the gas bubbles is achieved, without losing the saturation of the gas in the solution. However, the gas produced by that separation will be considered saturated in water due to the equilibrium between the liquid water and the gas in the atmosphere of the separation chamber. This gas is stayed in the upper part of the chamber, pressurizing it. This gas is discharged in a regulated manner by the upper part, trying with this controlled flow to maintain the pressure in the system. The solution saturated in the gas at the pressure of the chamber, but degassed by eliminating bubbles, is removed from the chamber through a pump. It is assumed that said solution is saturated from the chamber. The discharge pressure of that pump must be sufficient to pressurize the tank containing the cell pack.

The assumptions completing the modeling hypothesis previously stated are:

- Perfect agitation in all process systems (PSs) except gassed liquid in separation chamber.
- The half cells always operate at full volume without gas accumulation.
- All the ion OH^- is produced or consumed within the half cells, i.e., there is no OH^- in any other stream.
- Spatially uniform temperature throughout the device.
- Temporal constant temperature due to the action of the cooling system.
- The recirculation pumps allow to overcome the friction in the system and guarantee the flow between the half cells and the separation chambers.
- The gas mixture in the upper part of the separation chambers is considered as an ideal gas.

5.1.3 Process system definition

Figure 5.1 shows the process systems (PSs) that are taken to build the model. The number of each PS is placed in Roman next to each box. Although all the 16 process systems that appear are drawn, it is not necessary to make balances on all, since most of them present a very simple

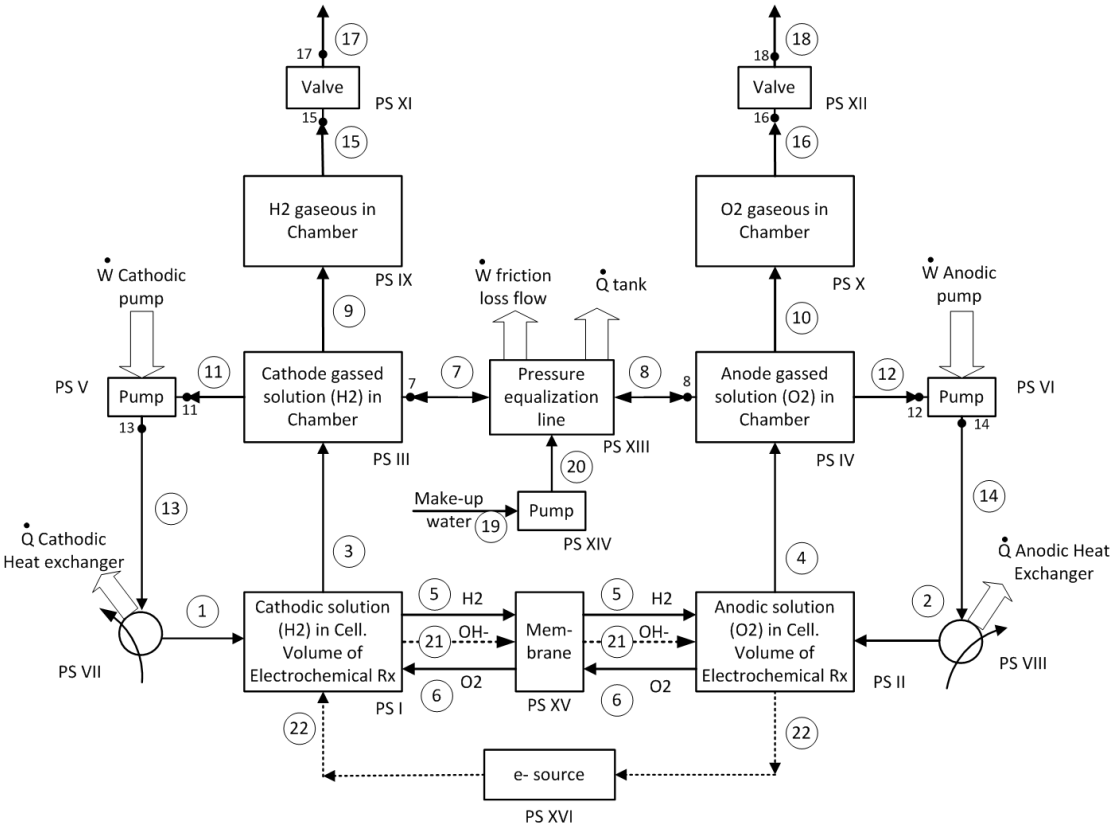

Figure 5.1: Flow diagram with the Process Systems numbered in Roman. Mass exchanges are identified with numbers inside circles.

action, which can be formulated with an algebraic expression. In addition, the symmetry of the processes (there are two half-circuits, one per each half-cell), facilitates the construction of the model. The following pairs of process systems are of interest and for them all balances must be raised (equal in their mathematical structure by symmetry, but with particular parameters): PSs I and II, PSs III and IV, PSs IX and X, and finally, PS XIII, which does not have symmetry. As already mentioned, the other PSs have trivial models, so no balance is deducted for them. While PSs I and II are the only ones with chemical reaction, all balances are worked on a molar basis instead of using the mass base.

5.1.4 Application of the conservation principle

The conservation law will be applied to the PSs of interest mentioned in the previous step. In this way, the basic structure of the model is obtained, which will allow answering the question

asked to the model in § 5.1.1.

PS I: Cathodic solution (H_2) in cell

This process system has the same structure of equations as PS II. Therefore, later on the PS II will only change the nomenclature and determine the parameters of the other half cell. The balances for the PS I are presented next.

Total Material Balance In this case, the balance is:

$$\frac{dN_I}{dt} = \dot{n}_1 + \dot{n}_6 - \dot{n}_{21} - \dot{n}_3 - \dot{n}_5 + \dot{n}_{22} + r_1 \sum_i \sigma_{i,1}, \tag{5.2}$$

with N_I are the total moles contained in the space containing the solution in the anodic half cell, the $\dot{n}_i$ are the molar flows with i indicating the number of the current, as indicated in Figure 5.1, and r_1 the rate at which the half-cell reaction proceeds, which is referred to as the electrochemical reaction 1. The final sum is on the stoichiometric coefficients $\sigma_{i,1}$ of the species i in the balanced electrochemical reaction 1, respecting the convention of using minus sign for reagents (consumed) and plus sign for products (appeared). Note that in (5.2) all flows are included, but due to the low mass of the electron, this last molar flow can be considered integrated to the mass of the ion OH^-, whose molecular mass is as the sum of the molecular masses of an oxygen and a hydrogen.

The total moles can be expressed as

$$N_I = \bar{\rho}_3 \, V_{mix,I}, \tag{5.3}$$

where $\bar{\rho}_1$ is the molar density of the mixture in $\frac{kg}{kmol}$ and $V_{mix,I}$ is the volume of the whole mixture (liquid and bubbles gas) contained in PS I. With the assumption of constant volume of the half cell replacing in (5.2) with the derivative of (5.3) and also recognizing that the molar flow of electrons is equal to the molar flow of OH^-, it is got to:

$$\frac{d\bar{\rho}_3}{dt} = \frac{1}{V_{mix,I}} \left[\dot{n}_1 + \dot{n}_6 - \dot{n}_3 - \dot{n}_5 + r_1 \sum_i \sigma_{i,1} \right]. \tag{5.4}$$

Hydrogen balance This balance is as shown next:

$$\frac{dN_{H_2,I}}{dt} = x_{H_2,1} \, \dot{n}_1 + x_{H_2,6} \, \dot{n}_6 - x_{H_2,21} \, \dot{n}_{21} - x_{H_2,3} \, \dot{n}_3 - x_{H_2,5} \, \dot{n}_5 + r_1 \, \sigma_{H_2,1}, \tag{5.5}$$

where $N_{O_2,I}$ is the mass of hydrogen (expressed in moles) contained in the PS I, $x_{H_2,i}$ is the molar fraction (in $\frac{kmol\,H_2}{kmol\,mix}$) of hydrogen in the current i, and $\sigma_{H_2,1}$ is the stoichiometric coefficient of

hydrogen in the cathodic reaction. It should be clarified that $x_{H_2,i}$ for current 3, and eventually for current 5 if the separation chamber is not operating correctly, it refers to both dissolved hydrogen and hydrogen in the form of bubbles.

To simplify this balance expression, it is known that the hydrogen concentrations in streams 6 and 21 is zero: $x_{H_2,6} = x_{H_2,21} = 0$ and also that the stoichiometric coefficient $\sigma_{H_2,1} = 1$, with which it is obtained

$$\frac{dN_{H_2,I}}{dt} = x_{H_2,1}\,\dot{n}_1 - x_{H_2,3}\,\dot{n}_3 - x_{H_2,5}\,\dot{n}_5 + r_1. \tag{5.6}$$

Another simplification is to express the total moles of hydrogen in this process system as

$$N_{H_2,I} = x_{H_2,I}\,N_I, \tag{5.7}$$

in which by applying the definition of derivative of a product, it is got to

$$\frac{dN_{H_2,I}}{dt} = dx_{H_2,I}\,\frac{dN_I}{dt} + N_I\,\frac{dx_{H_2,I}}{dt}, \tag{5.8}$$

which is replaced in the equation of Material Balance per component, concluding in

$$x_{H_2,I}\,\frac{dN_I}{dt} + N_I\,\frac{dx_{H_2,I}}{dt} = x_{H_2,1}\,\dot{n}_1 - x_{H_2,3}\,\dot{n}_3 - x_{O_2,5}\,\dot{n}_5 + r_1. \tag{5.9}$$

In this way the equation has two differentials, so it must be decided which of the two is the main differential and which will act as a parameter. In this case, since it is a balance for the hydrogen component, the main differential will be that of the concentration of hydrogen in the PS I, which by the assumption of perfect agitation is taken equal to that of the only outlet in a bundle, the current 3. In addition, the other differential as a parameter is no longer symbolized as a differential but as a change in the time of the variable. With all this, and that the outgoing flow through the membrane, $\dot{n}_5$ is formed only by H_2, it is got to:

$$\frac{dx_{H_2,3}}{dt} = \frac{1}{N_I}\left[x_{H_2,1}\,\dot{n}_1 - x_{H_2,3}\,\dot{n}_3 - \dot{n}_5 + r_1 - x_{H_2,3}\,\dot{N}_I\right], \tag{5.10}$$

which is the final expression for this Material Balance by component, in which the symbology for the parameter $\dot{N}_I$ is highlighted, which is remembered is no more than the change of the total moles in the PS I.

Oxygen Balance Analogously to hydrogen, the oxygen balance is presented next:

$$\frac{dN_{\mathrm{O}_2,I}}{dt} = x_{\mathrm{O}_2,1}\,\dot{n}_1 + x_{\mathrm{O}_2,6}\,\dot{n}_6 - x_{\mathrm{O}_2,21}\,\dot{n}_{21} - x_{\mathrm{O}_2,3}\,\dot{n}_3 - x_{\mathrm{O}_2,5}\,\dot{n}_5 + r_1\,\sigma_{\mathrm{O}_2,1}, \tag{5.11}$$

wherein the oxygen concentration in streams 5 and 21 is zero. Furthermore, remembering that oxygen does not participate in the electrochemical reaction 1 in this half cell, so $\sigma_{\mathrm{H}_2,1} = 0$, the outgoing and incoming flows that pass through the membrane, $\dot{n}_5$ and $\dot{n}_6$ are formed entirely by H_2 and O_2, respectively, and using the definition of $N_{\mathrm{O}_2,I} = x_{\mathrm{O}_2,I}\,N_I$ it is got to:

$$\frac{dx_{\mathrm{O}_2,3}}{dt} = \frac{1}{N_I}\left[x_{\mathrm{O}_2,1}\,\dot{n}_1 + \dot{n}_6 - x_{\mathrm{O}_2,3}\,\dot{n}_3 - x_{\mathrm{O}_2,3}\,\dot{N}_I\right], \tag{5.12}$$

final expression for this balance.

OH^- ion Balance It is remembered that this ion will be taken as a species with the molecular mass of the two atoms that form it, without considering the weight of the excess electron that characterizes it. The balance is

$$\frac{dN_{\mathrm{OH}^-,I}}{dt} = x_{\mathrm{OH}^-,1}\,\dot{n}_1 + x_{\mathrm{OH}^-,6}\,\dot{n}_6 - x_{\mathrm{OH}^-,21}\,\dot{n}_{21} - x_{\mathrm{OH}^-,3}\,\dot{n}_3 - x_{\mathrm{OH}^-,5}\,\dot{n}_5 + r_1\,\sigma_{\mathrm{OH}^-,1}. \tag{5.13}$$

Applying similar considerations to the previous balances, which in this case are: *i*) only the stream 21 has the ion OH^-, *ii*) the mole fraction of the ion in the stream 21 is 1 because that stream is only OH^-, and *iii*) the stoichiometric coefficient in the electrochemical reaction 1 is $\sigma_{\mathrm{OH}^-,1} = 2$. With this, the following expression is obtained:

$$\frac{dx_{OH^-,3}}{dt} = \frac{1}{N_I}\left[-\dot{n}_{21} + 2\,r_1\right], \tag{5.14}$$

in which using the consideration that all the production of ions OH^- is equal to the flow through the membrane, it becomes that the concentration of these ions does not change in the half cell, therefore:

$$\dot{n}_{21} = 2\,r_1, \tag{5.15}$$

which turns out to be the final expression for this balance. Note that in spite of being an algebraic equation, its origin is a balance, so the variable that produces ($\dot{n}_{21}$) is a state variable for the model.

Electron Balance Similar to the ion OH^- balance, the electron balance ends up being:

$$\dot{n}_{22} = 2\, r_1, \tag{5.16}$$

and again, it is a state variable of the model.

Water Balance Water is the last component that is considered, since the potassium ion, K^+ is not going to be represented in the model because it does not participate in the reactions. Therefore, the water fraction can be found directly with the constitutive equation:

$$x_{H_2O,3} = 1.0 - \sum x_{i,3}, \tag{5.17}$$

with i indicating all the other compounds different from water that go in stream 3. Again, $x_{H_2O,3}$ is a state variable of the model.

PS III: Cathode gassed solution (H_2) in Chamber

This process system has the same structure of equations as the PS IV due to process symmetry, as already said. Therefore, later on, for the PS IV only the nomenclature will be changed and the parameters of the other separation chamber will be determined. Next are the balances for the PS III.

Total Material Balance For the gas separation chamber, the total Material Balance is:

$$\frac{dN_{III}}{dt} = \dot{n}_3 + \dot{n}_7 - \dot{n}_9 - \dot{n}_{11}, \tag{5.18}$$

in which the flow in the stream 7 is defined entering but it could be going out, which would change its sign. This will be evident when the constitutive equation calculating $\dot{n}_7$ is determined. In the case of PS IV, the stream 8 is defined going out so both $\dot{n}_7$ and $\dot{n}_8$ will have the same sign in normal operation as will be seen in the analysis of PS XIII.

Total Volume Balance Since the levels of liquid solution in each SC are variables of interest to the modelling and control, it is useful to make a total volume balance in PSs III and IV. In that sense, the change in the volume, product of income and outcome of substance can be evaluated as

$$\frac{dV_{III}}{dt} = \dot{V}_3 + \dot{V}_7 - \dot{V}_9 - \dot{V}_{11}, \tag{5.19}$$

where $\dot{V}_i$ is the volumetric flow rate at the input or output i which is proposed in § 5.1.7. Recognizing that $V_{III} = A_{CS}\, L_{Lg,III}$, the equation for the calculation of the variable is defined as

$$\frac{dL_{Lg,III}}{dt} = \frac{1}{A_{CS}}\Big(\dot{V}_3 + \dot{V}_7 - \dot{V}_9 - \dot{V}_{11}\Big). \tag{5.20}$$

However, this model, in addition to not considering the rise time of the bubbles, dismiss the effect of the violent depressurizations that occur due to the rapid opening of valves. At that time, as the pressure varies dramatically, the solubility of the aqueous solution also changes, releasing a considerable amount of gas in the form of bubbles, which is called sudden vaporization. Then, the concept of volume change due to the gas that passes from solution to bubbles is incorporated and will be explained in § 5.1.7:

$$\frac{dL_{Lg,III}}{dt} = \frac{1}{A_{SC}}\Big(\dot{V}_3 - \dot{V}_7 - \dot{V}_9 - \dot{V}_{11} + \dot{V}_{bubbles}\Big). \tag{5.21}$$

Hydrogen Balance The balance of H_2 is as shown next:

$$\frac{dN_{\mathrm{H_2},III}}{dt} = x_{\mathrm{H_2},3}\,\dot{n}_3 + x_{\mathrm{H_2},7}\,\dot{n}_7 - \dot{n}_{\mathrm{H_2},9} - x_{\mathrm{H_2},11}\,\dot{n}_{11}, \tag{5.22}$$

where $N_{\mathrm{H_2},III}$ is the total mass of hydrogen in the gassed liquid that forms the PS III, $x_{\mathrm{H_2},i}$ is the molar fraction of the H_2 in the stream i, in units of $\frac{kg\,\mathrm{H_2}}{kgmix}$, with the mixture forming the current, and $\dot{n}_i$ is the molar flow of the current i in units of $\frac{kmol\,mix}{s}$. On the other hand, the flow corresponding to the output 9 (which was not separated as $x_{\mathrm{H_2},9}\,\dot{n}_9$ for convenience) will be briefly explained in § 5.1.7.

The total moles of hydrogen is replaced by its equivalence in terms of the total mass in the PS III. With this, and remembering that the main differential is the concentration in molar fraction and the secondary one is named as a speed parameter of change, the following balance is obtained:

$$\frac{dx_{\mathrm{H_2},III}}{dt} = \frac{1}{N_{III}}\Big[x_{\mathrm{H_2},3}\,\dot{n}_3 + x_{\mathrm{H_2},7}\,\dot{n}_7 - \dot{n}_{\mathrm{H_2},9} - x_{\mathrm{H_2},11}\,\dot{n}_{11} - x_{\mathrm{H_2},III}\dot{N}_{III}\Big]. \tag{5.23}$$

Oxygen Balance The balance is presented next:

$$\frac{dN_{\mathrm{O_2},III}}{dt} = x_{\mathrm{O_2},3}\,\dot{n}_3 + x_{\mathrm{O_2},7}\,\dot{n}_7 - x_{\mathrm{O_2},9}\,\dot{n}_9 - x_{\mathrm{O_2},11}\,\dot{n}_{11}. \tag{5.24}$$

Following a procedure similar to what was done before, it is obtained

$$\frac{dx_{\mathrm{O_2},III}}{dt} = \frac{1}{N_{III}}\Big[x_{\mathrm{O_2},3}\,\dot{n}_3 + x_{\mathrm{O_2},7}\,\dot{n}_7 - x_{\mathrm{O_2},9}\,\dot{n}_9 - x_{\mathrm{O_2},11}\,\dot{n}_{11} - x_{\mathrm{O_2},11}\dot{N}_{III}\Big] \tag{5.25}$$

which is the final balance per component for O_2 in PS III.

Ion OH^- and electron Balance As it is assumed that all ion and electron are consumed inside the half cell, it is not necessary to make a balance of these species in the PS III, because they do not arrive by any current.

Water Balance As for PS I, the water fraction can be found directly with the constitutive equation:

$$x_{\mathrm{H_2O},III} = 1.0 - \sum x_{i,III}, \tag{5.26}$$

with i indicating all the other compounds different from water that are in PS III.

PS V: Cathodic Solution recirculation pump

As initially commented, this process system has the same structure of equations as the PS VI. The balances for the PS V are presented here.

Total Material Balance For the RP, the total Material Balance is:

$$\frac{dN_V}{dt} = \dot{n}_{11} - \dot{n}_{13}. \tag{5.27}$$

Given that the mass within the PS can be considered to be constant, it is finally obtained that:

$$\dot{n}_{11} = \dot{n}_{13}. \tag{5.28}$$

This is a trivial equation that relates the outgoing flow of the SC with the flow that enters the HE. However, $\dot{n}_{11}$ is a state variable of the model basic structure.

Mechanical Energy Balance Following the analysis for this PS, the mechanical energy balances in the pump (from point 11 to 13) and in the recirculation circuit (from point 13 and 11) are

$$\eta \hat{W} = g(z_{13} - z_{11}) + \frac{P_{13} - P_{11}}{\rho_L} + \frac{{v_{13}}^2 - {v_{11}}^2}{2} + h_{f,11\to13}, \tag{5.29}$$

$$0 = g(z_{11} - z_{13}) + \frac{P_{11} - P_{13}}{\rho_L} + \frac{{v_{11}}^2 - {v_{13}}^2}{2} + h_{f,13\to11}, \tag{5.30}$$

being $\hat{W}$ the work per mass unit performed by the pump with its efficiency η, z_{11} and z_{13}, P_{11} and P_{13}, and v_{11} and v_{13} the heights, pressures and fluid velocities of entry and exit, respectively. Finally, the friction losses caused by the flow through pump between points 11 and 13 and through

the recirculation circuit are defined as $h_{f,11\to13}$ and $h_{f,13\to11}$, respectively. Considering negligible the modification of the density through the recirculation circuit and the internal pressure drops in the pump $h_{f,11\to13}$ and adding both equations, the mechanical energy balance for this process system is expressed as:

$$\eta_1 \hat{W}_1 = h_{f,13\to11}. \tag{5.31}$$

At this point, it is recalled that the friction losses between 13 and 11 are a function of the Reynolds number in the different sections and accessories, which as the same time is a function of the mass flow that is circulating. For continuity of flow, that mass flow can be labeled as $\dot{m}_{13}$, obtaining:

$$h_{f,13\to11} = f(\dot{m}_{13}) \Rightarrow f(\dot{m}_{13}) = \eta_1 \hat{W}_1. \tag{5.32}$$

In conclusion, a function is generated to calculate the mass flow $\dot{m}_{13}$.

Component Material Balances For this Process System there is no change in its composition so that directly the equations of the balance for the concentration variables at the output of the pump are as follows:

$$x_{\mathrm{H_2},13} = x_{\mathrm{H_2},11}, \tag{5.33}$$

$$x_{\mathrm{O_2},13} = x_{\mathrm{O_2},11}. \tag{5.34}$$

PS VII: Cathodic Heat Exchanger

This system is similar to PS VIII. Due to this, the PS VIII will change the nomenclature and take the parameters of the other section of the cooling system. Next are the balances for PS VII.

Total Material Balance For the Heat Exchanger, the total Material Balance is:

$$\frac{dN_{VII}}{dt} = \dot{n}_{13} - \dot{n}_1. \tag{5.35}$$

In this case also, in front of a null variation of the mass within the system, the following trivial equation is obtained:

$$\dot{n}_1 = \dot{n}_{13}. \tag{5.36}$$

Thermal Energy Balance In this model, as regards heat exchange, it is not considered given that it is more developed in other works and that in the present system the temperature remains constant from the control. Therefore no thermal energy balance is required.

Component Material Balances As it was in the case of the pump, these systems that do not present changes in the composition of the substance have trivial balances, as follows:

$$x_{\mathrm{H_2},1} = x_{\mathrm{H_2},13}, \tag{5.37}$$

$$x_{\mathrm{O_2},1} = x_{\mathrm{O_2},13}. \tag{5.38}$$

PS IX: H_2 gaseous in Chamber

This process system has, as previously stated, the same structure of equations as the PS X. Therefore, later for the PS X only nomenclature and proper parameters changes will be made. For simplicity using ideal gas model, the balances will be made on a molar basis. The balances for PS IX are as follows.

Total Material Balance For the gases contained in the gas separation chamber, the total Material Balance is:

$$\frac{dN_{IX}}{dt} = \dot{n}_9 - \dot{n}_{15}, \tag{5.39}$$

expression in which under the assumption of ideal gas behavior, the mol of the gas, using ideal gas equation, can be replaced by:

$$N_{IX} = \frac{P_{IX}\, V_{g,IX}}{R\, T}, \tag{5.40}$$

where $V_{g,IX}$ is the volume of the gas mixture, housed in the upper part of the chamber. In addition, P_{IX} and T are the pressure and temperature of the system in absolute units, and R is the universal constant of gases. If in addition the volume occupied by the gas is expressed as the product of the cross section A_T of the separation chamber (a vertical cylinder) and the height of the part of the chamber filled with gases $L_{g,IX}$, the following expression is obtained, in which the constants were separated:

$$N_{IX} = \frac{A_T}{R\, T} P_{IX}\, L_{g,IX} \tag{5.41}$$

expression in which the derivative of a product can be applied. With this, replacing in the original balance equation and considering that the main differential is the pressure differential,

while the height differential of the space occupied by the gas is a parameter ($\dot{L}_{g,IX} = \frac{dL_{g,IX}}{dt}$), the following expression is obtained:

$$\frac{dP_{IX}}{dt} = \frac{R\,T}{A_T\,L_{g,IX}}\left(\dot{n}_9 - \dot{n}_{15}\right) - \frac{P_{IX}}{L_{g,IX}}\,\dot{L}_{g,IX}, \tag{5.42}$$

which is the final expression of this total Material Balance, which allows to calculate the pressure in the separation chamber.

Hydrogen Balance The balance of H_2 is as shown next:

$$\frac{dN_{\mathrm{H_2},IX}}{dt} = x_{\mathrm{H_2},9}\,\dot{n}_9 - x_{\mathrm{H_2},15}\,\dot{n}_{15}, \tag{5.43}$$

where $N_{\mathrm{H_2},IX}$ is the total mol of hydrogen in the volume of gas that forms SdeP IX, $x_{\mathrm{H_2},i}$ is the molar fraction (in $\frac{kmol\,\mathrm{H_2}}{kmol\,mix}$), with the mixture forming the current, and $\dot{n}_i$ is the molar flow of the i current in units of $\frac{kmol\,mix}{s}$.

In the same way as was done previously, the total mol of hydrogen is replaced by its equivalence in terms of the total mol in the PS IX and the fraction of hydrogen in the output current in bulk (the current 15). This is because, on the assumption of perfect agitation, the concentration in the gas of the outlet is equal to the concentration of the gas contained in the PS. With this, and remembering that the main differential is the concentration in mol fraction and the secondary one is named as a speed parameter of change, it is got to:

$$\frac{dx_{\mathrm{H_2},15}}{dt} = \frac{1}{N_{IX}}\left[x_{\mathrm{H_2},9}\,\dot{n}_9 - x_{\mathrm{H_2},15}\,\dot{n}_{15} - x_{\mathrm{H_2},15}\dot{N}_{IX}\right] \tag{5.44}$$

which is the final balance per component for hydrogen in PS IX.

Oxygen Balance The balance is presented next:

$$\frac{dN_{\mathrm{O_2},IX}}{dt} = x_{\mathrm{O_2},9}\,\dot{n}_9 - x_{\mathrm{O_2},15}\,\dot{n}_{15} \tag{5.45}$$

Following a procedure similar to what was done for the balance of H_2, it is obtained

$$\frac{dx_{\mathrm{O_2},15}}{dt} = \frac{1}{N_{IX}}\left[x_{\mathrm{O_2},9}\,\dot{n}_9 - x_{\mathrm{O_2},15}\,\dot{n}_{15} - x_{\mathrm{O_2},15}\dot{N}_{IX}\right], \tag{5.46}$$

which is the final balance per component for oxygen in PS IX.

PS XI: Cathodic output valve

As initially commented, this process system has the same structure of equations as the PS XII.

Total Material Balance For the valve, the total Material Balance is:

$$\frac{dN_{XI}}{dt} = \dot{n}_{15} - \dot{n}_{17}. \tag{5.47}$$

Since it can be considered that moles inside the PS remains constant, it is finally obtained the trivial equation that relates the outgoing flow of the separation chamber with the output of the EHL:

$$\dot{n}_{15} = \dot{n}_{17}. \tag{5.48}$$

Mechanical Energy Balance (MEB) Following the analysis for this PS, the mechanical energy balance is

$$0 = g(z_{17} - z_{15}) + \frac{P_{17} - P_{15}}{\rho_g} + \frac{{v_{17}}^2 - {v_{15}}^2}{2} + h_{f,15\to17}, \tag{5.49}$$

similar to what was proposed for the MEB of PS V, z_{15} y z_{17}, P_{15} y P_{17}, y v_{15} y v_{17} are the relative heights, pressures, and inlet and outlet velocities, respectively, while $h_{f,15\to17}$ are the friction losses caused by the flow through the valve. If the heights z_{15} and z_{17} are considered equal, the load losses on the valve are ignored and some work is carried out recognizing that the volumetric flow rate $\dot{V} = A\,v$, it is got the calculation of the output volumetric flow as

$$\dot{V}_{17} = C_{v,1} u_1 \sqrt{\frac{P_{17} - P_{15}}{\rho_{g,XI}}}, \tag{5.50}$$

being the definition of the parameter C_v informed by the manufacturer of the valve and recognizing u_1 as the control variable.

PS XIII: Pressure equalization line

In Figure 5.1, the connection scheme between the two separation chambers and the pressure tank can be seen. The equalization line communicates to the two separation chambers, passing through the space of the tank that contains the cell pack. That tank and the lines of conduction that communicate it with the cameras, represent a significant volume of liquid, which can be taken as another process system. In this sense, there is mass transfer between both chambers and that volume, producing cross contamination to the chambers. This contamination occurs by two mechanisms: *i*) convective bulk transport, by the macroscopic movement of solution between the volume of the pressure equalization tank and each chamber, due to the difference in pressures, and *ii*) the mass transfer itself, by mesoscopic movement of oxygen and hydrogen,

trying to match the chemical potential of each substance in the chambers and the pressure equalization tank. This last mechanism is much slower than the first, but it becomes significant in the absence of fluid flow or when the bulk flow is established. In contrast, the first mechanism is typical of mixing or homogenization by flow in a tank to which a stream of substance with different solute concentration arrives. It is emphasized that the direction of the flows to and from the equalization tank to the chambers can change direction. This must be taken into account in the programming of the mathematical solution of the model. To represent the entire situation of concentration change in the equalization tank, the following balance equations are established for said tank.

Total Material Balance As it is a closed and pressurized system, it is assumed that its total volume is constant (remember that this PS does not include the liquid inside the chambers). Adding that the density varies slightly, it can be assumed that there is no appreciable change in the total mass of this PS. With all this, assuming a movement of liquid between 7 and 8 (greater pressure in the chamber of O_2), the balance in molar base is

$$\frac{dN_{XIII}}{dt} = 0 = \dot{n}_{20} + \dot{n}_8 - \dot{n}_7, \tag{5.51}$$

in which if it operates in a steady state, i.e. there is no water injection $\dot{n}_{20} = 0$, $\dot{n}_8 = \dot{n}_7$. That shows the equality in value of these flows, but it must be remembered that one is always positive (enters $PSXIII$) and the other is negative (leaves $PSXIII$).

All of the above leads us to believe that in steady state, the changes in concentration in the equalization tank are due only to mass transfer by molecular diffusion. It should be noted that when the steady state is abandoned, the other mechanism, i.e. homogenization by bulk flows, appears and is more drastic in its effect on concentration, than the effect of molecular diffusion. Therefore, the two mechanisms must be considered. That looks better by making the mass balance per component presented next:

Hydrogen Balance This balance is presented generically with the *in* subscript for the incoming flow and the *out* subscript for the outgoing flow. This is because the flow that enters brings the concentration of the chamber that produces it, while the flow out does so with the concentration in the $PSXIII$

$$\frac{dN_{\mathrm{H_2},out}}{dt} = x_{\mathrm{H_2},in}\,\dot{n}_{in} - x_{\mathrm{H_2},out}\,\dot{n}_{out} + A_{line}\,\Phi_{\mathrm{H_2}}, \tag{5.52}$$

in which A_{line} is the area of mass transfer, which is equal to the flow area of the pipe and $\Phi_{\mathrm{H_2}}$ is the molar transfer flux in $\frac{kmol_{\mathrm{H_2}}}{m^2\,s}$. The molar concentration of hydrogen in process system XIII, $x_{\mathrm{H_2},XIII}$, is defined as the variable to be calculated in this differential equation, as previously performed, to obtain

$$\frac{dx_{\mathrm{H_2},XIII}}{dt} = \frac{1}{N_{XIII}}\Big(x_{\mathrm{H_2},in}\,\dot{n}_{in} - x_{\mathrm{H_2},XIII}\,\dot{n}_{out} + A_{line}\,\Phi_{\mathrm{H_2}} - x_{\mathrm{H_2},XIII}\dot{N}_{XIII}\Big). \tag{5.53}$$

In a similar way to that was discussed in the total mass balance, when there is no net flow, the mass transfer by diffusion continues to act, as evidenced in (5.52). This transfer flux mass only depends on concentrations and not on bulk flows. In this sense, when there are bulk flows and these are in the opposite direction to the concentration gradient that will generate mass transfer by diffusion, the term of the flux $\Phi_{\mathrm{H_2}}$ remains active. Obviously, its effect on the concentration is going to be very small compared to the one that causes the bulk flow, but still produces mass transfer.

Oxygen Balance All of the above is repeated for the analysis of the change in oxygen concentration in this PS as follows:

$$\frac{dx_{\mathrm{O_2},XIII}}{dt} = \frac{1}{N_{XIII}}\Big(x_{\mathrm{O_2},in}\,\dot{n}_{in} - x_{\mathrm{O_2},XIII}\,\dot{n}_{out} + A_{line}\,\Phi_{\mathrm{O_2}} - x_{\mathrm{O_2},XIII}\dot{N}_{XIII}\Big). \tag{5.54}$$

Mechanical Energy Balance Following the analysis for this PS, the mechanical energy balance from points 8 to 7 is

$$0 = g(z_8 - z_7) + \frac{P_8 - P_7}{\rho_{Sln\mathrm{KOH}}} + \frac{{v_8}^2 - {v_7}^2}{2} + h_{f,8\to7}, \tag{5.55}$$

being z_8 and z_7, P_8 and P_7, and v_8 and v_7 the heights, pressures and velocity of entry and exit, respectively. Finally, the friction losses caused by the flow through the equalization pressure line between 8 and 7 are defined as $h_{f,8\to7}$. Considering negligible the change of velocity between inlet and outlet when the steady state is reached, the MEB for this PS is expressed as

$$h_{f,8\to7} = f(\dot{m}_8) = g(z_7 - z_8) + \frac{P_7 - P_8}{\rho_{Sln\mathrm{KOH}}}. \tag{5.56}$$

It is recalled that the friction losses between 7 and 8 are a function of the Reynolds number in the different line sections and accessories, which at the same time is a function of the mass flow that is circulating.

At this point, it is necessary to state that the instantaneous establishment of the flow is not fulfilled in any piping system. A sudden difference in separation chambers pressure is not immediately converted in flow change between points 7 and 8, as it could be expected. The friction of the fluid during its flow and the elasticity of liquid filling the line impose a delay to any sudden flow change. To represent these phenomena, an adjustment of previous balance is needed. The mass flow calculated in (5.56) will be labeled as the theoretical mass flow $\dot{m}_{theo}$ and a capacitance model will be adopted for the calculation of real molar flows $\dot{n}_7$ and $\dot{n}_8$, i.e.,

$$\frac{d\dot{n}_i}{dt} = \frac{1}{\tau}\left(\frac{\dot{m}_{theo}}{\mathfrak{M}_i} - \dot{n}_i\right), \tag{5.57}$$

where τ will be identified from data.

PSs XIV, XV and XVI

The injection pump (PS XIV), the membrane (PS XV) and the source of electrons (PS XVI) do not provide any variable to the system of equations but are identified to give completeness to the scheme.

5.1.5 Model basic structure

After reviewing all the balance equations obtained in previous step, the basic structure of the model is reported in Table 5.1. Those balance equations providing information to answer the questions asked to the model are maintained in the model basic structure.

5.1.6 Variables, parameters and constants

In Table 5.2 the nomenclature used for the variables, parameters and constants belonging to this model is presented, while Table 5.3 is used to count them.

5.1.7 Constitutive and assessment equations

For each of the structural parameters, those that appear in the basic model structure, its constitutive or assessment equation is proposed in Table 5.4. After that, the equations for the new parameters that arise from the previous equations, which are called *functional parameters*, are summarized in Table 5.5. Finally, model constants considered are presented in Table 5.6. Those constitutive and assesment equations that are considered relevant to clarify, are explained next:

Table 5.1: Balance equations forming the **model basic structure**.

#	Equation	Process System
1	$\frac{d\bar{\rho}_3}{dt} = \frac{1}{V_{mix,I}}\left[\dot{n}_1 + \dot{n}_6 - \dot{n}_3 - \dot{n}_5 + r_1 \sum_i \sigma_{i,1}\right]$	SP_I
2	$\frac{dx_{\mathrm{H}_2,3}}{dt} = \frac{1}{N_I}\left[x_{\mathrm{H}_2,1}\,\dot{n}_1 - x_{\mathrm{H}_2,3}\,\dot{n}_3 - \dot{n}_5 + r_1 - x_{\mathrm{H}_2,3}\,\dot{N}_I\right]$	SP_I
3	$\frac{dx_{\mathrm{O}_2,3}}{dt} = \frac{1}{N_I}\left[x_{\mathrm{O}_2,1}\,\dot{n}_1 + \dot{n}_6 - x_{\mathrm{O}_2,3}\,\dot{n}_3 - x_{\mathrm{O}_2,3}\,\dot{N}_I\right]$	SP_I
4	$\dot{n}_{21} = 2\,r_1$	SP_I
5	$\dot{n}_{22} = 2\,r_1$	SP_I
6	$\frac{dN_{III}}{dt} = \dot{n}_3 + \dot{n}_7 - \dot{n}_9 - \dot{n}_{11}$	SP_{III}
7	$\frac{dL_{Lg,III}}{dt} = \frac{1}{A_{SC}}\left(\dot{V}_3 - \dot{V}_7 - \dot{V}_9 - \dot{V}_{11} + \dot{V}_{bubbles}\right)$	SP_{III}
8	$\frac{dx_{\mathrm{H}_2,III}}{dt} = \frac{1}{N_{III}}\left[x_{\mathrm{H}_2,3}\,\dot{n}_3 + x_{\mathrm{H}_2,7}\,\dot{n}_7 - \dot{n}_{\mathrm{H}_2,9} - x_{\mathrm{H}_2,11}\,\dot{n}_{11} - x_{\mathrm{H}_2,III}\dot{N}_{III}\right]$	SP_{III}
9	$\frac{dx_{\mathrm{O}_2,III}}{dt} = \frac{1}{N_{III}}\left[x_{\mathrm{O}_2,3}\,\dot{n}_3 + x_{\mathrm{O}_2,7}\,\dot{n}_7 - \dot{n}_{\mathrm{O}_2,9} - x_{\mathrm{O}_2,11}\,\dot{n}_{11} - x_{\mathrm{O}_2,III}\dot{N}_{III}\right]$	SP_{III}
10	$\dot{n}_{11} = \dot{n}_{13}$	SP_V
11	$0 = \eta_1\,\hat{W}_1 - \frac{P_{13}-P_{11}}{\rho_{L,11}} \Rightarrow f(\dot{m}_{13}) = h_{f,13\to11}$	SP_V
12	$x_{\mathrm{H}_2,13} = x_{\mathrm{H}_2,11}$	SP_V
13	$x_{\mathrm{O}_2,13} = x_{\mathrm{O}_2,11}$	SP_V
14	$x_{\mathrm{H}_2,1} = x_{\mathrm{H}_2,13}$	SP_{VII}
15	$x_{\mathrm{O}_2,1} = x_{\mathrm{O}_2,13}$	SP_{VII}
16	$\frac{dP_{15}}{dt} = \frac{R\,T}{A_T\,L_{g,IX}}\left(\dot{n}_9 - \dot{n}_{15}\right) - \frac{P_{15}}{L_{g,IX}}\,\dot{L}_{g,IX}$	SP_{IX}
17	$\frac{dx_{\mathrm{H}_2,15}}{dt} = \frac{1}{N_{IX}}\left[x_{\mathrm{H}_2,9}\,\dot{n}_9 - x_{\mathrm{H}_2,15}\,\dot{n}_{15} - x_{\mathrm{H}_2,15}\dot{N}_{IX}\right]$	SP_{IX}
18	$\frac{dx_{\mathrm{O}_2,15}}{dt} = \frac{1}{N_{IX}}\left[x_{\mathrm{O}_2,9}\,\dot{n}_9 - x_{\mathrm{O}_2,15}\,\dot{n}_{15} - x_{\mathrm{O}_2,15}\dot{N}_{IX}\right]$	SP_{IX}
19	$\dot{n}_{15} = \dot{n}_{17}$	SP_{XI}
20	$\dot{V}_{17} = C_{v,1}\,u_1\sqrt{\frac{P_{17}-P_{15}}{\rho_{g,XI}}}$	SP_{XI}
21	$\frac{dN_{XIII}}{dt} = \dot{n}_{XIII,in} - \dot{n}_{XIII,out} + \dot{n}_{20}$	SP_{XIII}
22	$0 = \frac{P_8-P_7}{\rho_L} - h_{f,8\to7} \Rightarrow f(\dot{m}_8) = \frac{P_8-P_7}{\rho_L}$	SP_{XIII}
23	$\frac{dx_{\mathrm{H}_2,XIII}}{dt} = \frac{1}{N_{XIII}}\left[x_{\mathrm{H}_2,XIII,in}\,\dot{n}_{XIII,in} - x_{\mathrm{H}_2,XIII,out}\,\dot{n}_{XIII,out} + A_{line}\Phi_{\mathrm{H}_2} - x_{\mathrm{H}_2,XIII}\dot{N}_{XIII}\right]$	SP_{XIII}
24	$\frac{dx_{\mathrm{O}_2,XIII}}{dt} = \frac{1}{N_{XIII}}\left[x_{\mathrm{O}_2,XIII,in}\,\dot{n}_{XIII,in} - x_{\mathrm{O}_2,XIII,out}\,\dot{n}_{XIII,out} + A_{line}\Phi_{\mathrm{O}_2} - x_{\mathrm{O}_2,XIII}\dot{N}_{XIII}\right]$	SP_{XIII}

Volume change in SC $\dot{V}_{bubbles}$

Previously was incorporated the concept of volume change due to the gas that passes from solution to bubbles in (5.21). The volume occupied by the gas in the form of bubbles is calculated

Table 5.2: List of symbols

Symbol	Name	Symbol	Name
$\bar{\rho}_i$	Molar density of stream i	$V_{mix,I}$	Volume in PS I
$\dot{n}_i$	Molar flow in stream i	r_j	Reaction rate for reaction j
$\sigma_{X,j}$	Stoichiometric coefficient of X in reaction j	$x_{X,3}$	Concentration of species X in molar fraction
N_I	Total moles in PS I	M_{III}	Total mass in PS III
$\dot{m}_i$	Mass flow in stream i	$w_{X,III}$	Concentration of species X in mass fraction
η_1	Pump efficiency	$\hat{W}_1$	Specific work of the Pump
P_j	Pressure in point j	$\rho_{L,i}$	Mass density in stream i
R	Ideal gas constant	T	System temperature
$\mathfrak{M}_X$	Molar mass of species X	A_T	Chamber cross area
$L_{g,IX}$	Height of gas volume	$\rho_{g,XI}$	Mass density of gas in PS XI
$\dot{V}_i$	Volumetric flow in stream i	$h_{f,a\to b}$	Friction energy loss from a to b

Table 5.3: Variables, parameters and constants of the model.

	Instance	Total
Variables	$\bar{\rho}_3$, $x_{\mathrm{H}_2,3}$, $x_{\mathrm{O}_2,3}$, n_{21}, n_{22}, M_{III}, $w_{\mathrm{H}_2,III}$, $w_{\mathrm{O}_2,III}$, m_{11}, m_{13}, $w_{\mathrm{H}_2,13}$, $w_{\mathrm{O}_2,13}$, $w_{\mathrm{H}_2,1}$, $w_{\mathrm{O}_2,1}$, P_{15}, $w_{\mathrm{H}_2,15}$, w_{O_2}, m_{17}, V_{17}, m_7, m_8	21
Parameters	$\bar{\rho}_i$, $\dot{n}_i$, r_j, $x_{X,3}$, N_I, M_{III}, $\dot{m}_i$, $w_{X,III}$, η_1, $\hat{W}_1$, P_j, $\rho_{L,i}$, T, $L_{g,IX}$, $\rho_{g,XI}$ $\dot{V}_i$, $h_{f,a\to b}$	38
Structural Constants	$V_{mix,I}$, $\sigma_{X,j}$, R, $\mathfrak{M}_X$, A_T, n_{cell}, L_{SC}	16

with the ideal gas law:

$$V_{bubbles} = R\,T\,\frac{n_{bubbles}}{P_{IX}}. \tag{5.58}$$

Taking the derivative of the last equation, it is obtained

$$\dot{V}_{bubbles} = R\,T\left(\frac{\dot{n}_{bubbles}}{P_{IX}} + \frac{\dot{P}_{IX}}{n_{bubbles}}\right), \tag{5.59}$$

where $\dot{n}_{bubbles}$ is the migration of dissolved gas to bubbles and vice versa. The amount of gas present in the gaseous solution will be

$$n_{bubbles} = n_{\mathrm{H}_2,bubbles} + n_{\mathrm{O}_2,bubbles}. \tag{5.60}$$

Analyzing only hydrogen, it is obtained

$$n_{\mathrm{H}_2,bubbles} = \left(x_{\mathrm{H}_2,III} - x_{\mathrm{H}_2,sat}\right) N_{III}, \tag{5.61}$$

Table 5.4: Constitutive and assessment equations for structural parameters

#	Parameter	Equation
1	$\dot{n}_n$	$\dot{n}_n = \dot{V}_n\,\bar{\rho}_n$
3	$\dot{n}_5$	$\dot{n}_5 = \left(\Phi_{\mathrm{H_2-O_2},Fick} + \Phi_{\mathrm{H_2-O_2},Darcy}\right) A_{cell}\,n_{cell}$
4	$\dot{n}_6$	$\dot{n}_6 = \left(\Phi_{\mathrm{O_2-H_2},Fick} + \Phi_{\mathrm{O_2-H_2},Darcy}\right) A_{cell}\,n_{cell}$
5	r	$r = \eta_F \frac{n_{cell}}{\sigma_{\mathrm{e^-},2}\,F}\,I$
6	N_M	$N_M = V_{mix,M}\,\bar{\rho}_m$
8	$\dot{N}_M$	$\dot{N}_M = V_{mix,M}\,\dot{\bar{\rho}}_m$
10	$\dot{n}_q$	$\dot{n}_q = \left(n_{\mathrm{H_2},N,b} + n_{\mathrm{O_2},N,b}\right) \frac{FC_{flash}}{\tau_b}$
12	$\dot{n}_r$	$\dot{n}_r = \frac{\dot{m}_r}{\mathfrak{M}_r}$
14	$\dot{V}_3$	$\dot{V}_3 = \dot{V}_1 + \dot{V}_{\mathrm{H_2},r_1} - \dot{V}_{\mathrm{H_2O},r_1} - \dot{V}_5 + \dot{V}_6$
15	$\dot{V}_p$	$\dot{V}_p = \frac{\dot{m}_p}{\rho_{SlnKOH}}$
17	$\dot{V}_q$	$\dot{V}_q = \dot{n}_q \frac{R\,T}{P_M}$
19	$\dot{V}_r$	$\dot{V}_r = \dot{m}_r \frac{w_{\mathrm{H_2O},r}}{\rho_{SlnKOH}}$
21	$\dot{V}_{b,N}$	$\dot{V}_{b,N} = -\left(n_{\mathrm{H_2},N,b} + n_{\mathrm{O_2},N,b}\right) R\,T \frac{\dot{P}_Q}{{P_Q}^2}$
23	$x_{D,p}$	$x_{D,p} = min(x_{D,n}, x_{D,sat,M})$
27	$x_{D,q}$	$x_{D,q} = \frac{n_{D,N,b}}{n_{\mathrm{H_2},N,b} + n_{\mathrm{O_2},N,b}}$
31	$x_{D,r}$	$x_{D,r} = min(x_{D,n}, x_{D,sat,M})$
35	$\dot{V}_4$	$\dot{V}_4 = \dot{V}_2 + \dot{V}_{\mathrm{O_2},r} + \dot{V}_{\mathrm{H_2O},r_2} + \dot{V}_5 - \dot{V}_6$
36	$h_{f,a\to b}$	$h_{f,a\to b} = \sum_S \left(K_S \frac{{v_S}^2}{2}\right)$
39	$L_{g,Q}$	$L_{g,Q} = L_{SC} - L_{Lg,N}$
41	$\dot{L}_{g,Q}$	$\dot{L}_{g,Q} = -\frac{dL_{Lg,N}}{dt}$
43	N_Q	$N_Q = \frac{P_Q\,A_{SC}\,L_{g,Q}}{R\,T}$
45	$\dot{N}_Q$	$\dot{N}_Q = \dot{n}_q - \dot{n}_t$
47	$\dot{m}_{theo}$	$f(\dot{m}_{theo}) = h_{f,7\to 8}(\dot{m}_{theo}) + g(L_{g,III} - L_{g,IV}) + \frac{P_{15}-P_{16}}{\rho_{SlnKOH}}$

Indexes: $a \to b$: flow from point a to b, D: H_2 or O_2 , m: flows 1 or 2, n: flows 3 or 4, p: flows 7 or 8, q: flows 9 or 10, r: flows 11 or 12, t: flows 15 or 16, M: PSs I or II, N: PSs III or IV, Q: PSs IX or X,

whose derivative is

$$\dot{n}_{\mathrm{H_2},bubbles} = \left(x_{\mathrm{H_2},III} - x_{\mathrm{H_2},sat}\right)\dot{N}_{III} + \left(\frac{dx_{\mathrm{H_2},III}}{dt} - \frac{dx_{\mathrm{H_2},sat}}{dt}\right) N_{III}, \tag{5.62}$$

where the only unknown parameter left is $\frac{dx_{\mathrm{H_2},sat}}{dt}$. Expressing this concentration based on the saturation concentration that is calculated from Henry's law and differentiating, it is arrived at:

$$\frac{dx_{\mathrm{H_2},sat}}{dt} = x_{\mathrm{H_2},sat}\left(\frac{\dot{x}_{\mathrm{H_2},15}}{x_{\mathrm{H_2},15}} + \frac{\dot{P}_{IX}}{P_{IX}} - \frac{\dot{N}_{III}}{N_{III}} + \frac{\dot{L}_{Lg,III}}{L_{Lg,III}}\right), \tag{5.63}$$

whose derivatives are already in the basic structure of the model.

Table 5.5: Constitutive and assessment equations for functional parameters

#	Parameter	Equation
1	$\Phi_{D-E,Fick}$	$\Phi_{D-E,Fick} = D_D \frac{C_{D,n_D} - C_{D,n_E}}{z_{cell}}$
3	$C_{D,n}$	$C_{D,n} = min(x_{D,n}\,\bar{\rho}_n\,, C_{D,sat,M})$
7	$C_{D,sat,M}$	$C_{D,sat,M} = K_{He,D}\,x_{D,n}\,P_N$
11	$\Phi_{D-E,Darcy}$	$\Phi_{D-E,Darcy} = \epsilon_D^{Darcy} \frac{P_{N_D} - P_{N_E}}{z_{cell}}$
13	$n_{D,N,b}$	$n_{D,N,b} = max(x_{D,N} - x_{D,sat,M}, 0)\,N_{III}$
17	$x_{D,sat,M}$	$x_{D,sat,M} = \frac{C_{D,sat,M}}{\bar{\rho}_n}$
21	$\mathfrak{M}_i$	$\mathfrak{M}_i = x_{\mathrm{H_2O},i}\mathfrak{M}_{SlnKOH} + x_{\mathrm{H_2},i}\mathfrak{M}_{\mathrm{H_2}} + x_{\mathrm{O_2},i}\mathfrak{M}_{\mathrm{O_2}}$
25	$\mathfrak{M}_{SlnKOH}$	$\mathfrak{M}_{SlnKOH} = \left(\frac{1-C}{\mathfrak{M}_{\mathrm{H_2O}}} + \frac{C}{\mathfrak{M}_{\mathrm{KOH}}}\right)^{-1}$
26	$\dot{V}_m$	$\dot{V}_m = \dot{V}_r$
28	$\dot{V}_{D,r_z}$	$\dot{V}_{D,r_z} = \dot{n}_{D,r_z} \frac{R\,T}{P_{N_D}}$
30	$\dot{n}_{F,r_z}$	$\dot{n}_{F,r_z} = \sigma_{F,r_z}\,r$
34	$\dot{V}_{\mathrm{H_2O},r_z}$	$\dot{V}_{\mathrm{H_2O},r_z} = \frac{\dot{n}_{\mathrm{H_2O},r_z}\,\mathfrak{M}_{\mathrm{H_2O}}}{\rho_{\mathrm{H_2O}}}$
36	$\dot{V}_o$	$\dot{V}_o = \dot{n}_o \frac{R\,T}{P_N}$
38	K_S	Taken from [84]
39	f_{Darcy}	$f_{Darcy} = \left\{ -2\,log\left[\frac{\epsilon}{3.71ID} - \frac{5.02}{Re}\,log\left(\frac{\epsilon}{3.71ID} + \frac{14.5}{Re}\right)\right]\right\}^{-2}$ for turbulent flows [177]
40	Re	$Re = \frac{\rho_{SlnKOH}\,v_S\,ID}{\mu_{SlnKOH}}$
41	v_S	$v_S = \frac{1}{A_S}\frac{\dot{m}_S}{\rho_{SlnKOH}}$

Indexes: D and E: H_2 or O_2 , F: H_2 , O_2 or H_2O , n: flows 3 or 4, o: flows 5 or 6, r: flows 11 or 12, t: flows 15 o 16, z: reactions 1 (Cathodic side) or 2 (Anodic side), M: PSs I or II, N: PSs III or IV, Q: PSs IX or X.

Molar flow of H_2 gas inside SC $\dot{n}_{\mathrm{H_2},9}$

The molar flow $\dot{n}_{\mathrm{H_2},9}$ is analyzed as the rise of the bubbles immersed in the solution until they separate on the free surface of the liquid. It ill be modelled as the gradual separation of the bubbles present in the liquid with a time constant to be adjusted:

$$\dot{n}_{\mathrm{H_2},9} = \frac{n_{bubbles}}{\tau_{bubbles}}. \tag{5.64}$$

Molar transfer flux in SP XIII $\Phi_{\mathrm{H_2}}$

The definition of the local molar transfer coefficient will be used:

$$k_{x,\mathrm{H_2}} = \frac{\mathfrak{D}_{\mathrm{H_2,KOH}}}{z}, \tag{5.65}$$

being z the distance that the solute must travel. It should be remembered that the flux occurs between the midpoint (bulk) of the pressurization tank BTP and the midpoint (bulk) of each of

Table 5.6: Values of fixed parameters and constants. Piping dimensions are presented separately in Table 4.1

Symbol	Value
Parameters	
$V_{mix,N}$	1.71×10^{-3} m^3
$\sigma_{H_2O,1}$	-2
$\sigma_{e^-,1}$	-2
$\sigma_{H_2,1}$	1
$\sigma_{OH^-,1}$	2
$\sigma_{OH^-,2}$	-2
$\sigma_{O_2,2}$	0.5
$\sigma_{H_2O,2}$	1
$\sigma_{e^-,2}$	2
$\eta_{pump,i}$	10%
$\dot{W}_i$	26.7 W
T	300 K
η_F	90%
C	30%w/w
D_{H_2}	1.3236×10^{-7} m^2 s^{-1}
K_{He,H_2}	8.3355×10^{-6} mol m^{-3} Pa^{-1}
$\epsilon_{H_2}^{Darcy}$	$1.4 \times 10^{-16} \times P_{H_2}$ mol m^{-1} s^{-1} Pa^{-1} [171]
D_{O_2}	4.4120×10^{-8} m^2 s^{-1}
K_{He,O_2}	1.6816×10^{-5} mol m^{-3} Pa^{-1}
$\epsilon_{O_2}^{Darcy}$	$0.7 \times 10^{-16} \times P_{O_2}$ mol m^{-1} s^{-1} Pa^{-1} [171]
K_{cell}	5
ϵ	0.0024 m
Constants	
R	8.314 kJ (kmol K)$^{-1}$
$\mathfrak{M}_{H_2}$	2.016 kg kmol^{-1}
$\mathfrak{M}_{O_2}$	31.998 kg kmol^{-1}
ρ_{SlnKOH}	1281.3 kg m^3
g	9.81 m s^{-2}
F	96485.3365 C mol^{-1}
$\mathfrak{M}_{H_2O}$	18.015 kg kmol^{-1}
$\mathfrak{M}_{KOH}$	56.1056 kg kmol^{-1}
μ_{SlnKOH}	0.0012 kg (m s)$^{-1}$

the gas separation chambers. Those points are indicated as SCH and SCO for the separation chambers of H_2 and O_2, respectively. The molar transfer flux Φ_{H_2} is calculated by the following constitutive equation, deduced directly from Fick law:

$$\Phi_{H_2} = k_{x,H_2,7}\left(C_{H_2,SCH} - C_{H_2,BTP}\right) - k_{x,H_2,8}\left(C_{H_2,BTP} - C_{H_2,SCO}\right), \tag{5.66}$$

which can be rewritten considering that the molarity C can be expressed as the product of the molar concentration x and the molar density $\bar{\rho}$, which are variables already analysed. Then it is obtained

$$\Phi_{H_2} = \left[k_{x,H_2,7}\left(x_{H_2,7} - x_{H_2,XIII}\right) - k_{x,H_2,8}\left(x_{H_2,XIII} - x_{H_2,8}\right)\right]\bar{\rho}_{SlnKOH}, \tag{5.67}$$

which will be the constitutive equation to determine the mass transfer by molecular diffusion of H_2 throughout the equalization system. The molar transfer flux of the O_2 will be similar taking into account that it diffuses from SCO to SCH:

$$\Phi_{O_2} = \left[k_{x,O_2,7}\left(x_{O_2,7} - x_{O_2,XIII}\right) - k_{x,O_2,8}\left(x_{O_2,XIII} - x_{O_2,8}\right)\right]\bar{\rho}_{SlnKOH}. \tag{5.68}$$

Molar injection flow $\dot{n}_{20}$

At times when water is injected, $\dot{n}_{20}$ is not null and at that moment it is no longer valid that $\dot{n}_7 = \dot{n}_8$. What needs to be defined is what proportion of the injection flow circulates to each SC. For simplicity, looking the place where the injection line is connected to the recirculation line, it is defined that the entire injection flow goes to the SCO.

5.1.8 Parameter identification

With the proposed structure, the identification of the free parameters was carried out, whose values appear in Table 5.6. These parameters combine values obtained from the literature with identification by using the well-known least-squares method. The output errors, which measure the difference between model and experiments, are evaluated in order to compute such parameters.

5.1.9 Degrees of freedom analysis

A solvable model is obtained when its degrees of freedom (the difference between the number of unknown variables and parameters, and equations) is null. The model presents 42 variables, 50 structural parameters and 49 functional parameters. There are 141 equations in total that equal the number of unknown variables and parameters. Therefore, the model is solvable.

5.2 Model solution and result analysis

The model is solved using Matlab®. Using the code obtained in this work, which is simple due to the lumped parameter characteristics of PBSM, several operative conditions of the electrolyzer have been simulated. These conditions allow to evaluate the behavior of this PBSM regarding operation data taken from the actual assembly. In the following subsections, three different simulations are presented. First, two step-disturbances showing the response in the cell give

qualitative information that can be compared with the real system. Second, it is presented the bubbles behavior when valves are opened and current changes. And third, processes of pressurization and operation are compared between simulations and real data.

5.2.1 Analysis of cell behavior

Two step disturbances have been applied at 600 s and 1200 s of the simulation. The order of such disturbances is: first an electric current step from 20 A to 24 A, and next an increase of 50% in membrane diffusivity. While the increment in the electric current could be caused by a change in the power source, the modification in the membrane diffusivity shows the consequence of its degradation but, in that case, it would be progressive. Figure 5.2a presents the modeled dynamic behavior of molar flow in the electrolytic cell. Four observable facts can be enumerated in the graph:

i) there is a step in the production of hydrogen corresponding to the increase in the electric current,

ii) the concentration of H_2 at the entrance of the cell corresponds to the increase in the solubility of the gas compared to the growth of the pressure in the system,

iii) the molar flow of contamination towards the anodic half cell slowly grows due also to the greater quantity of dissolved gas, and

iv) H_2 at the exit of the half cell is, except during transients, the difference between the other three flows.

In Figure 5.2b, the changes of pressure in the H_2 separation chamber are illustrated with the gas exit valve closed. The pressure increases as gas accumulates in the upper part of the chamber. It can be seen that, when there is an increase in the electric current, the rate of change of the pressure slightly increases ($t = 600$ s). This fact is given by the increment in the H_2 production. On the contrary, in response to a greater diffusivity ($t = 1200$ s), the slope of the curve decreases slightly. This fact occurs since more gas flows from the cathode chamber to the anodic chamber and, therefore, it does not go to the corresponding chamber. On the other hand, the level of solution increases with the growing presence of bubbles from the gases that were produced. Since the bubbles begin to detach from the free surface, the volume stops increasing and, on the contrary, begins to decrease due to the slow consumption of water in the electrochemical process.

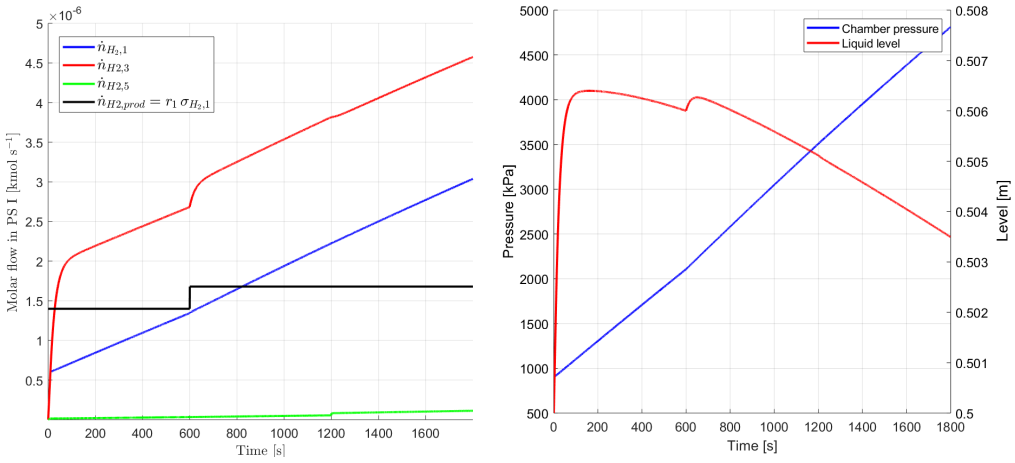

(a) (b)

Figure 5.2: (a) Modeled dynamic response of molar flows in the electrolytic cell. (b) Pressure and gassed liquid level modeled response in the gas separation chamber. Molar flow subindex correspond to numbers in Figure 5.1.

5.2.2 Simulation of bubbles evolution

The following simulation has been developed to analyze the bubbles behavior in the separation chamber as was described in § 5.1.4. Figure 5.3 illustrates the response of the model including the valve opening. When the valve is opened, on the left of the figure it can be seen that the level rises due to the sudden change in pressure. Then, it quickly decreases due to the discharge of bubbles which is observed on the right. Moreover, in Figure 5.4 there is a change of the electric current. On the left, it can be seen that, due to the increase of the electric current input, the slope of the saturation concentration rises due to the faster growth of the pressure. In turn, since there is more gas production, there are more bubbles in the system, which can be observed in the comparative zooms on the left and right between both lines. On the right, a peak in the bubbles molar flow can be seen due to the transient that is experienced until the flows in and out the separation chamber stabilize.

5.2.3 Pressurization and operation tests

Two typical tests of electrolyzer operation have been considered: *i)* pressurization from 1000 to 2000 kPa and *ii)* normal operation at 1000 kPa. In the first case, represented in Figure 5.5, the valves are closed while the approximately linear growth of the pressure is observed. Meanwhile, the hydrogen level decreases and the oxygen level increases as the equalization line compensates

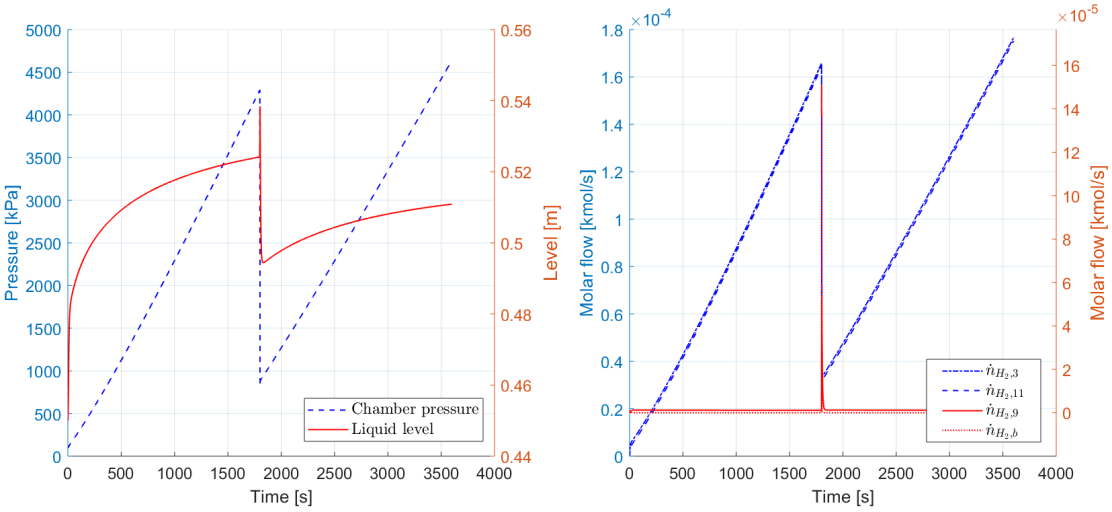

Figure 5.3: Model response in the H_2 separation chamber to a valve opening.

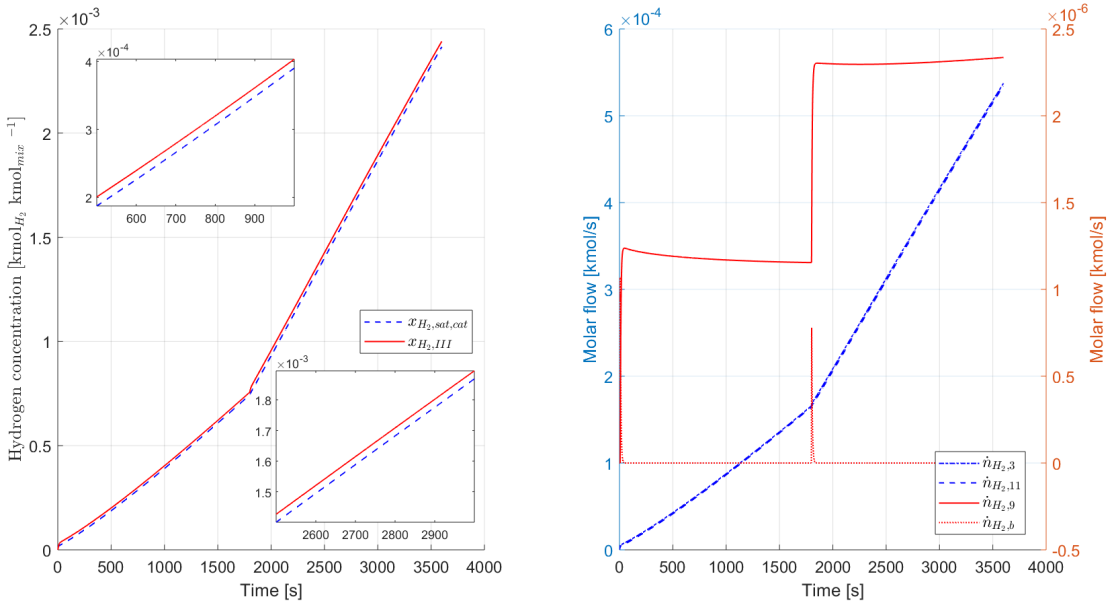

Figure 5.4: Model response in the H_2 separation chamber to a electric current input change. Left side shows the pressure and level in the separation chamber. In the right side can be seen the molar flows inside the separation chamber, due to the scales difference, the biggest flows 3 and 11 can be read in the left axis while flows 9 and bubbles are in the right axis.

the higher production of H_2 over O_2. In this way it was possible to identify the curve of the level sensors and the Faraday efficiency.

On the other hand, the period of operation shown in Figure 5.6 has been characterized by

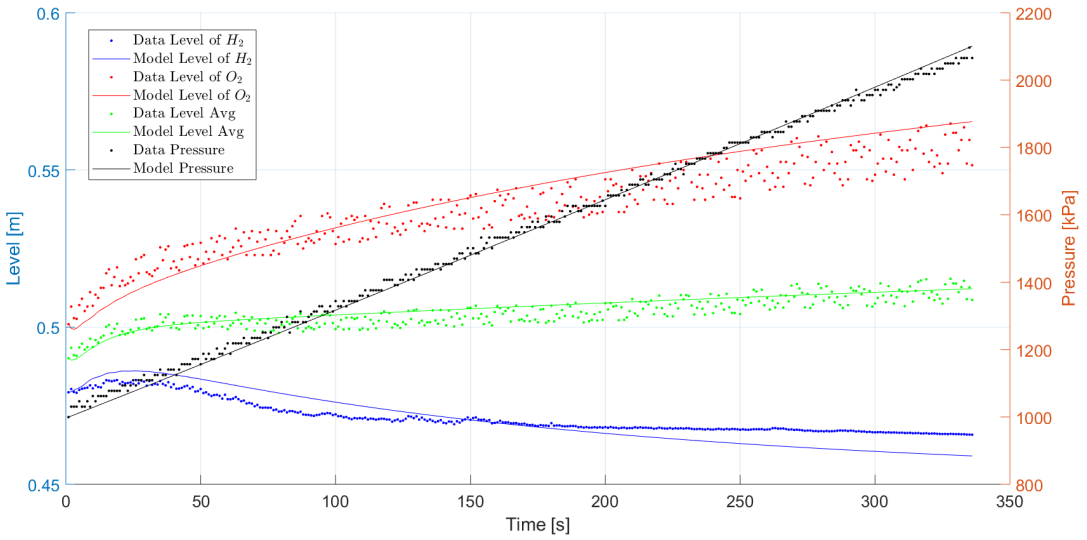

Figure 5.5: Comparison of pressurization between the real system (dotted line) and the model (solid line). In this case, the electrolyzer is operating with output valves closed.

having openings and closures of the outlet valves that are controlled from the error in the desired working pressure and the level difference between both chambers. This original control has clear flaws as can be seen in the large depressurization that occurred from $t = 75\,\text{s}$. When opening a valve, the pressure of the assembly decreases while the level in the corresponding chamber increases due to the depressurization of that side and the compensation through the equalization line. In this case, the errors obtained are greater than the case of pressurization due to inaccuracies in the acquisition of valve positions and the lack of precision in level measurements, as observed from $t = 40\,\text{s}$ to $t = 80\,\text{s}$ in the modeled levels. These features show there is flebility for a better fitting of the model for facing rapid changes in the operating conditions. However, the model has an adequate representation of the electrolyzer behavior under these operative conditions. This can be concluded from the observation of the relative errors calculated as follows:

$$re_z = \frac{|z_{data} - z_{model}|}{z_{data}}, \tag{5.69}$$

where z is any of the analyzed variables (SCs levels and system pressure). These relative errors are, on average, less than 2% for each variable.

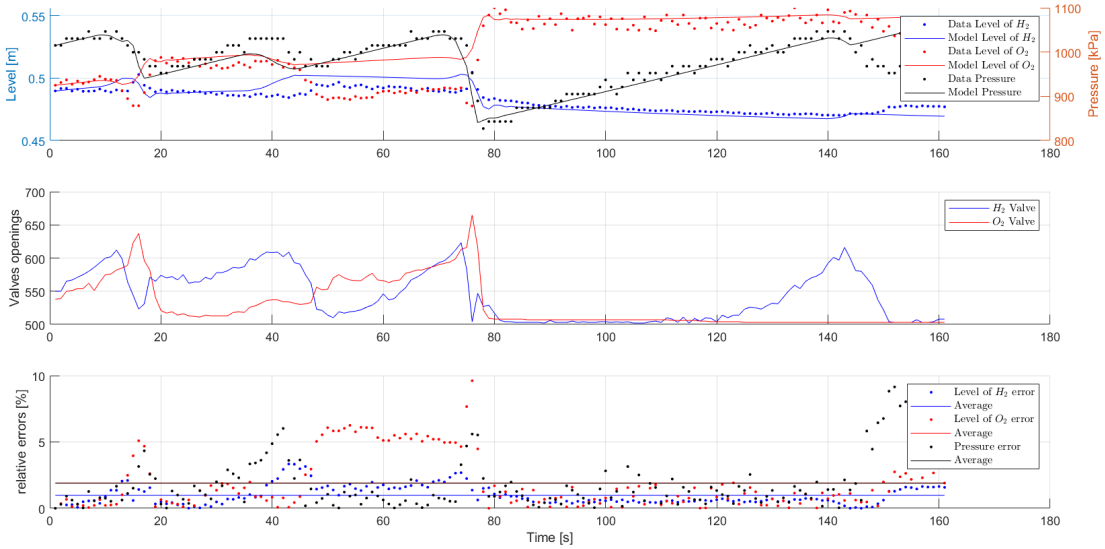

Figure 5.6: Upper figure: comparison of normal operation at 1000 kPa between the real system (dotted line) and the model response (solid line). In the second figure, it can be seen the opening valves, above $u_{min} = 600$ the valve is open. The third figure shows the relative errors between data collected and model outputs.

5.3 Summary

A phenomenological-based semiphysical model of hydrogen production in an alkaline self-pressurized electrolyzer has been proposed. Inherent characteristics of this kind of modelling methodology provides additional information concerning phenomena taking place in the process. This fact allows further analysis to be made, e.g., controllability, observability and identifiability. Such information can be used to have a better understanding of the electrolyzer design and operation, with the added capability of a possible model-based controller synthesis for this equipment. The proposed model is capable of representing the dynamical evolution of the level, pressure and all the concentrations in the system. Therefore, this model, referred to as a simulation-oriented model, will be the basis in the next section to make a control-oriented model necessary to design controllers for the operation of the alkaline electrolyzer.

Part III

Performance improvement in alkaline electrolyzers through control strategies

Chapter 6

Control-oriented model description

6.1 Introduction

In Chapter 5, a Simulation-Oriented Model (SOM) developed under the phenomenological-based semi-physical modeling method was described and presented. This highly-detailed model has 25 differential equations (i.e., 25 states) and 17 additional variables, 50 structural parameters and 49 functional parameters. The model has two inputs, two disturbances and six outputs that are presented in Table 6.1.

Table 6.1: List of inputs, disturbances and outputs

Symbol	Description
Inputs	
u_{H_2}	H_2 outlet valve opening
u_{O_2}	O_2 outlet valve opening
Disturbances	
I	Electrical input current
P_{tank}	External pressure in the storage tank
Outputs	
$L_{Lg,III}$	Liquid level solution in H_2 SC
$L_{Lg,IV}$	Liquid level solution in O_2 SC
P_{IX}	Pressure in H_2 SC
P_X	Pressure in O_2 SC
$x_{H_2,15}$	H_2 purity in the H_2 outlet
$x_{O_2,16}$	O_2 purity in the O_2 outlet

Such a model is suitable for simulation purposes but not for control design. Therefore, in this chapter, a Control-Oriented Model (COM) will be developed considering the objective of the control implementation, which is the action on the valve openings to reduce the cross-

contamination in the gas streams. First, and as an intermediate step, the following section presents a reduction of the model based on physical meanings. After that, a linearization around several operating points is performed and shown in § 6.3. Moreover, a second reduction by numerical meanings is carried out. These steps are graphically explained in Figure 6.1.

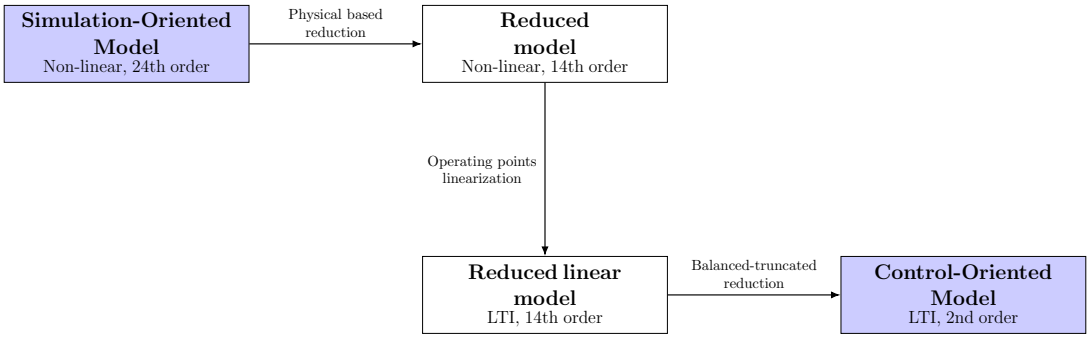

Figure 6.1: Graphical explanation of the steps taken to go from a Simulation-Oriented Model to a Control-Oriented Model.

6.2 Model reduction on physical basis

As stated above, the SOM is not suitable for control design. Therefore, to this end, those variables that produce smaller effects on the controlled variables might be neglected under some assumptions and guaranteed conditions that are explained next.

Although the ultimate goal is to maximize the purity of the gases, this is a consequence of the pressure and concentration on both sides of the membrane, as was indicated in § 3.1.4. Hence, the concentrations of impurities are not taken into account for the controller, whose objective, in effect, will be to maintain the liquid levels and system pressure equalized. Moreover, under the hypothesis of reaching gas purities greater than 99%, gas contamination is neglected, which means x_{O_2} and x_{H_2} are considered null on the cathodic and anodic sides of the electrolyzer, respectively. Furthermore, in gas region (PS_{IX} and PS_X), pure gases are considered (i.e., $x_{\mathrm{H}_2,15} = x_{\mathrm{O}_2,16} = 1$). Due to the latter hypothesis, saturation of pure gas at each cell can be assumed in order to calculate diffusion across the membrane, i.e.,

$$C_{\mathrm{H}_2,sat,I} = K_{He,\mathrm{H}_2} P_{IX}, \tag{6.1}$$

$$C_{\mathrm{O}_2,sat,II} = K_{He,\mathrm{O}_2} P_X, \tag{6.2}$$

Table 6.2: List of states included in the nonlinear reduced model

Symbol	Description
$\bar{\rho}_3$	Molar density in H_2 half-cell
$x_{H_2,3}$	Concentration of H_2 in H_2 half-cell
$\bar{\rho}_4$	Molar density in O_2 half-cell
$x_{O_2,4}$	Concentration of O_2 in O_2 half-cell
N_{III}	Total moles in H_2 SC
$L_{Lg,III}$	Height of liquid solution level in H_2 SC
$x_{H_2,III}$	Concentration of H_2 in H_2 SC
N_{IV}	Total moles in O_2 SC
$L_{Lg,IV}$	Height of liquid solution level in O_2 SC
$x_{O_2,IV}$	Concentration of O_2 in O_2 SC
P_{IX}	Pressure in H_2 SC
P_X	Pressure in O_2 SC
$\dot{n}_7$	Molar flow from the PT to H_2 SC
$\dot{n}_8$	Molar flow from O_2 SC to the PT

where K_{He,H_2} and K_{He,O_2} are the Henry's law constants for H_2 and O_2, respectively. Besides, according to the ideal gas law, the gas moles behave equally no matter the substance, hence the accountancy of the number of moles at each line is the only thing that really matters. Therefore, the contaminating moles of O_2 (or H_2) at the cathode (or anode) are treated as H_2 (or O_2). More clearly, the second equation presented in Table 5.1 is modified as

$$\frac{dx_{H_2,3}}{dt} = \frac{1}{N_I}\left[x_{H_2,1}\,\dot{n}_1 - x_{H_2,3}\,\dot{n}_3 - \dot{n}_5 + \mathbf{\dot{n}_6} + r_1 - x_{H_2,3}\,\dot{N}_I\right], \tag{6.3}$$

where $\dot{n}_6$ are the moles of O_2 that pass through the membrane to the cathode cell. The mole fraction of O_2 in the anode cell is similarly modified.

In addition, despite having two paths of diffusion, i.e., through the membrane and through the equalization line, the latter is smaller than the former (10^6 times). This is mainly due to a longer path through the equalization line (approximately 3 m) against just the thickness of the membrane (approximately 5×10^{-4} m). Then, the diffusion through the equalization line can be neglected along with the corresponding states.

Based on the previous assumptions, the model can be reduced to 14 states, which have a physical meaning and are listed in Table 6.2. The remaining states are considered constant while the parameters, which are represented by algebraic equations, are not modified. To summarize, a graphical description of the final states is presented in Figure 6.2.

Different scenarios with pulse-type signals in the disturbances i and P_{tank} and control inputs u_{H_2} and u_{O_2} were simulated to compare the responses of the original model and the reduced COM. Figures 6.3 to 6.5 show the results when the initial operating conditions correspond to $I = 30$ A/ and $P_{H_2} = 4000$ kPa (an operating point in the center of the considered operating

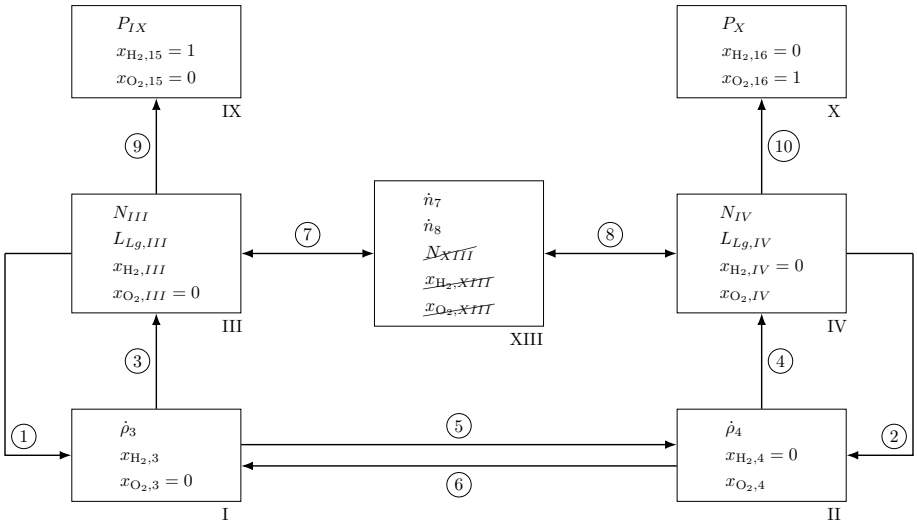

Figure 6.2: Flow diagram of the reduced system indicating the variables defined as constant and the neglected ones.

range) and a pulse-type signal in the current, the pressure in the tank and the opening of the O_2 valve are applied, respectively. The duration of that pulse was 10 s and the amplitude was 30 A. Moreover, Figures 6.6 and 6.7 show two examples of disturbances when the operating points are $I = 10$ A/$P_{H_2} = 1000$ kPa and $I = 50$ A/$P_{H_2} = 7000$ kPa, respectively. These values correspond to the limits of the selected range, which will be discussed in § 6.3. Finally, in Figure 6.8, a constant step in electrical current is imposed.

In the top-plot of Figures 6.3 to 6.8, the evolutions of the pressure P_{H_2} for the full original model (solid black line) and the same pressure for the reduced COM (dashed red line) can be observed. The second and third plots compare the evolutions of the levels L_{H_2} and L_{O_2}, respectively. The bottom plot shows the difference of levels ΔL for the original and the reduced models, respectively. The relative errors, which are defined as

$$re = 100\% \frac{|y_{\text{original}} - y_{\text{reduced}}|}{|y_{\text{original}}|}, \tag{6.4}$$

and the absolute error, in case of the level difference, can be seen in solid blue lines. In this last case, the nominal values are close to zero and the relative error is impractical. Notice that the maximum approximation error is 2×10^{-5} m in ΔL, which is quite small comparing with the maximum value of this signal in these figures. In all cases, it can be observed that the pressure and levels in both separation chambers did not present differences while the difference in level

has an increasing decoupling, although of small amount. Recalling that the control inputs will be the system pressure and the level difference in SCs, it can be concluded that this reduced model is capable of giving accurate information about these variables.

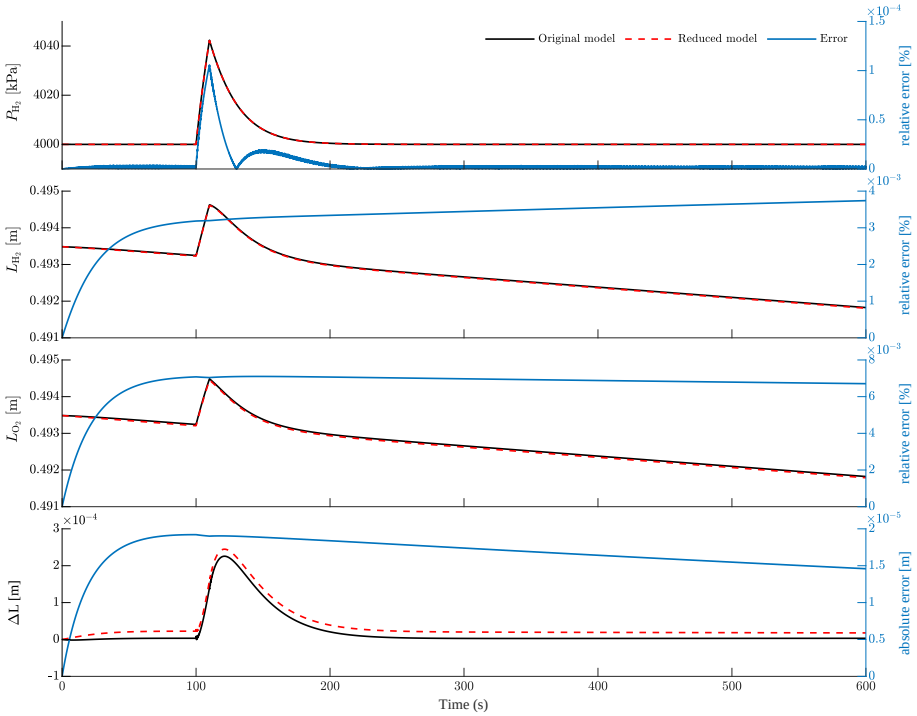

Figure 6.3: Comparison between the responses of the full nonlinear model and the reduced COM when a pulse of 10 s duration is applied in the electrical current when $P_{H_2} = 40$ bar and $I = 30$ A.

6.3 Model linearisation and second reduction

In the next chapter, two control strategies will be developed: a traditional PI control and a $\mathcal{H}_\infty$ optimal controller. In the second case, a linear model is needed in order to be able to apply the different control design methods. While this is well-known in the case of $\mathcal{H}_\infty$ controllers, in the case of classical PI control, linearisation will be also necessary in order to decouple both control actions.

Therefore, the operating conditions of the electrolyzer must be defined in order to linearised the reduced model. Assuming the control objective of tracking P_{ref} given in (7.6) and the regulation of ΔL around 0 are satisfied, the operating conditions can be parameterized by the

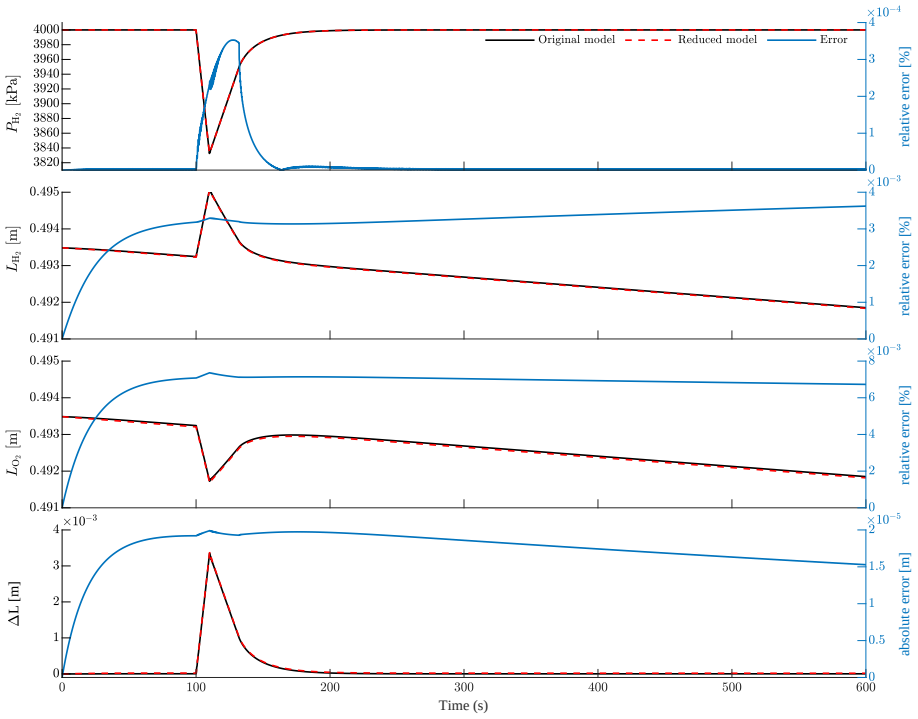

Figure 6.4: Comparison between the responses of the full nonlinear model and the reduced COM when a pulse of 10 s duration is applied in the pressure of the storage tank when $P_{H_2} = 40$ bar and $I = 30$ A.

steady-state values of the tank pressure $\bar{P}_{\text{tank}}$ and the current $\bar{I}$. Thus, the system operating region is defined as

$$\mathcal{O} = \left\{ (\bar{P}_{\text{tank}}, \bar{I}) \, : \, 0 \text{ kPa} \leq \bar{P}_{\text{tank}} \leq 7000 \text{ kPa} \right. \tag{6.5}$$

$$\left. \text{and } 10 \text{ A} \leq \bar{I} \leq 50 \text{ A} \right\}. \tag{6.6}$$

Although the electrolyzer was designed to operate up to 20000 kPa, in this first approximation a maximum operating pressure of 7000 kPa was selected in order to escalate the problem. On the other hand, the maximum electrical current is limited in two ways: due to the integrity of the electrolytic cell and the available power source.

Next, the reduced nonlinear model introduced in § 6.2 is numerically linearised at a representative operating point $(\bar{P}_{\text{tank}}, \bar{I}) \in \mathcal{O}$. To select this point, the linearisation is performed over a grid of operating points in $\mathcal{O}$. The magnitude of the frequency responses for these operating points is shown in Figure 6.9 in gray lines and the selected nominal model is represented by a thicker blue line. This nominal model will be used to design the considered linear controllers. It

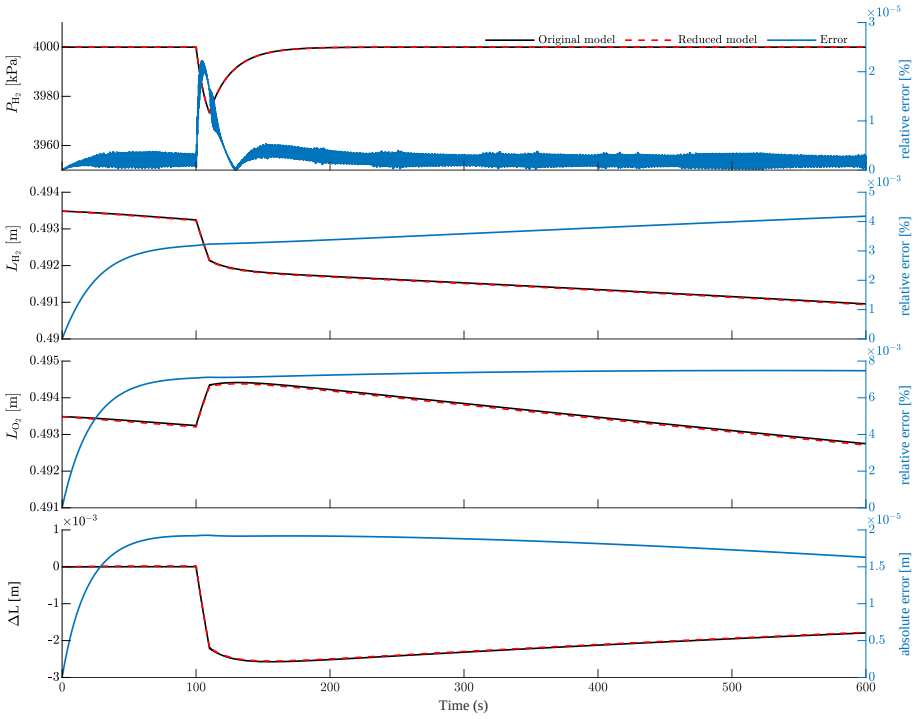

Figure 6.5: Comparison between the responses of the full nonlinear model and the reduced COM when a pulse of 10 s duration is applied in the opening of O_2 valve when $P_{H_2} = 40$ bar and $I = 30$ A.

can be observed that there is no drastic changes in the frequency responses at different operating points. This fact suggests that linear controllers can achieve a suitable performance.

The selected nominal dynamics are approximated by the model

$$y(s) = G(s)\begin{bmatrix}\hat{I}(s)\\ \hat{u}(s)\end{bmatrix} = \begin{bmatrix}G_d(s) & G_c(s)\end{bmatrix}\begin{bmatrix}\hat{I}(s)\\ \hat{u}(s)\end{bmatrix}, \tag{6.7}$$

where

$$\hat{u} = \begin{bmatrix}\hat{u}_{H_2}\\ \hat{u}_{O_2}\end{bmatrix} = \begin{bmatrix}u_{H_2} - \bar{u}_{H_2}\\ u_{O_2} - \bar{u}_{O_2}\end{bmatrix}, \qquad y = \begin{bmatrix}P_{H_2} - \bar{P}_{H_2}\\ \Delta L\end{bmatrix}. \tag{6.8}$$

The variable $\hat{u}$ is the vector of control inputs, and y is the vector of the controlled variables. The incremental current $\hat{I} = I - \bar{I}$ acts as a disturbance to be rejected. All of these variables are incremental values with respect to $\bar{I}$, $\bar{u}_{H_2}$, $\bar{u}_{O_2}$, and $\bar{P}_{H_2}$, where the last three variables are functions of the operating point $(\bar{P}_{tank}, \bar{I})$.

In the case of $\mathcal{H}_\infty$ strategy, the order of the controller will be the order of the nominal model plus the order of all the weighting functions. Therefore, to simplify the real-time implementation,

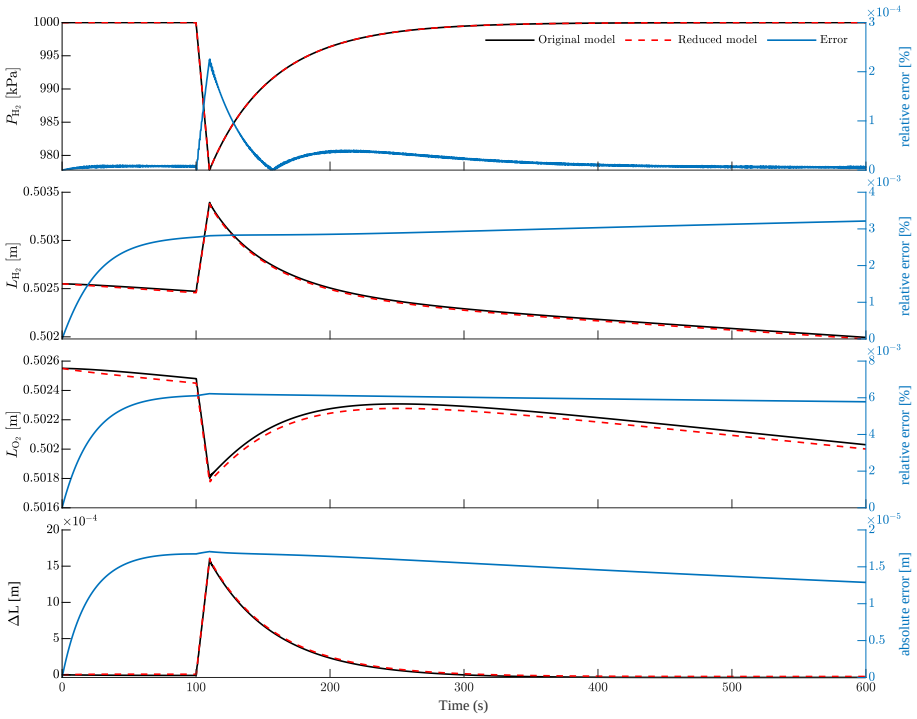

Figure 6.6: Comparison between the responses of the full nonlinear model and the reduced COM when a pulse of 10 s duration is applied in the pressure of the storage tank when $P_{H_2} = 10$ bar and $I = 10$ A.

the order of $G(s)$ can be numerically reduced. As can be seen in Figure 6.9, the nominal model $G_c(s)$ exhibits a frequency response similar to a first-order system for each channel. Therefore, using a standard balanced-truncated reduction method [68], the linear time-invariant (LTI) nominal model of 14-th order is reduced by to a 2-nd order LTI model [163, 223]. The full and reduced models are compared in Figure 6.10. As observed in this figure, the reduced model is dominated by two poles.

6.4 Summary

After constructing a complete SOM, in this chapter the design of a control-oriented model based on the previous one was presented. First, the model was reduced based on physical concepts and considering the control objectives. This step was validated by comparing both original and reduced models in several scenario simulations. Second, the model was linearised around several operating points. After that, a unique linearised model was selected due to the similar frequency

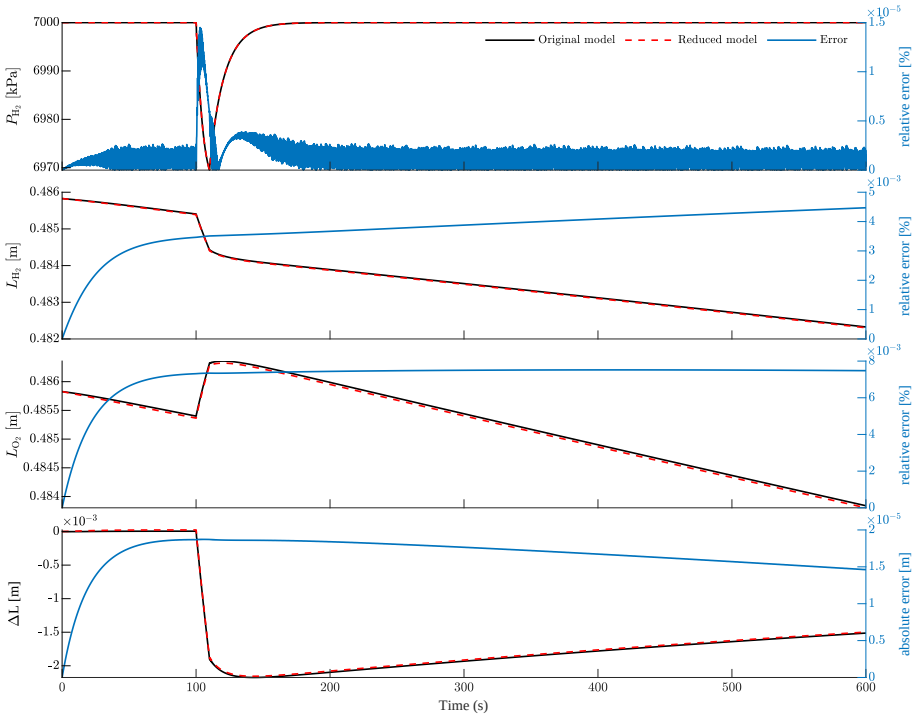

Figure 6.7: Comparison between the responses of the full nonlinear model and the reduced COM when a pulse of 10 s duration is applied in the opening of O_2 valve when $P_{H_2} = 70$ bar and $I = 50$ A.

responses at the different operating points. Finally, a second reduction by numerical means was carried out to get a 2-nd order LTI model. These successive operations were described graphically in Figure 6.1. This reduced 2-nd order LTI model, named $G_r(s)$, will be used to design two control strategies in the following chapter.

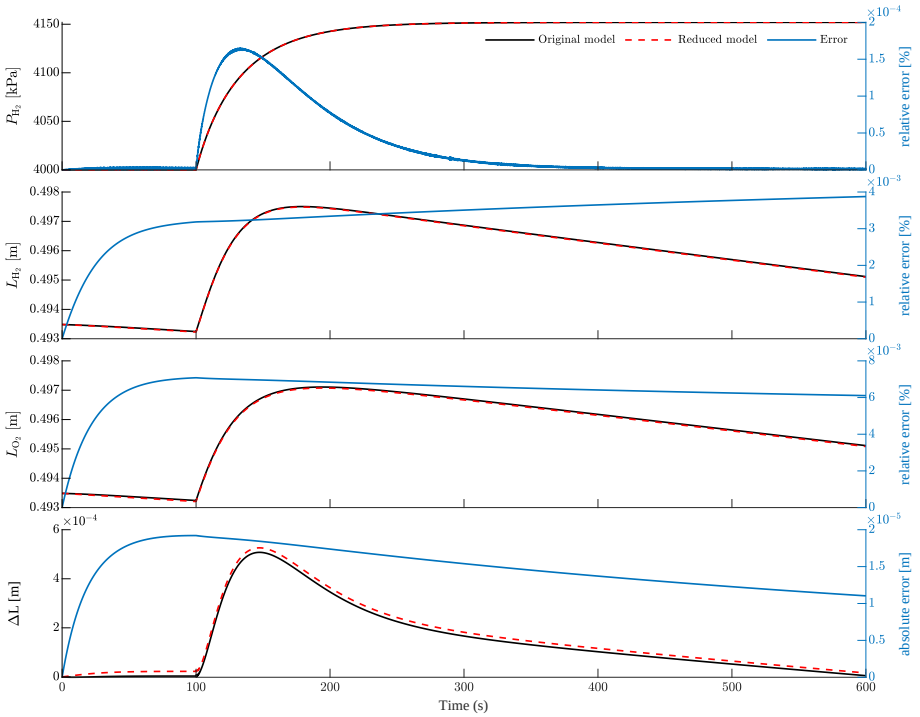

Figure 6.8: Comparison between the responses of the full nonlinear model and the reduced COM when a constant step is applied in the electrical current when $P_{\mathrm{H_2}} = 40$ bar and $I = 30$ A.

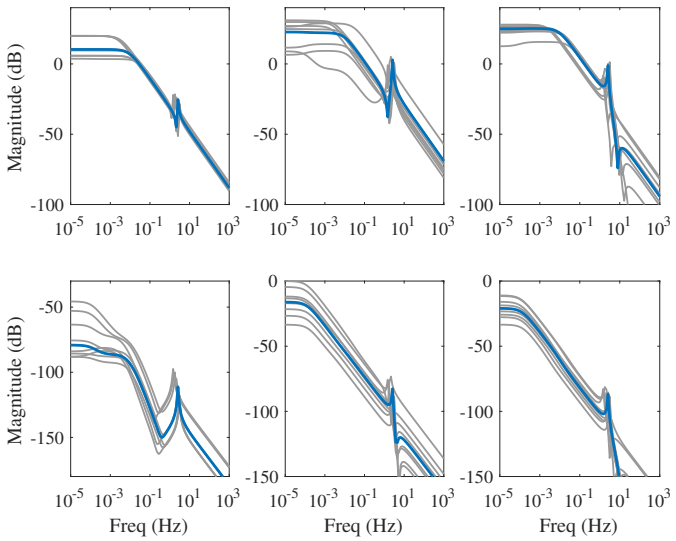

Figure 6.9: Frequency responses of the linearised model at several operating points (gray lines) and the nominal model $G(s)$ (blue lines).

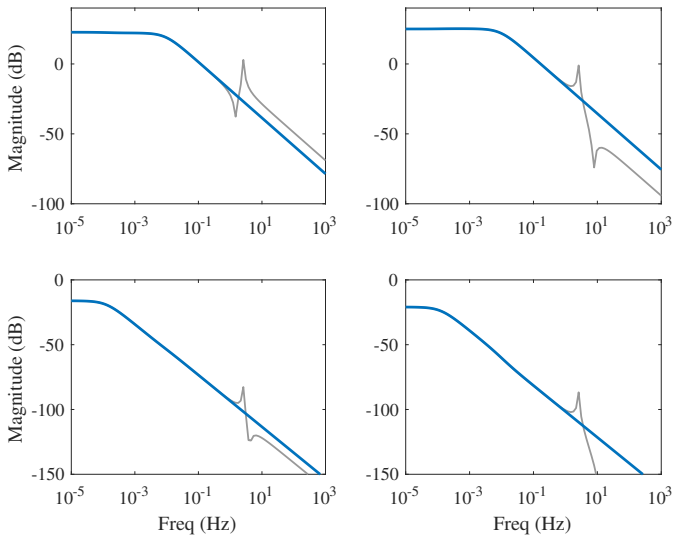

Figure 6.10: Frequency response of the nominal plant (gray) and the reduced plant (blue).

Chapter 7

Design and simulation of control strategies

7.1 Control scheme

In this chapter, two linear controllers are proposed for mitigating the cross-contamination of gases through the membrane in the alkaline electrolyzer presented in Chapter 4 [43, 44]. As was mentioned before, the former is a classical PI control used frequently in industry, while the latter is a model-based $\mathcal{H}_\infty$ optimal controller.

Before their presentation, it is necessary to describe the control scheme which was partially mentioned previously. An alkaline electrolyzer requires several control loops for an efficient and safe operation. The control of both the refrigeration system and the make-up pump ensures a safe operation of the electrolyzer while the H_2 production is controlled by the outlet valves.

The refrigeration system and the make-up pump are controlled independently by hysteresis cycles. These control actions are defined by the following sets of constraints:

$$\begin{aligned} L_{Lg,III} \leq L_{\min} \text{ and } L_{Lg,IV} \leq L_{\min} &\Rightarrow u_{\text{pump}} = 1, \\ L_{Lg,III} \geq L_{\max} \text{ or } L_{Lg,IV} \geq L_{\max} &\Rightarrow u_{\text{pump}} = 0, \end{aligned} \tag{7.1}$$

$$\begin{aligned} T_{H_2} + T_{O_2} \geq 2\ T_{\max} &\Rightarrow u_{RS} = 1, \\ T_{H_2} + T_{O_2} \leq 2\ T_{\min} &\Rightarrow u_{RS} = 0, \end{aligned} \tag{7.2}$$

where L_{O_2}, L_{H_2}, T_{O_2} and T_{H_2} are the liquid solution levels and temperatures in O_2 and H_2 SCs, respectively. These variables are measured by the transmitters LT1, LT2, TT1 and TT2, respectively (see Figure 4.4). The limits imposed are $L_{\min} = 0.45$ m, $L_{\max} = 0.5$ m, $T_{\min} =$

39.5 °C and $T_{\max} = 40.5$ °C. Finally, the control actions u_{pump} and u_{RS} manage the activation of the injection pump, the refrigeration system pump and the radiator, respectively.

As previously indicated, in alkaline electrolysis, a pressure difference between both half-cells generates the gas crossover. Therefore, the control objective is to keep the liquid solution levels equalized in both SCs (measured by LT1 and LT2 in Figure 4.4) while H_2 and O_2 are delivered at a certain pressure (measured by PT1 and PT2 in Figure 4.4). This objective is achieved acting over two motorized outlet valves (MVO and MVH in Figure 4.4). The operating ranges for pressure p and electric current I are 0-7000 kPa and 10-50 A, respectively. It is important to note that this electrolyzer, with an electrode area of $A_{cell} = 143$ cm^2, works in a current density j with a range of 70-350 mA/cm^2 under the direct relationship

$$j = \frac{I}{A_{cell}}. \tag{7.3}$$

With the aim of having a suitable resolution in these wide operating ranges and considering the H_2 production capacity of 0.5 Nm^3/h, needle-type outlet valves with a relatively small maximum flow coefficient, e.g., $C_v = 0.004$, must be used. In order to be able to control the system with only one valve per outlet line, the pressure in both storage tanks should be similar.

Another variable to be controlled is the difference between the liquid levels in both SCs, defined as

$$\Delta L = L_{Lg,III} - L_{Lg,IV}. \tag{7.4}$$

This variable must be kept around a set-point $\Delta L_{\text{ref}} = 0$. This condition will contribute to the natural action of the equalization line circuit by keeping the pressure equalized on both sides of the membrane. In other words, if the control dynamics are slow enough, the equalization line ensures that the pressure in both SCs is almost the same, and the same happens in the electrolytic cells. As stated by Schalenbach et al [172], the Zirfon$^{\text{TM}}$ membrane is highly permeable to pressure differences. These pressures P_{III} and P_{IV} depend on the pressure of each SC and the pressure exerted by the column of liquid. In order to understand the effect of the liquid level difference in each SC, an example is presented next. A difference in level $\Delta L = 2$ mm represents a pressure difference of 25 Pa. Considering only this difference, a contaminating flow of H_2 from cathode to anode $\dot{n}_5 = 1.71 \times 10^{-9}$ kmol s^{-1} occurs (see Figure 5.1). The purity of the gases generated will depend on the rate of O_2 production. Therefore, with a low current density $j = 70$ mA/cm^2, an impurity of 0.24 % will be obtained. Finally, controlling the difference

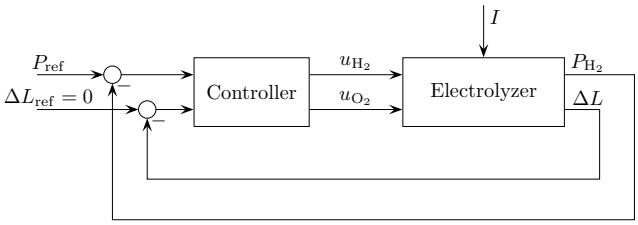

Figure 7.1: Proposed control scheme.

in level and pressure generates a high purity of the supplied gases. However, the absence of contamination is unavoidable due to the natural diffusion that occurs in the studied process.

The control scheme proposed to achieve the objectives is presented in Figure 7.1. The controller produces two valve opening values, u_{H_2} and u_{O_2}, taking values between 0 (minimum opening) and 10 (maximum opening). The control values are computed to ensure that

$$P_{XI} \to P_{\text{ref}}, \tag{7.5a}$$

$$\Delta L \to 0. \tag{7.5b}$$

In normal operation, this pressure is set externally in order to follow smoothly the pressure of the storage tanks P_{tank}. Accordingly, the reference for the pressure P_{ref} is defined as

$$P_{\text{ref}} = P_{\text{tank}} + P_{gap}, \text{ subject to } |dP_{\text{ref}}/dt| < \alpha, \tag{7.6}$$

being α a rate limit in kPa/s. This rate limit ensures that a sudden change in the storage pressure does not generate an excessive variation in the pressure at both sides of the membrane, with the consequent cross-contamination. Moreover, the pressure gap between P_{ref} and P_{tank}, $P_{\text{gap}} = 50$ kPa, is needed to compensate the action of the retention valves (RVO and RVH).

7.2 PI control

The system to be controlled, namely as $G_c(s)$, has two control inputs and two controlled outputs. It can be observed in Figure 6.9 that the control loops are coupled and a multivariable approach is required.

As mentioned before, the simplest control approach consists in decoupling the loops and then designing two independent controllers [14]. For this purpose, the reduced and linearised plant,

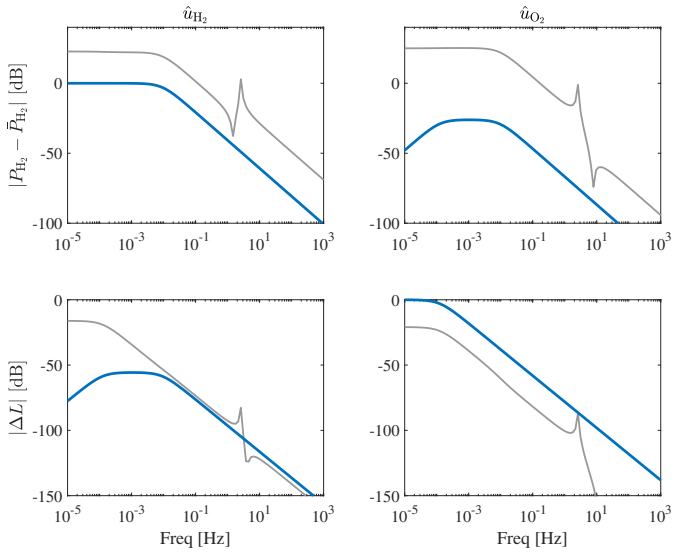

Figure 7.2: Frequency responses of the nominal plant $G_c(s)$ (gray lines) and decoupled plant $G_{\text{dec}}(s)$ (blue lines) used for the PI controller desing.

$G_r(s)$ is right-multiplied by the inverse of its DC-gain, that is,

$$G_{\text{dec}}(s) = G_r(s)G_r(0)^{-1}. \tag{7.7}$$

Figure 7.2 compares the frequency response of the original and the decoupled plants, respectively. It can be observed that the diagonal elements dominate the dynamics and the off-diagonal present a small response in the frequency range of interest, as compared to the original nominal model $G_c(s)$.

The transfer functions corresponding to the diagonal elements of the decoupled plant present a dominant dynamic behaviour similar to a first-order system, i.e., it can be approximated by

$$G_{\text{dec}}(s) \approx \begin{bmatrix} \frac{k_1}{s-a_1} & 0 \\ 0 & \frac{k_2}{s-a_2} \end{bmatrix}. \tag{7.8}$$

Consider the PI controller for each channel j,

$$K_{\text{PI}}(s) = k_{p,j}\frac{s-b_j}{s}, \tag{7.9}$$

with $b_j = -k_{i,j}/k_{p,j}$ and being $k_{p,j}$ and $k_{i,j}$ the proportional and integral gains of the controller, respectively. Then, the controller parameters can be tuned by locating the zero b_j slightly at the left of the model dominant pole a_j and then adjusting the gain $k_{p,j}$ until a suitable closed-loop response is obtained.

The resulting closed-loop scheme combining the diagonal elements $G_{\text{dec},jj}(s)$, $(j = 1, 2)$ and the PI controllers is stable for all values of $k_{p,j}$. Nevertheless, a limit on these parameters comes from the lack of perfect decoupling, measurement noise levels, and the saturation of the control action. All these issues must be checked by simulation using the complete nonlinear model.

Next, a model-based robust controller will also be designed and compared with the previous one.

7.3 $\mathcal{H}_\infty$ optimal control

Alternatively, the controller can be designed in the frame of multivariable optimal control. In this case, the control design objectives are expressed as

$$\min_{\tilde{K}(s)} \frac{\|z\|_2}{\|w\|_2}, \tag{7.10}$$

where z is a performance variable and w a disturbance. Therefore, the controller design consists in defining a control setup and in selecting z and w according to the control specifications with suitable weighting functions [163, 223].

In the electrolyzer case, tracking a pressure reference P_{ref} while rejecting the disturbance I is sought. Hence, the performance variable z represents the pressure and level errors, and the disturbance w, of the system pressure and the current, i.e.,

$$z = W_e(s)M(s)\begin{bmatrix} P_{\text{H}_2} - P_{\text{ref}} \\ \Delta L \end{bmatrix}, \qquad w = W_u(s)\begin{bmatrix} P_{\text{ref}} \\ \hat{I} \end{bmatrix}, \tag{7.11}$$

where

$$M(s) = \begin{bmatrix} 1 & 0 \\ 0 & 1 \end{bmatrix}\frac{1}{s}, \tag{7.12}$$

$$W_e(s) = \begin{bmatrix} k_{e,1} & 0 \\ 0 & k_{e,2} \end{bmatrix}, \tag{7.13}$$

$$W_u(s) = \begin{bmatrix} k_{u,1} & 0 \\ 0 & k_{u,2} \end{bmatrix}\frac{s/0.1\omega_c + 1}{s/10\omega_c + 1}, \tag{7.14}$$

being $k_{e,j}$, $k_{u,j}$ and ω_c design parameters. The weighting function $M(s)W_e(s)$ penalizes the low frequencies of the pressure and level errors and $W_u(s)$ penalizes the magnitude at high frequencies of the control actions. The closed-loop setup is shown in Figure 7.3.

The final controller is obtained after solving the optimization problem (7.10) and left-multiplying the resulting $\tilde{K}(s)$ by $M(s)$, that is,

$$K_\infty(s) = M(s)\tilde{K}(s). \tag{7.15}$$

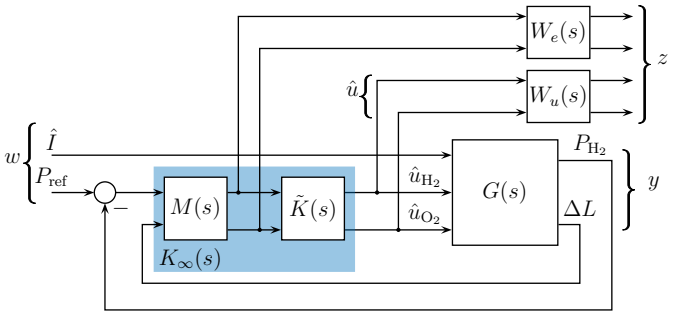

Figure 7.3: Control setup for the design of the $\mathcal{H}_\infty$ controller.

This factorization is needed to ensure the existence of a stabilizing controller.

7.4 Simulation results

The numerical simulations were performed with the previously designed controllers (based on the COM presented in Chapter 6) combined with the full-nonlinear model of the electrolyzer, called the SOM developed in Chapter 5. The simulations were performed in MatLab/Simulink with the variable-step solver Bogacki-Shampine (ode23). Five different scenarios were considered and discussed below. In the first situation, a large depressurization occurs while a constant electric current is applied. In the second scenario, the electrolyzer produces gases at constant pressure but the electric current fluctuates, as if it was provided by renewable energy sources. The third simulation is a pressurization when the electrolyzer has a lower pressure than the tank, so in order to supply H_2, the system must increase its pressure. In the fourth situation, a simple model of the evolution of the tank is added so the control must follow the tank pressure according to the gas consumption. Finally, the fifth scenario uses throttle valves which simulate the action of the tanks. This situation is the closest to the actual situation in the current laboratory set, which will be discussed in § 8.1. Previous reported results do not consider a dynamic model based on the phenomenology of the system for controller design, therefore a potential comparison with this work would be unfair.

The controllers were designed as indicated in § 7.2 and § 7.3. Regarding the PI tuning, once the plant is decoupled, it can be approximated by a first order model. Thus, the PI parameters were chosen in order to locate the PI zero slightly at the left of the dominant pole (about 5%)

and reduce the plant pole effect. The dominant poles of the decoupled plant are

$$a_1 = -0.0576\,\text{rad/s}, \qquad a_2 = -0.00078\,\text{rad/s}. \tag{7.16}$$

Therefore, the controller zeros were seleceted as $b_j = 1.05\,a_j$ $(j = 1, 2)$. Then the gains were adjusted until have fast responses without saturating the control actions. This was tuned using standard Matlab tuning tools, resulting in the following parameters:

$$k_{i,1} = 0.18, \qquad k_{p,1} = 3, \tag{7.17}$$

$$k_{i,2} = 0.16, \qquad k_{p,2} = 200. \tag{7.18}$$

Regarding the $\mathcal{H}_\infty$ controller, the design was cast as a standard mixed-sensitivity problem. Here, the performance output was selected as

$$z = [W_e e \; W_u u]^T, \tag{7.19}$$

as shown in Figure 7.3. Therefore, the $M.W_e$ penalizes the low frequency values of the pressure and level error, where M ensures integral action in the final controller. On the other hand, the weight W_u penalizes the high frequency values of the control input. The aim of the weight W_u is to limit the control action and the controller bandwidth to provide robustness. Then, the design parameters in the weighting functions were set as

$$\begin{aligned} k_{e,1} &= 0.1, \quad k_{e,2} = 4, \\ k_{u,1} &= 0.8, \quad k_{u,2} = 0.8, \end{aligned} \tag{7.20}$$

and $\omega_c = 0.7$ rad/s. The particular values of the weighting functions W_e and W_u in Equation (7.20) were found as usual by checking the closed-loop $\mathcal{H}_\infty$ norm of the plant augmented with the weights and the closed-loop response of the linear model.

Both controllers were designed using approximated linear models but imposing robustness constraints in order to consider the differences with the complete nonlinear model.

7.4.1 Scenario 1: Depressurization

This scenario analyzes a depressurization process caused by a sudden change in the tank pressure P_{tank}. This pressure drop can be caused by a preparation for a prolonged maintenance shutdown or by the system management when low energy is forecasted.

Figure 7.4 shows the system responses with the PI controller (dashed lines) and the $\mathcal{H}_\infty$ controller (solid lines). In the upper plot, a sudden change of P_{tank} from 7000 to 1000 kPa and

the reference P_{ref} computed according to (7.6) with a rate limit of 5 kPa/s, can be observed. The current density is required to remain constant at 0.21A/cm^2 (i.e., electric current $I = 30$ A). Both controllers achieve a suitable pressure reference tracking. There are more visible differences between both controllers in the evolution of level difference ΔL. The $\mathcal{H}_\infty$ controller achieves a faster convergence to the reference. On the other hand, impurity does not increase due to smooth control actions involving equalized pressures on both sides of the membrane. Instead, the impurity decreases due to the production of gases at a lower pressure. The goal of this simulation is to achieve a depressurization without extra contamination during this process, which is reached with both controllers. In Figure 7.4, it can be seen that the control actions u_{H_2} and u_{O_2} do not exceed the actuator limits.

7.4.2 Scenario 2: Electric current fluctuations

In this scenario, the current density changes while the pressure reference P_{ref} is kept constant. The simulations using both controllers are compared in Figure 7.5. As can be seen, valves openings virtually follow the fluctuation of the current density due to the direct relationship between current density and gas production. Both controllers manage to maintain the reference pressure with a maximum error of 0.5% and the level difference in less than 2 mm. Because of this, O_2 impurity, that is always the highest value, is below 1%.

7.4.3 Scenario 3: Pressurization

In this scenario, electrical current density is kept constant while system pressure increases. This is the case, for example, when electrolyzer starts from cold start (i.e., $P_{\text{H}_2} = 100$ kPa) and the pressure has to reach the pressure reference P_{ref} while the storage tank is loaded and its pressure $P_{\text{tank}} = 4000$ kPa. Simulations performed for large pressure differences result in some problems which will be discussed later. Therefore, only the last pressurization step is presented in Figure 7.6. In both cases, an anti-windup strategy is needed. This can be observed at $t \cong 200$ s when the pressure error change its sign but the action of the control does not change until $t > 460$ s for $\mathcal{H}_\infty$ controller and $t > 480$ s for PI controller.

Another interesting behaviour to highlight is the level error that accumulates during pressurization. This is because during this process there is no gas outlet to equalize levels. Moreover, since the H_2 mole production is two times O_2 , this difference usually occurs. The deeper the pressurization, the greater the difference in level of liquid solution. Therefore, in this prototype,

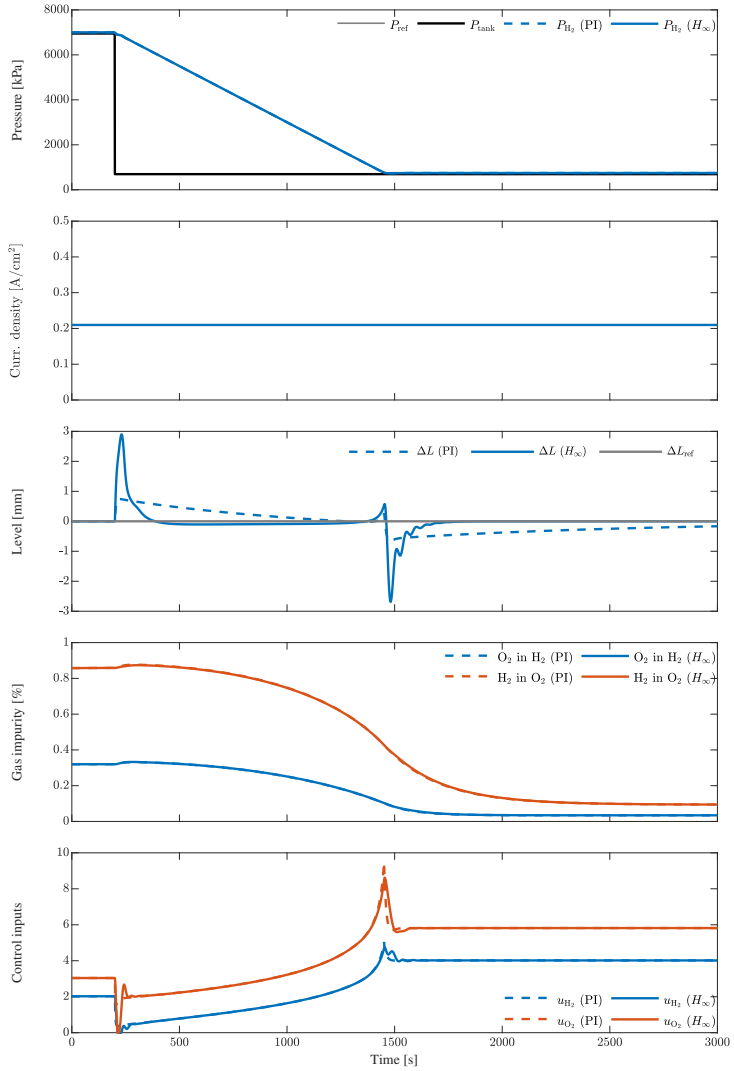

Figure 7.4: Simulation results corresponding to Scenario 1 using the PI controller (dashed lines) and the $\mathcal{H}_\infty$ controller (solid lines).

a single pressurization step from atmospheric pressure to P_{tank} is not practicable. About the level difference, there are different possible answers. First, to accept this error with its consequent contamination in a specific period of time. Second, to have an alternative gas outlet to the ambient that allows hydrogen releasing in a controlled manner. The big disadvantage of this, of course, is the waste of gas. Third, to make a design change in the electrolyzer by making the hydrogen separation chamber cross section twice the one of the oxygen separation chamber. The author of this thesis is not aware if there is any real case where this path has been tested.

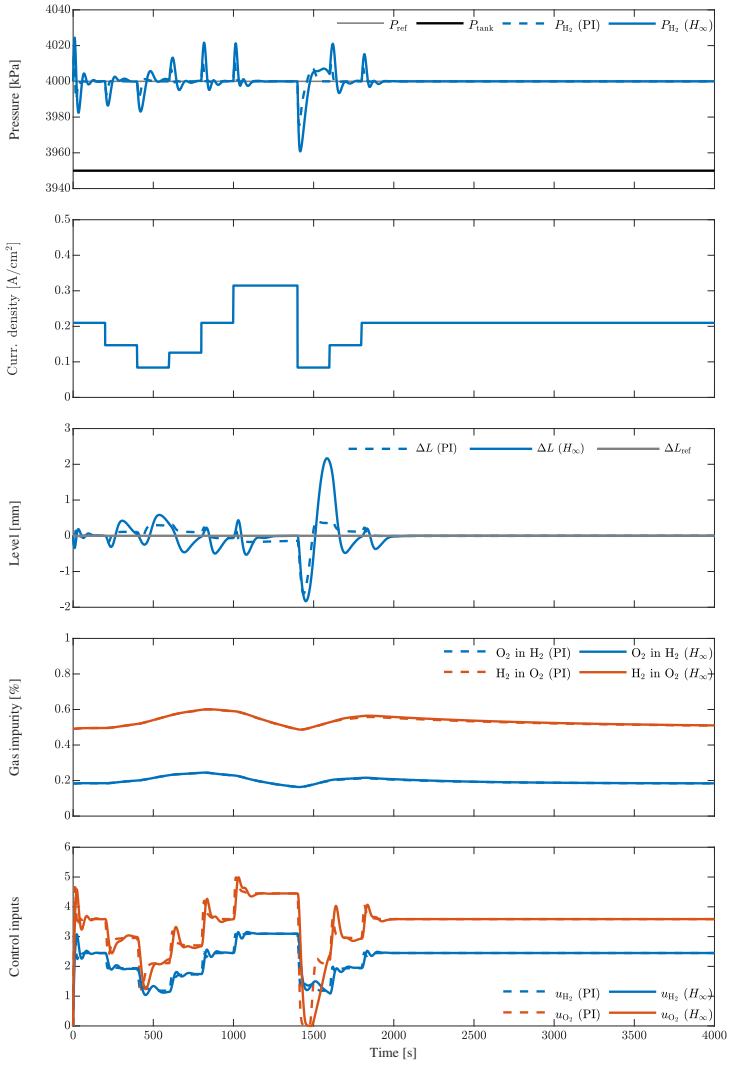

Figure 7.5: Simulation results corresponding to Scenario 2 using the PI controller (dashed lines) and the $\mathcal{H}_\infty$ controller (solid lines).

However, it is important to clarify that in fact the slow difference in levels is not the cause of the contamination but rather the control actions after it. This is due to the action of the equalization line, which in this situation is capable of compensating the pressure in both SC and, in consequence, in both half cells. Perhaps, a different strategy can be designed for this process in particular.

Finally, comparing the two control strategies, both eventually equalize the levels while delivering gases at the selected pressure with the same valves opening. However, $\mathcal{H}_\infty$ control has a more fluctuating and higher response on control actions. Because of this, the gas impurities are

greater than for the PI controller. The problem with the $\mathcal{H}_\infty$ control strategy can be justified as its optimization was concentrated for minor errors. Therefore, as stated before, this could be solved with a particular control for this case. The last remark in this case is that, again, when the controllers found the equilibrium point, both strategies tend to have the same contamination.

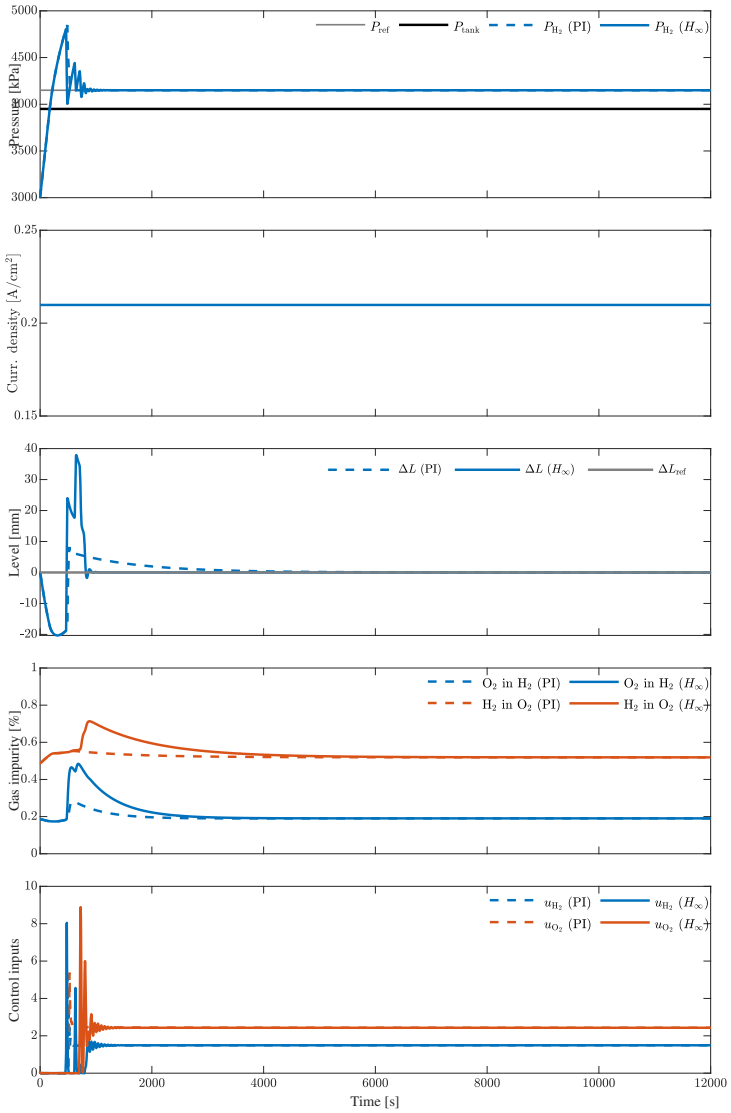

Figure 7.6: Simulation results corresponding to Scenario 3 using the PI controller (dashed lines) and the $\mathcal{H}_\infty$ controller (solid lines).

7.4.4 Scenario 4: Storage tank and consumption

In this fourth scenario, a simple consumption profile is proposed. Besides, the model of the storage tanks is added. Considering ideal gases, the following equation can be written to a rigid tank as a control volume:

$$P_{\text{tank}}\, V_{\text{tank}} = n_{\text{tank}}\, R\, T. \tag{7.21}$$

The pressure of the tank, P_{tank}, is the value taken as the reference for the controllers. The tank volume, V_{tank}, is a parameter of design of the complete system. In order to define tank size, it is necessary to specify the type of renewable energy source and the despachability requirements. The first issue means to know its fluctuability along a single day, and also in each season. Moreover, cases as solar sources, characteristics as cloud effect are important. About the second need, the more demanding the consumption profile (i.e., little tolerance to receive less energy than demanded, or to have moments of power shortage), the greater storage capacity it must have. Furthermore, the storage system has to be designed for a maximum pressure which also limitates its capacity. This issue is out of scope, so a system is defined in order to show a more interesting behaviour which means to select a small storage system. Taking the derivatives with respect to time in Equation (7.21) and considering, in this first approximation, negligible temperature changes,

$$\dot{P}_{\text{tank}}\, V_{\text{tank}} = \dot{n}_{\text{tank}}\, R\, T. \tag{7.22}$$

In addition, the change of moles in the tank, $\dot{n}_{\text{tank}}$, is generated by the inflow from the electrolyzer and the outflow to the consumption, i.e.,

$$\dot{P}_{\text{tank}} = (\dot{n}_{17} - \dot{n}_{\text{cons}})\, \frac{R\, T}{V_{\text{tank}}}. \tag{7.23}$$

Finally, P_{tank} is added as a new state for the extended plant which is then used as input for the control system and a consumption profile, $\dot{n}_{\text{cons}}$, is generated as a new disturbance of the plant.

Figure 7.7 shows the response of the two control strategies designed. Both are capable of following the pressure reference with small level error. As was seen in other cases, $\mathcal{H}_\infty$ controller has a relative more aggressive action that generates a higher level error but compensates it faster. Therefore, similar impurities can be observed. Increasing impurity is due to the increasing operation pressure.

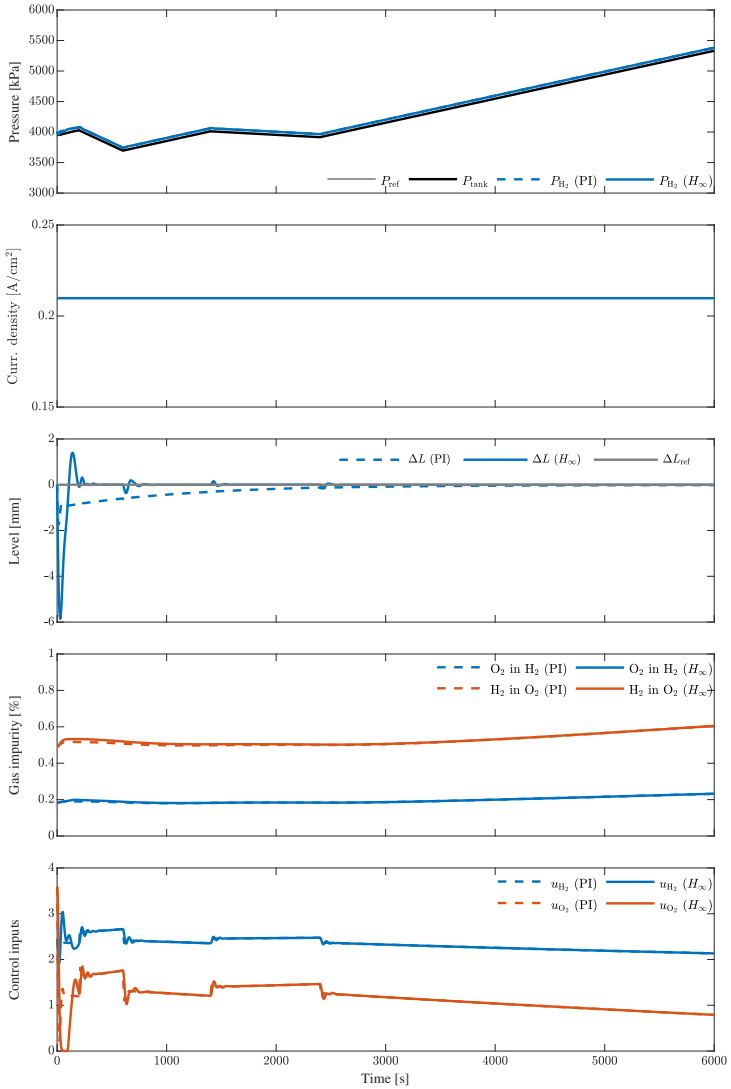

Figure 7.7: Simulation results corresponding to Scenario 4 using the PI controller (dashed lines) and the $\mathcal{H}_\infty$ controller (solid lines).

7.4.5 Scenario 5: Manual valves

The following scenario seeks to replicate the experiments that can be performed in the laboratory in the absence of a suitable gas storage system. As will be explained in Chapter 8, a manual valve was installed downstream of the H_2 outlet line which will restrict the release of gas to the atmosphere. This will simulate the tank pressure which, as previously explained, is used to define the operating pressure. An intermediate buffer tank is installed between the outlet line and the manual valve in order to have a delay in response.

It can be seen that for a certain opening value of the manual valve and given a constant flow of H_2 produced, due to the constant current, the buffer tank pressure tends to stabilize at a fixed value. The time constant of this process is given by the volume of the buffer tank used. Consequently, the pressure of the electrolyzer follows this pressure due to the control action while the liquid levels remain even. Given this, the variation in purity is directly due to the pressure of the system and is part of the nature of the process. As previously stated, further reducing contamination below this will depend on the materials and construction design. Only at the beginning of the valve opening changes, a fluctuation in the control action can be seen which generates a relatively greater contamination. This is slightly observable in the most abrupt change close to t = 18000s and at the beginning of the simulation where the $\mathcal{H}_\infty$ control imposes more fluctuating openings and therefore there is a little more H_2 in O_2.

7.4.6 Controller comparison

Particularly in scenario 1, the $\mathcal{H}_\infty$ control has a higher transient error but converges to zero faster that in the PI case. Overall, the performance of both controllers is similar and depends on the tuning of the PI and the weight selection for the $\mathcal{H}_\infty$ control procedure. Both controllers were designed from a common COM and seeking for the best performance/robustness compromise. In case of the PI controller, the tuning procedure consists in adjusting four parameters (the proportional and integral constants for each channel). In the $\mathcal{H}_\infty$ control, the design is based on an optimal algorithm and the controller is tuned by the proper selection of a set of weighting transfer functions. The PI controller might be preferred by some control engineers as it is based on a more intuitive SISO tuning procedure. However, this method relies on non-perfect decoupling that can affect the final closed-loop performance. Instead, the $\mathcal{H}_\infty$ controller requires more sophisticated design tools but is designed directly from the MIMO model in an optimal way, based on the performance/robustness weights that take care of low/high frequency requirements.

7.5 Summary

In the quest to raise the operating pressure of alkaline electrolyzers, control strategies are needed to decrease gas cross-contamination and, consequently, increase the purity of the supplied gases. In that sense, modelling and control are key issues in operation and design improvements. Two different controllers that were tested in closed loop with a high-fidelity nonlinear model of the electrolyzer were presented here. They were able to maintain impurity below 1% in all cases,

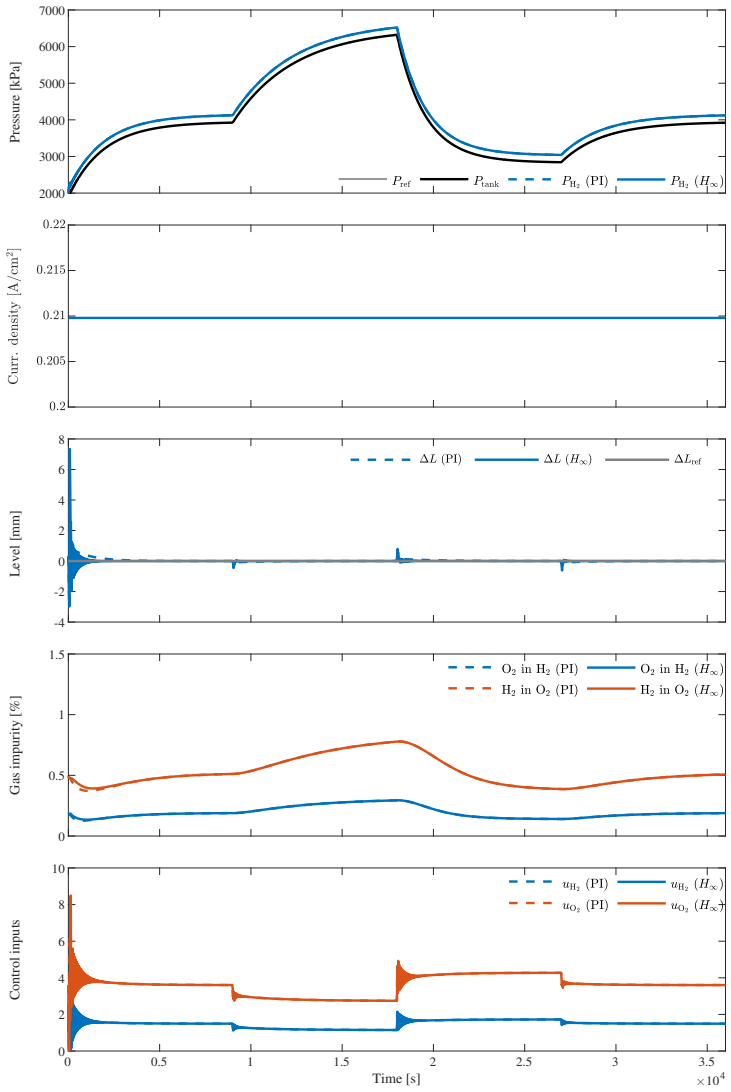

Figure 7.8: Simulation results corresponding to Scenario 5 using the PI controller (dashed lines) and the $\mathcal{H}_\infty$ controller (solid lines).

keeping, practically on all scenarios, the liquid solution level difference between both SCs below 4mm and a maximum pressure error of 0.5%.

Simulation results show that, with a suitable design, both controllers are capable of achieving satisfactory performance. Design and implementation issues will define which one is more practical. The design of the PI controller requires less model information, but the final parameters must be checked by extensive simulations. $\mathcal{H}_\infty$ optimal control is a multivariable system tool and the design results more systematic.

Naturally, the following section shows the tests carried out on the real system in order to validate the model, once again, and the control strategies developed.

Chapter 8

Experimental results from electrolyzer prototype

8.1 Experimental setup

A special test space was built in the laboratory with the prototype high-pressure alkaline electrolyzer. This experimental area has an anti-explosive electrical installation in a distant space with remote connection. To track the tests, in addition to monitoring the measured variables, there are cameras to view the physical equipment.

The equipment configuration presented in Chapter 4, which can be seen in Figure 4.4, is similar to other equipment configurations referred to in the literature. Such are the cases of the Hydrogen and Renewable Integration (HARI) Project in the United Kingdom [157], the tests conducted by the German company Linde [175], the analysis of the process conditions developed in a laboratory electrolyzer in Germany [79] and the modelling carried out by the Centro Nacional del Hidrógeno in Spain [162]. The previous examples include commercial equipment, such as the Hydrogenics electrolyzer used in the HARI Project, and equipment developed ad-hoc by research groups. In all cases, the equipment is designed to operate at a maximum pressure of 30 bar as dictated by the state of the art. Due to this it may be possible that there are cases where the presence of recirculation pumps is not documented or that the recirculation circuits are mixed. Precisely Haug et al [79], when analyzing the process conditions, compares the responses of the equipment having separate, mixed or mixed recirculations. In some cases the analysis includes the interaction with renewable energies, such as solar or wind, and in other cases controlled sources of direct current are used. As commented in Chapter 3, no developments in control

strategies were found except for the cases of Schug [175] and Sánchez et al [162]. In the first case, there are two independent loops that control both outlet valves, the hydrogen one with respect to the system pressure and the oxygen one with respect to the pressure variation in both separation chambers. However, no further details are available. On the other hand, in the second case, there are no details either, but it is reported that the system pressure is controlled with a pressure regulator at the hydrogen outlet while the difference in level is controlled with solenoid valves actuated by PWM. In the present work, as previously described, the aim is to develop a MIMO-type control based on needle-type valves that allow finding a stable operating point, considering that it also seeks to work at higher pressures, which means the problems of contamination increase.

For the development of current experimentation, modifications were made to the electrolyzer for the new valves. In turn, a column was added that functions as a KOH solution trap prior to the valves. These changes can be seen in the scheme together with a photograph in Figure 8.1. Next, the position of the outlet line were modified and a lever was added to be able to set a precise opening of the output to define the output pressure (see Figure 8.2). Next, two manual valves were added between the electrolyzer and the environment to emulate the storage tanks as described in § 7.4.5. Moreover, a buffer tank was installed before the manual needle valve in order to smooth out changes in outlet pressure which is used as a reference for the control loop. This solution does not have the same response as a storage tank but allows to corroborate the operation of the control strategies in similar situations.

In order to obtain a better response from the control system, the independent control of the motors that operate the needle valves was modified. This is because the system was modified from a valve that operates in a half-turn range, to one that operates in ten turns. This control loop, similar to a servomotor, receives the command from the control described in this thesis and operates a pulse width modulator to eliminate the error. This description can be summarized as

$$
\begin{aligned}
e_k &= \alpha_{\text{des}} - \alpha_{\text{cur}}, \\
PWM &= k_p\, e_k + k_i\, T_{i,k}, \\
T_{i,k+1} &= T_{i,k} + T_s\, e_k,
\end{aligned}
$$

where e_k is the error between the desired position and the current position (measured by an incremental encoder), PWM is the percentage defined for the pulse width, k_p and k_i are the constants set for this PI control and T_s is the period of the control cycle. The maximum voltage

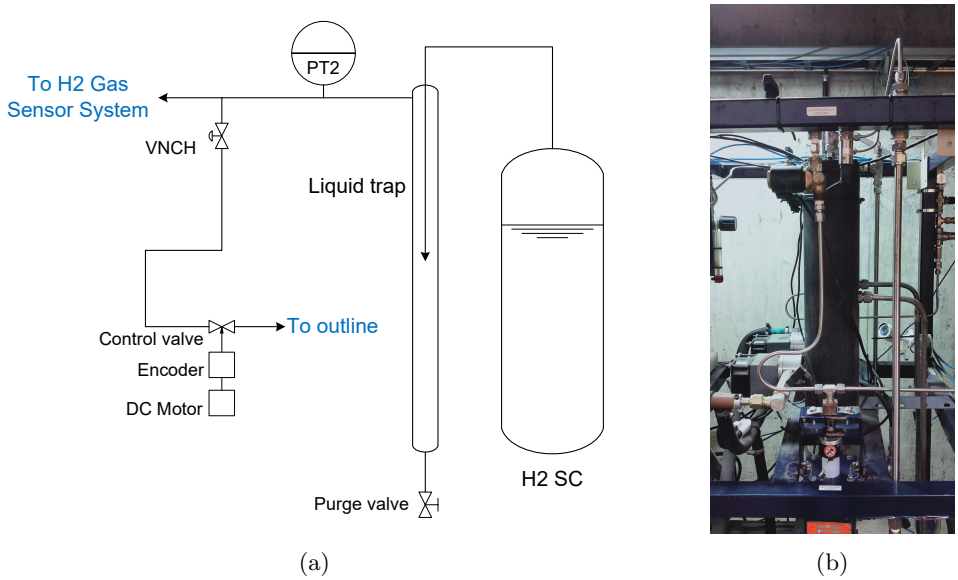

(a) (b)

Figure 8.1: Scheme of the pipeline (a) and photograph (b) of the new outlet line with the installation of the new needle-type valves.

(a) (b)

Figure 8.2: Photographs of the new position of the output lines for O_2 (a) and H_2 (b). In the case of H_2, the needle valve can be seen after the manual valve.

applied in this control was changed from 12 V to 24 V in order to have faster reactions according to the change of valves.

Finally, the power supply is a set of switching power supplies that allows a diverse series-

parallel configuration to achieve a wider range of current and voltage. In turn, this arrangement is controlled by an IGBT driven by a PWM of a manually defined value. A general photograph of the installation of the electrolyzer along with the power supply and the computer which is remotely connected to the lab facilities, is presented in Figure 8.3.

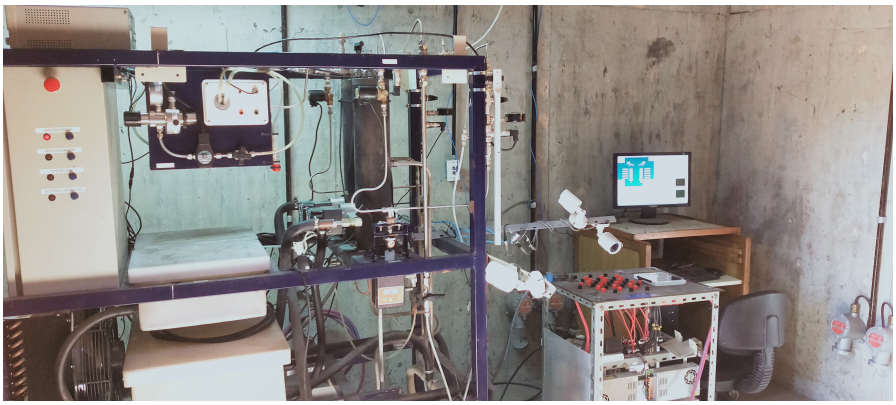

Figure 8.3: General photograph of the test setup. In the electrolyzer can be identified the gas sensor system at the left of the separation chambers and the cameras added to the structure.

8.2 Experiments

The analysis carried out began with a series of tests for different values of pressure and current in permanent operation. These tests, which are presented in § 8.2.1, made it possible to verify the correct operation of the modifications made. In addition, they served as a source of information to compare with the data obtained with the previous control. After that, tests similar to the simulations previously presented in § 7.4 were carried out. On the one hand, a test of a current profile is shown in § 8.2.2. On the other hand, a test that simulates a change in the hydrogen tank pressure with the previously mentioned manual valve can be observed in § 8.2.3. The following experiments were carried out with the designed PI and $\mathcal{H}_\infty$ control strategies. The test campaigns were carried out separately and modifications in the power source had to be made before starting with the $\mathcal{H}_\infty$ control. Therefore, it can be seen in the next experiments that the current density imposed when the $\mathcal{H}_\infty$ control is used is higher than in those tests using the PI strategy. This means that gas production increased.

8.2.1 Permanent operation

In these tests, a combination of constant and variable openings has been applied in the manual outlet valve of the small buffer tank. In Figures 8.4 and 8.5, two tests can be observed where the throttling is such that a stabilization pressure is not reached. On the contrary, the pressure in the tank rises due to the difference in molar flow rates at the inlet and at the outlet. In this way, it was possible to carry out pressure sweeps at a relatively constant electrical current in the electrolyzer in a wide operating range.

Figure 8.4 shows the performance of the electrolyzer with the PI control while in Figure 8.5, the $\mathcal{H}_\infty$ control is applied. In both cases, it is observed that the fluctuation in the current is proportional to the temperature of the system, as already discussed. It can be seen that the cooling system is responsible for limiting the temperature around 40 °C without problem. This is because the electrical source operates at constant voltage. In case the test would have been carried out at constant current with a source dedicated to that effect, a decrease in the applied voltage as the temperature increases would have been obtained, and vice versa. As explained in Chapter 3, increasing temperature decreases overpotentials.

Moreover, the loop that controls the water injection operates twice in the first test and once in the second one by replenishing the water consumed during the electrolysis process. It is seen in those cases that the levels increase rapidly along with the pressure while the temperature decreases smoothly due to the ambient temperature well below the system temperature. Since this control is independent, the valves act on this sudden change in the variables, resetting the errors relatively quickly.

Regarding both controls, for this test a pressure difference was defined

$$P_{gap} = P_{\text{tank}} - P_{\text{ref}} = 50\,\text{kPa}. \tag{8.1}$$

It is observed that the control has no difficulties in following this variation. However, there is some fluctuation in the valve openings due to the high variation in the measurement of liquid levels within the separation chambers. This is mainly due to the nature of the sensors used. They measure the capacitance of a pair of concentric tubes immersed in the solution. Due to the high conductivity of the solution, the capacity will be that of the gas volume above it. In turn, the liquid-free surface does not stay still for two reasons. On the one hand, by the bubbling of the gases produced that rise through the separation chamber and are separated from the solution

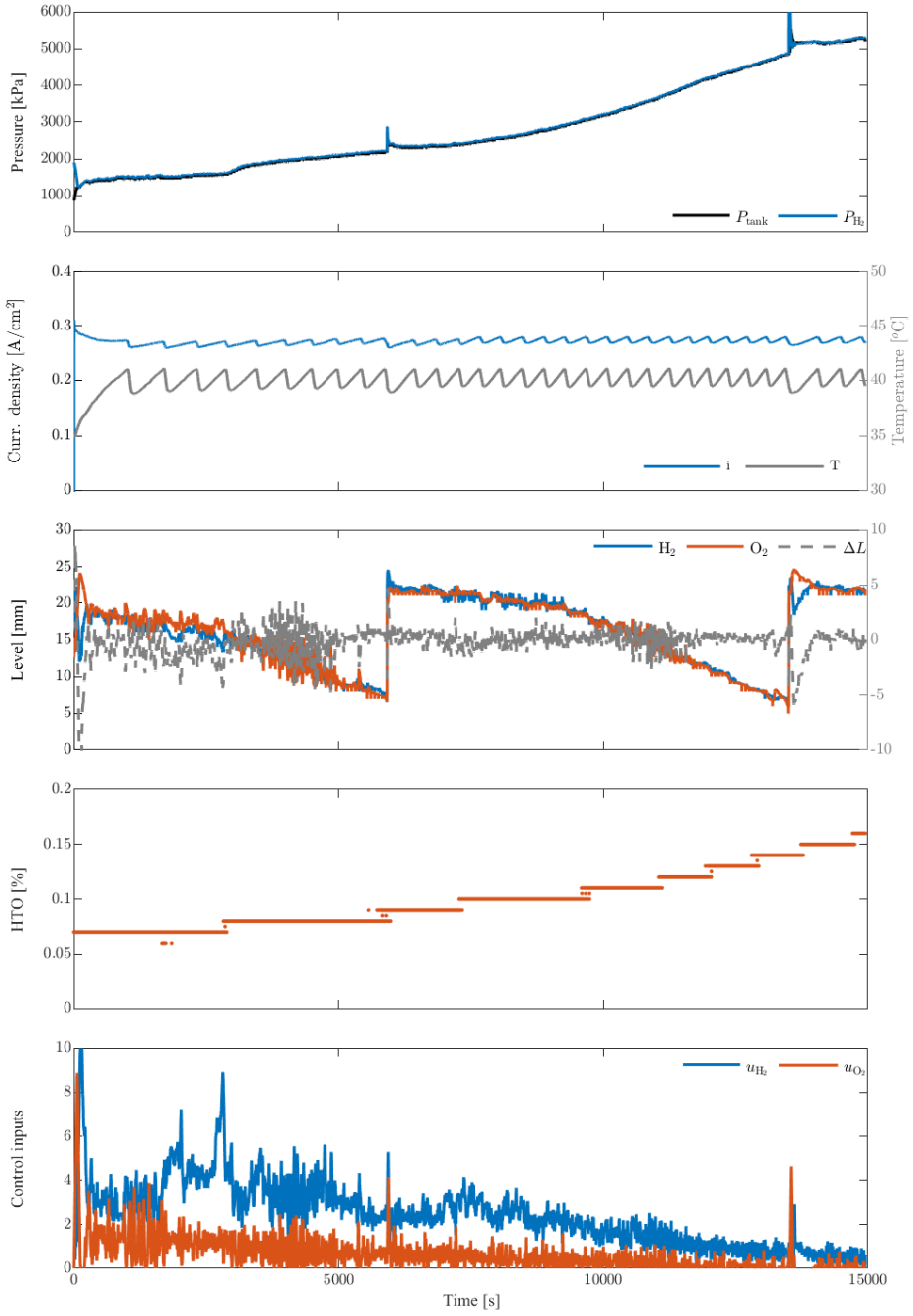

Figure 8.4: Main results of the experiments carried out with the prototype alkaline electrolyzer with an increase in the operating pressure using PI control.

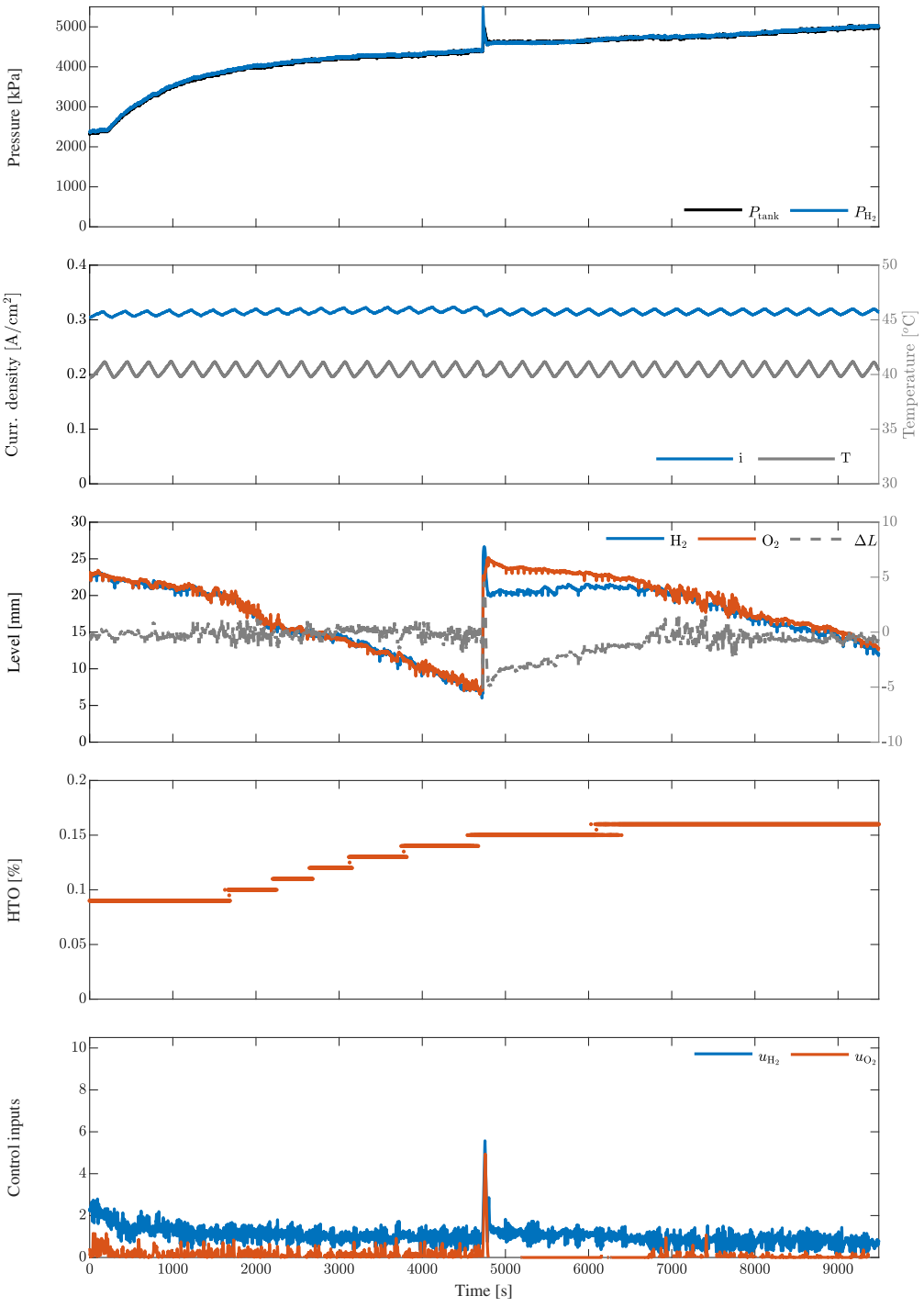

Figure 8.5: Main results of the experiments carried out with the prototype alkaline electrolyzer with an increase in the operating pressure using $\mathcal{H}_\infty$ control.

and, on the other, by the recirculation flow imposed by the recirculation pumps. It is because of this variation in levels that control actions also vary. In any case, this variation is limited.

Furthermore, analyzing the final objective of these controls, the purity obtained is high enough. Or in other words, cross contamination remains low. In electrolytic cells, the diffusion of H_2 towards the O_2 side is always greater than the opposite. For this reason, this value, which is commonly known as HTO (which stands for H_2 to O_2), is represented in Figure 8.4. The trend is that contamination increases as system pressure increases. This is because, as was said in Chapter 5, at higher pressures, there is more dissolved gas and therefore more gas diffuses through the membrane. It is important to note that the purities obtained in this case are significantly higher than those obtained in the previous test campaign with the original control (e.g., $HTO = 0,34\%$ @50bar and $HTO = 0,19\%$ @30bar).

Finally, comparing both tests and control strategies, it can be observed that the PI control has greater valves openings and greater fluctuations as well, hence higher actuator action. The first fact is possibly related to the different situation in the manual valve after the buffer tank. On the contrary, the second fact is a possible cause of contamination. This means that more opening fluctuation in the valves generates more level difference in SC (level difference standard deviation in PI test $\sigma = 1.366$ mm while in the $\mathcal{H}_\infty$ test, $\sigma = 1.056$ mm). However, it can be observed that H_2 purity is comparable at the same system pressure.

8.2.2 Variations in electric current

Strictly speaking, the electric current is not varied directly, as was commented in the previous subsection, but rather the duty cycle value is defined. Experiments lasting more than 3 hours are presented in Figure 8.6 and Figure 8.7. Again, the first experiment was carried out using the PI control and the second one with the $\mathcal{H}_\infty$ strategy.

In this occasion, the operating temperature was defined around 50 °C, which results in a higher current than at 40 °C. It is seen that the temperature rises for high duty cycle values (referred to higher electrical current values) forcing the refrigeration system to operate. On the contrary, for low values of electric current, the loss of heat itself to the environment is sufficient so that in the long term the temperature would be well below that defined value. It can be seen that for $DC = 85\%$ ($t \in (5600\text{ s}, 8000\text{ s})$ for the PI control and $t \in (3600\text{ s}, 6000\text{ s})$ for the $\mathcal{H}_\infty$ control) there is a difference between both tests. This is due to the higher current density in the second part of the experiment campaign, when $\mathcal{H}_\infty$ was implemented, as mentioned before.

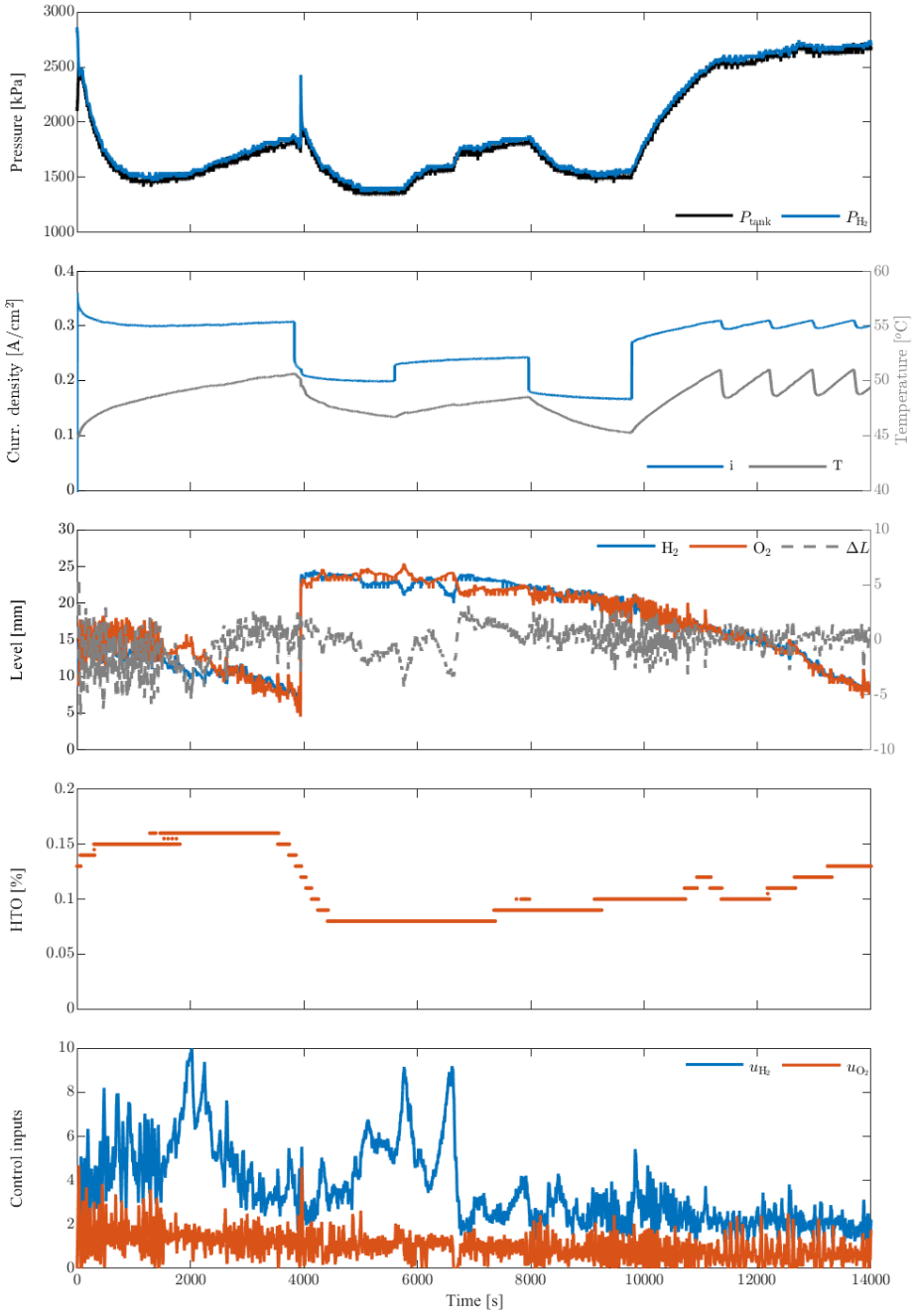

Figure 8.6: Main results of the experiments carried out with the prototype alkaline electrolyzer with variations in the power supply using PI control.

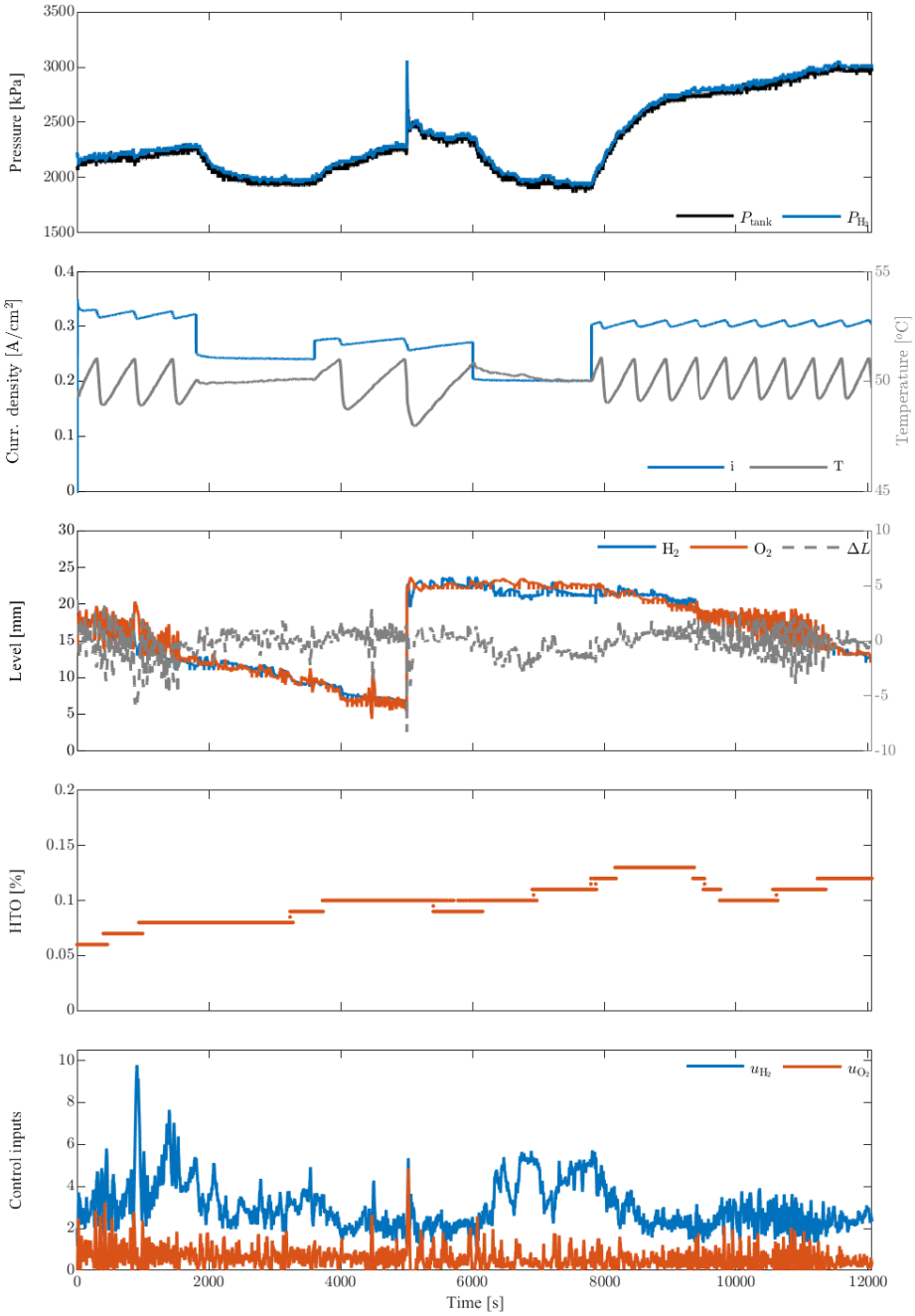

Figure 8.7: Main results of the experiments carried out with the prototype alkaline electrolyzer with variations in the power supply using $\mathcal{H}_\infty$ control.

These tests was started with a relatively low tank pressure that rose and fell in accordance with the imposed high or low electrical currents. This is because the flow produced in each case is proportional to the current. The mass balance within the buffer tank, which was explained in § 8.1, indicates that the pressure in this tank will vary depending on the difference between the inlet and outlet flows.

In turn, the relationship between the electrical current and gas production implies that the valve openings will be directly related to current variation. However, this correspondence is difficult to be seen since the valves, again, follow the fluctuation of the solution-free surface levels in the separation chambers, keeping the error close to 0. However, in the case of the $\mathcal{H}_\infty$ strategy the H_2 valve opening seems to increase at lower current densities, specially remarkable in $t \in (6000\text{ s}, 7800\text{ s})$.

H_2 contamination in O_2, which is always the greater than the opposite flow, is limited by presenting two competing causes. On the one hand, the higher the current, the more gas is produced in each electrode. Therefore, the gas which manages to cross the membrane, in this case H_2, is proportionally diluted in the greater amount of O_2 produced. On the other hand, the higher the operating pressure, the more contamination there will be due to the nature of the diffusion. Both control strategies manage to have impurities below $HTO = 0.15\%$. The difference at initial time between both tests is justified by the past actions in each experiment. While in PI control the system was pressurized up to 30 bar, in $\mathcal{H}_\infty$ control, electrolyzer and buffer pressures start at similar values around 21 bar.

8.2.3 Changes in pressure tank

As the third and last test example carried out, the change in the pressure of the buffer tank is shown in Figures 8.8 and 8.9. This is accomplished by the sudden opening of the manual outlet valve. The time constant between the step applied to the valve and the pressure of the buffer tank is directly related to its capacity (volume). In turn, to reduce sudden changes in the electrolyzer there is a slope limit in the reference pressure that the control follows. That is why it is observed how initially the pressure of the buffer tank decreases faster than the pressure of the electrolyzer that follows a line with a slope identified as α in § 7.1.

In this case, a constant duty cycle and an operating temperature of around 40 °C were also maintained. Here it can be seen how the control acts on the valves, opening them considerably, which is related to the greater difference in pressure. In turn, in the PI control case, the maximum

range of the H_2 valve is reached and the level difference increases, which implies gas crossover. However, the contamination remains low and this strategy is relatively better than a sudden depressurization because the last option would cause large amounts of dissolved gas to separate with its consequent increased contamination.

It can be seen that the $\mathcal{H}_\infty$ strategy is able to maintain the level difference closer to 0, which implies less contamination. This can also be justified by noting that the H_2 valve has not reached the upper limit. Moreover, the difference in the initial value of HTO is due to the history before the initial time of the test. In the PI test, the system was producing gases near to 50 bar for half an hour while in the $\mathcal{H}_\infty$ test the starting pressure was reached rapidly, and then the test was started.

8.2.4 Control implementation comparison

In this Chapter, the control strategies were tested on the real system. The software implementation was developed in C code copying the form of discrete matrices from the state space, as follows:

$$x_{k+1} = A_z\ x_k + B_z\ e_k, \tag{8.2}$$

$$u_k = C_z\ x_k + D_z\ e_k, \tag{8.3}$$

being x_k and x_{k+1} the actual and future states of the controller. Moreover, e_k and u_k are the errors in level difference and pressure, and the desired valves openings, respectively. Finally, the matrices A_z, B_z, C_z and D_z are defined for each control strategy. Furthermore, the length of the state vector depends on the controller (i.e., in this case two states for PI control and six states for $\mathcal{H}_\infty$ control). In this way, the implementation was similar for both controllers. The difference lies in the time elapsed in each control cycle due to the number of calculations. However, there were no difficulties in this regard.

Besides, like the results of the comparison in the simulations, both controllers had an adequate performance equalizing the levels in the SCs and delivering gases at the desired pressure linked to the pressure tank. Numerically speaking, two parameters can be defined in order to compare the performance, i.e.,

$$\pi_{\Delta L} = \overline{|\Delta L|}, \tag{8.4}$$

$$\pi_{\mathrm{HTO}} = \max(\mathrm{HTO}). \tag{8.5}$$

Table 8.1: Numerical comparison between experiments with PI and $\mathcal{H}_\infty$ controllers

Experiment	$\pi_{\Delta L}(mm)$		$\pi_{\text{HTO}}(\%)$	
	PI	$\mathcal{H}_\infty$	PI	$\mathcal{H}_\infty$
Permanent operation	0.8228	0.8349	0.16	0.16
Variations in electric current	1.1147	0.8469	0.16	0.13
Changes in pressure tank	2.8305	1.3265	0.20	0.15

These parameters summarize the final objective of the controllers: to minimize the error difference in the levels ($\pi_{\Delta L}$) in order to reduce the contamination by gas crossing in the produced gases (π_{HTO}). Table 8.1 shows these results, which concludes that, in general, both controllers have similar responses. However, slightly better performance can be observed in the case of the $\mathcal{H}_\infty$ control, especially in the deep depressurization experiment.

8.3 Summary

In this chapter, the experimental setup was presented along with some of the tests carried out with their respective results. In the tests on the prototype electrolyzer in the laboratory, it was possible to verify the correct operation of both controls in different scenarios. In all cases, the contamination was quite below 1% in the O_2 line, which is the one that always presents the greatest contamination given the greater diffusivity of H_2. In turn, these results were compared with those obtained with the previous setup and control. Even though it is within the expected range of the difference between simulation and reality, it can be seen that the real purity values are also higher than the simulated ones in § 7.4. This is probably related to the fact that the identification of the plant was carried out with the previous results where the control generated greater fluctuations in levels and pressure and therefore, there was greater contamination.

Finally, it can be seen that the valves normally operate in the lower part of their range. This has been the smallest commercial valve that could be found. At the design level this can be improved by building larger cell packages that generate a higher flow rate of produced gases. On the other hand, in order not to lose the objective of covering a wide operating range, a set of valves could be used that allow regulation at low and high flow rates.

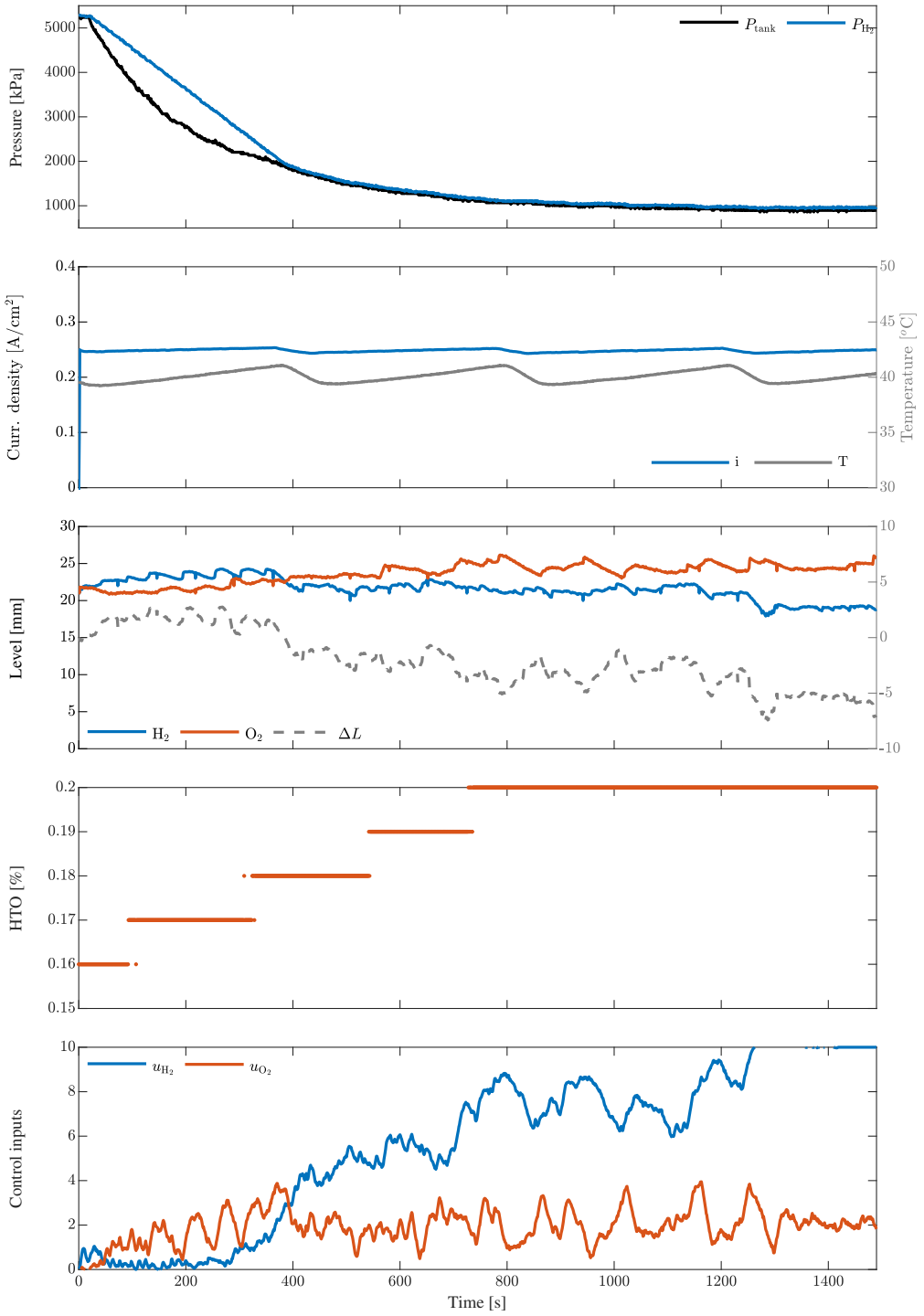

Figure 8.8: Main results of the experiments carried out with the prototype alkaline electrolyzer with a sudden opening in the manual needle valve and the consequent decrease in tank pressure using PI control.

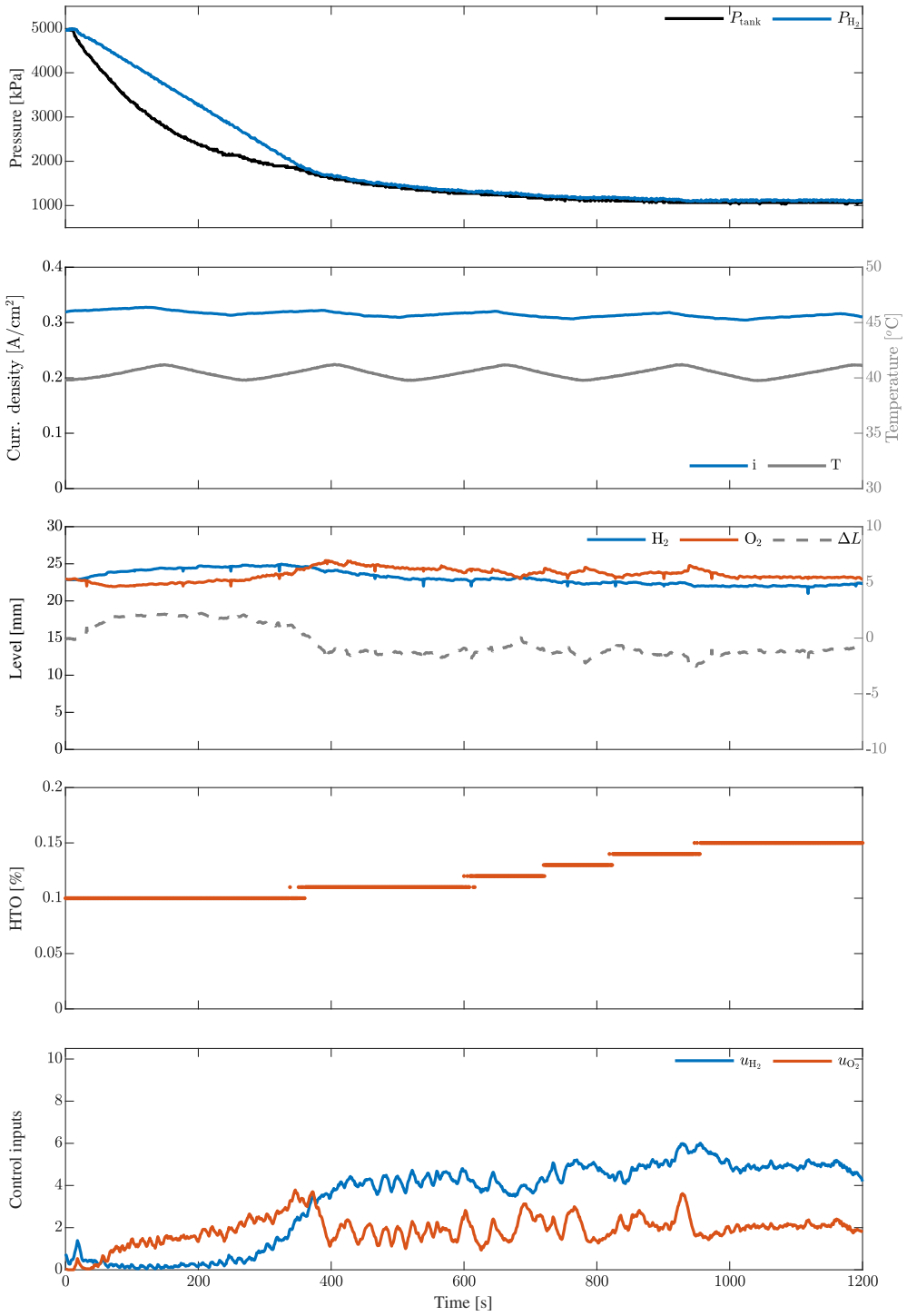

Figure 8.9: Main results of the experiments carried out with the prototype alkaline electrolyzer with a sudden opening in the manual needle valve and the consequent decrease in tank pressure using $\mathcal{H}_\infty$ control.

Part IV

Concluding Remarks

Chapter 9

Contributions and concluding remarks

9.1 Contributions

For several years, there has been a growing and sustained interest in renewable energy and the use of hydrogen as an energy vector. Global efforts to improve these technologies are evident.

Throughout this doctoral thesis, the operation of high-pressure alkaline electrolysers was investigated with three objectives. On the one hand, the experimental knowledge gathered with the prototypes made was consolidated. High-pressure production, while theoretically more efficient, has several drawbacks. That is why it is understood that there is not enough information on its use. The *first contribution* of this thesis is the exhaustive analysis of the operation of high pressure alkaline electrolyzers, which will allow the evaluation of substantial improvements in the design of new prototypes that allow progress in the implementation of this particular technological solution.

On the other hand, it was sought to contribute to an area of knowledge that was not being exploited, such as the modeling and control of these devices. So, the *second contribution* of the present thesis is the development of a dynamic model of the complete electrolyzer system, not only of the electrolytic cell. At the same time, the phenomenological-based semiphysical modelling carried out allows adapting to the diverse electrolyzers directly by changing the parameters which have real meaning. Therefore a simulation high order model and a control-oriented reduced order model were generated.

Finally, as a *third contribution*, the control scheme was described and two control strategies

were developed for the main actuators of the electrolyzer that are relevant to minimize cross contamination in both gas lines. Moreover, as was discussed, after an exhaustive revision of the related literature, these two controllers, a traditional PI and the other based on optimal control tools, are the first published. Both controllers were implemented in the electrolyzer system and their capability of producing gases at a certain pressure and equalizing levels in the separation chambers, which means minimizing the gas crossover in the electrolytic cells, were tested.

9.2 Answering the research questions

The conclusions of this dissertation are summarized by answering the *key research questions* presented in Chapter 1 as follows:

(Q1) *What is the current state of hydrogen production according to the extended idea of using it as an energy vector?*

Although the use of hydrogen as an energy vector is an idea proposed some decades ago, it still needs a lot of effort in order to be well established. Its main difficulty is the necessity to develop both supply and demand for this product as an energy vector. Although the production and consumption of hydrogen have a long tradition, this new perspective means producing H_2 from renewable sources, what is known as green hydrogen, with the ultimate goal of storing energy to later be used again in the energy sector or in transportation. Moreover, its fate is directly linked to the insertion of renewable energies because its own maturation is justified in an ecofriendly scenario. Currently, its cost is closer to that of hydrocarbons but a global decision is still required to sustain it while it is established as a possible option.

As discussed in Chapter 2, several technologies are being developed and among them, electrolysis is the best option to connect with renewable sources. Therefore, all efforts made to improve this technology could be used to get closer to this global solution.

(Q2) *How developed is the modelling and control of alkaline electrolysis since this technology is long established?*

Surprisingly, there is a lack of dynamic models which integrate the entire system and publications about control strategies especially designed for alkaline electrolysis. Existing models are generally dedicated to steady state and focus on electrolytic cells. However, in

recent years some new research has been found showing that other groups are also interested in this topic.

In the case of control strategies, as described in Chapter 3, no information could be found. It is clear that commercial systems have some form of control loops but they have no systematic development. The control strategies presented in Part III could be an interesting starting point.

(Q3) *How to describe the complete operation of alkaline electrolyzers involving all processes and auxiliary systems?*

Since high-pressure alkaline electrolyzers are in a prototype stage even while this technology is well known from decades ago, it was important to describe precisely and entirely the operation of this system. Chapter 4 is a concise description of the last prototype and condenses all the experience obtained in the process of designing and operating the previous ones.

(Q4) *How to design a model capable of describing the main operating variables of the electrolyzer, especially gas concentrations?*

Linked to the *key research question* (Q2), the phenomenological-based semiphysical model presented in Chapter 5 is distinguished by the treatment of the electrolyzer as a complete and complex system. The virtue of the method used in this thesis is that each process system is relatively simple to construct and modify. In this sense, changes in some auxiliary system can be updated directly in the general model, as is usual in compartmental model construction. Furthermore, the simplifying hypotheses considered in this thesis could be updated with more precise descriptions by modifying only the definition of the functional parameters considered.

(Q5) *Is it possible to design better control strategies in order to improve performance (i.e., purity of output gases) in high pressure operation?*

In this especial case, it is difficult to answer this question since there are no other control strategies to compare with. In the gathered experience with the previous control loops used in the prototypes, which were empirically developed, the control strategies developed in Part III have smoother actions that imply better performance in decreasing diffusion. However, no control strategies for commercial systems could be found so a lack of comparison should be accepted.

9.3 Directions for future research

This thesis has endeavoured to understand in depth the dynamics of high pressure alkaline electrolyzers. These efforts have the ultimate goal of developing this technology taking care of the purity of the gases at higher operating pressure. However, this is just the beginning for the study of possible improvements. Therefore, some ideas for future research and possible upgrades are:

- The control strategies developed in Part III should be tested in larger systems. Even the distributed control system would be used for electrolyzer arrays. This would probably be the future of the application of this technology in large wind farms or solar plants.
- Throughout the completion of this thesis, several design proposals have been discussed in order to be implemented in future prototypes. Although some of them were partially implemented for the final experiments, other ideas need their own design. Among these ideas, it is worth highlighting the auxiliary partial depressurization system for cleaning the solution, the combination of slow (fine) and fast (coarse) control valves, or the utilization of catalysts inside the chambers to achieve even higher pressures.
- A detailed investigation of the behaviour of the bubbles within the cell and in the separation chambers would provide more information for the design of the parts. Some lines of research have been identified around this topic but they are just beginning.
- The dynamic model presented in Part II can be expanded with information from other investigations in order to take into account the thermal and electrical behaviour. This would complete the model and interface with neighboring systems. This is the case of renewable sources which could feed the electrolyzer.
- Experimental closed-loop data from this thesis could be used to refine the simulation and control-oriented models.
- Taking advantage of the configuration developed both in the simulation and in the experimental field, more control strategies could be designed in order to have more comparative results.

References

[1] Fuel cells and infrastructure technologies program, multi-year research, development and demonstration plan. Technical report, U.S. Department of Energy, 2007.

[2] D. Abbott. Keeping the energy debate clean: How do we supply the world's energy needs? *Proceedings of the IEEE*, 98:42–66, 2009.

[3] M. A. Abdalla, S. Hossain, O. B. Nisfindya, A. A. T., M. Dawoodb, and A. K. Azada. Hydrogen production, storage, transportation and key challenges with applications: A review. *Energy Conversion and Management*, 165:602–627, 2018.

[4] R. M. Abouatallah, D. W. Kirk, S. J. Thorpe, and J. W. Graydon. Reactivation of nickel cathodes by dissolved vanadium species during hydrogen evolution in alkaline media. *Electrochimica Acta*, 47:613–621, 2001.

[5] C. Acar and I. Dincer. Comparative assessment of hydrogen production methods from renewable and non-renewable sources. *International journal of hydrogen energy*, 39(1):1–12, 2014.

[6] D. Aili, M. K. Hansen, J. W. Andreasen, J. Zhang, J. O. Jensen, N. J. Bjerrum, and Q. Li. Porous poly (perfluorosulfonic acid) membranes for alkaline water electrolysis. *Journal of Membrane Science*, 493:589–598, 2015.

[7] U. Albrecht, M. Altmann, J. Michalski, T. Raksha, and W. Weindorf. *Analyse der Kosten Erneuerbarer Gase*. Ponte Press, Ottobrunn, Germany, 2013.

[8] F. Allebrod, C. Chatzichristodoulou, and M. B. Mogensen. Alkaline electrolysis cell at high temperature and pressure of 250°C and 42bar. *Journal of Power Sources*, 229:22–31, 2013.

[9] H. Alvarez, R. Lamanna, P. Vega, and S. Revollar. Metodología para la obtención de modelos semifísicos de base fenomenológica aplicada a una sulfitadora de jugo de caña de azúcar. *Revista Iberoamericana de Automática e Informática Industrial*, 6:10–20, 2009.

[10] E. Amores, J. Rodríguez, and C. Carreras. Influence of operation parameters in the modeling of alkaline water electrolyzers for hydrogen production. *International Journal of Hydrogen Energy*, 39:13063–13078, 2014.

[11] L. An, T. S. Zhao, Z. H. Chai, P. Tan, and L. Zeng. Mathematical modeling of an anion-exchange membrane water electrolyzer for hydrogen production. *International Journal of Hydrogen Energy*, 39:19869–19876, 2014.

[12] S. Anantharaj, S. Ede, K. Karthick, S. Sam Sankar, K. Sangeetha, P. Karthik, and S. Kundu. Precision and correctness in the evaluation of electrocatalytic water splitting: revisiting activity parameters with a critical assessment. *Energy & Environmental Science*, 11:744–771, 2018.

[13] M. L. Arlt, G. F. Cardoso, and D. Weng. Hydrogen storage applications in industrial microgrids. In *2017 IEEE Green Energy and Smart Systems Conference (IGESSC)*, pages 1–6, Nov 2017.

[14] K. J. Aström and T. Hägglund. *Advanced PID control*. Instrumentation, Systems, and Automation Society, Research Triangle Park, USA, 2006.

[15] T. Audichon, E. Mayousse, S. Morisset, C. Morais, C. Comminges, T. W. Napporn, and K. B. Kokoh. Electroactivity of RuO_2–IrO_2 mixed nanocatalysts toward the oxygen evolution reaction in a water electrolyzer supplied by a solar profile. *international journal of hydrogen energy*, 39(30):16785–16796, 2014.

[16] S. P. Badwal, S. Giddey, and C. Munnings. Hydrogen production via solid electrolytic routes. *Wiley Interdisciplinary Reviews: Energy and Environment*, 2:473–487, 2013.

[17] S. P. Badwal, S. Giddey, and C. Munnings. Emerging technologies, markets and commercialization of solid-electrolytic hydrogen production. *Wiley Interdisciplinary Reviews: Energy and Environment*, 7:286–304, 2018.

[18] J. Balej. Water vapour partial pressures and water activities in potassium and sodium hydroxide solutions over wide concentration and temperature ranges. *International Journal of Hydrogen Energy*, 10(4):233–243, 1985.

[19] M. Ball and M. Weeda. The hydrogen economy - vision or reality? *International Journal of Hydrogen Energy*, 40:7903–7919, 2015.

[20] B. K. Barman and K. K. Nanda. Cofe nanoalloys encapsulated in n-doped graphene layers as a pt-free multifunctional robust catalyst: Elucidating the role of co-alloying and n-doping. *ACS Sustainable Chemistry & Engineering*, 6(10):12736–12745, 2018.

[21] H. Barthels, W. Brocke, K. Bonhoff, H. Groehn, G. Heuts, M. Lennartz, H. Mai, J. Mergel, L. Schmid, and P. Ritzenhoff. Phoebus-Jülich: an autonomous energy supply system comprising photovoltaics, electrolytic hydrogen, fuel cell. *International Journal of Hydrogen Energy*, 23:295–301, 1998.

[22] B. Bauer, F. Effenberger, and H. Strathmann. Anion-exchange with improved alkaline stability. *Desalination*, 79:125–144, 1990.

[23] M. Bernt, A. Siebel, and G. H. A. Analysis of voltage losses in pem water electrolyzers with low platinum group metal loadings. *Journal of the Electrochemical Society*, 165:F305, 2018.

[24] R. Bhandari, C. Trundewind, and P. Zapp. Life cycle assessment of hydrogen production via electrolysis - a review. *Journal of Cleaner Production*, 85:151–163, 2014.

[25] L. Burke and A. Moynihan. Oxygen electrode reaction. part 1.—nature of the inhibition process. *Transactions of the Faraday Society*, 67:3550–3557, 1971.

[26] A. Buttler and H. Spliethoff. Current status of water electrolysis for energy storage, grid balancing and sector coupling via power-to-gas and power-to-liquids: A review. *Renewable and Sustainable Energy Reviews*, 82:2440–2454, 2018.

[27] D. Call and B. Logan. Hydrogen production in a single chamber microbial electrolysis cell lacking a membrane. *Environmental Science and Technology*, 42:3401–3406, 2008.

[28] M. Carmo, D. L. Fritz, J. Mergel, and D. Stolten. A comprehensive review on PEM water electrolysis. *International Journal of Hydrogen Energy*, 38:4901–4934, 2013.

[29] M. Carmo, G. P. Keeley, D. Holtz, T. Grube, M. Robinius, Martin Müller, and D. Stolten. PEM water electrolysis: Innovative approaches towards catalyst separation, recovery and recycling. *International Journal of Hydrogen Energy*, 44:3450–3455, 2019.

[30] M. Chandesris, V. Médeau, N. Guillet, S. Chelghoum, D. Thoby, and F. Fouda-Onana. Membrane degradation in PEM water electrolyzer: Numerical modeling and experimental evidence of the influence of temperature and current density. *International Journal of Hydrogen Energy*, 40:1353–1366, 2015.

[31] P. Charvin, S. Abanades, G. Flamant, and F. Lemort. Two-step water splitting thermochemical cycle based on iron oxide redox pair for solar hydrogen production. *Energy*, 32:1124–1133, 2007.

[32] R. Chaubey, S. Sahu, O. James, and S. Maity. A review on development of industrial process and emerging techniques for production of hydrogen from renewable and sustainable sources. *Renewable and Sustainable Energy Reviews*, 23:443–462, 2015.

[33] G. Chen, X. Chen, and P. L. Yue. Electrochemical behavior of novel Ti/IrOx-Sb_2O-SnO_2 anodes. *The Journal of Physical Chemistry B*, 106(17):4364–4369, 2002.

[34] K. Chen et al. Materials degradation of solid oxide electrolysis cells. *Journal of The Electrochemical Society*, 163(11):F3070, 2016.

[35] J. Cheng, H. Zhang, G. Chen, and Y. Zhang. Study of $Ir_xRu_{1-x}O_2$ oxides as anodic electrocatalysts for solid polymer electrolyte water electrolysis. *Electrochimica Acta*, 54(26):6250–6256, 2009.

[36] S. Cherevko. Stability and dissolution of electrocatalysts: Building the bridge between model and "real world" systems. *Current Opinion in Electrochemistry*, 8:118–125, 2018.

[37] J. Chi and H. Yu. Water electrolysis based on renewable energy for hydrogen production. *Chinese Journal of Catalysis*, 39(3):390–394, 2018.

[38] T. Corrales-Sánchez, J. Ampurdanés, and A. Urakawa. MoS_2-based materials as alternative cathode catalyst for PEM electrolysis. *International journal of hydrogen energy*, 39(35):20837–20843, 2014.

[39] F. Crnkovic, S. Machado, and L. Avaca. Electrochemical and morphological studies of electrodeposited Ni–Fe–Mo–Zn alloys tailored for water electrolysis. *International Journal of Hydrogen Energy*, 29:249–254, 2004.

[40] A. Cruden, D. Infield, M. Kiaee, T. G. Douglas, and A. Roy. Development of new materials for alkaline electrolysers and investigation of the potential electrolysis impact on the electrical grid. *Renewable Energy*, 49:53–57, 2013.

[41] M. David, H. Alvarez, C. Ocampo-Martinez, and R. Sánchez-Peña. Phenomenological based model of hydrogen production using an alkaline self-pressurized electrolyzer. In *18th European Control Conference (ECC)*, pages 4344–4349, 2019.

[42] M. David, H. Alvarez, C. Ocampo-Martinez, and R. Sánchez-Peña. Dynamic modelling of alkaline self-pressurized electrolyzers: a phenomenological-based semiphysical approach. *International Journal of Hydrogen Energy*, 45(43):22394–22407, 2020.

[43] M. David, F. Bianchi, C. Ocampo-Martinez, and R. Sánchez-Peña. H_2 purity control of high-pressure alkaline electrolyzers. In *16th IFAC Symposium on Advanced Control of Chemical Processes (ADCHEM)*, volume 54, pages 109–114, 2021.

[44] M. David, F. Bianchi, C. Ocampo-Martinez, and R. Sánchez-Peña. Model-based control design for H_2 purity regulation in high-pressure alkaline electrolyzers. *Journal of the Franklin Institute*, 358:4373–4392, 2021.

[45] M. David and C. Ocampo-Martinez. Current status of water electrolysis for energy storage. In *Comprehensive renewable energy, 2nd edition*. Elsevier Ltd, 2021. (in press).

[46] M. David, C. Ocampo-Martinez, and R. Sánchez-Peña. Advances in alkaline water electrolyzers: A review. *Journal of Energy Storage*, 23:392–403, 2019.

[47] M.-R. de Valladares. Global trends and outlook for hydrogen. *International Energy Agency, December 2017*, 2017.

[48] I. Dincer and C. Acar. Review and evaluation of hydrogen production methods for better sustainability. *International Journal of Hydrogen Energy*, 40:11094–11111, 2014.

[49] J. Divisek, P. Malinowski, J. Mergel, and H. Schmitz. Improved construction of an electrolytic cell for advanced alkaline water electrolysis. *International Journal of Hydrogen Energy*, 10:383–388, 1985.

[50] Z. Dobó and A. B. Palotás. Impact of the voltage fluctuation of the power supply on the efficiency of alkaline water electrolysis. *International Journal of Hydrogen Energy*, 41:11849–11856, 2016.

[51] Z. Dobó and A. B. Palotás. Impact of the current fluctuation on the efficiency of alkaline water electrolysis. *International Journal of Hydrogen Energy*, 42:5649–5656, 2017.

[52] S. Dutta. A review on production, storage of hydrogen and its utilization as an energy resource. *Journal of Industrial and Engineering Chemistry*, 20:1148–1156, 2014.

[53] M. El-Deab, M. Awad, A. Mohammad, and T. Ohsaka. Enhanced water electrolysis: electrocatalytic generation of oxygen gas at manganese oxide nanorods modified electrodes. *Electrochemistry Communications*, 9:2082–2087, 2007.

[54] M. Faraj, M. Boccia, H. Miller, F. Martini, S. Borsacchi, M. Geppi, and A. Pucci. New LDPE based anion-exchange membranes for alkaline solid polymeric electrolyte water electrolysis. *International Journal of Hydrogen Energy*, 37:14992–15002, 2012.

[55] M. Felgenhauer and T. Hamacher. State-of-the-art of commercial electrolyzers and on-site hydrogen generation for logistic vehicles in South Carolina. *International Journal of Hydrogen Energy*, 40:2084–2090, 2015.

[56] Q. Feng, G. Liu, B. Wei, Z. Zhang, H. Li, and H. Wang. A review of proton exchange membrane water electrolysis on degradation mechanisms and mitigation strategies. *Journal of Power Sources*, 366:33–55, 2017.

[57] F. Fouda-Onana, M. Chandesris, V. Médeau, S. Chelghoum, D. Thoby, and N. Guillet. Investigation on the degradation of meas for pem water electrolysers part i: Effects of testing conditions on mea performances and membrane properties. *International Journal of Hydrogen Energy*, 41(38):16627–16636, 2016.

[58] FreedomCAR & Fuel partnership. *Hydrogen production: Overview of technology options*, 2009. https://www1.eere.energy.gov/hydrogenandfuelcells/pdfs/h2_tech_roadmap.pdf.

[59] S. H. Frensch, F. Fouda-Onana, G. Serre, D. Thoby, S. S. Araya, and S. K. Kær. Influence of the operation mode on pem water electrolysis degradation. *International Journal of Hydrogen Energy*, 44(57):29889–29898, 2019.

[60] A. Gago, S. Ansar, B. Saruhan, U. Schulz, P. Lettenmeier, N. Cañas, P. Gazdzicki, T. Morawietz, R. Hiesgen, J. Arnold, et al. Protective coatings on stainless steel bipolar plates for proton exchange membrane (PEM) electrolysers. *Journal of Power Sources*, 307:815–825, 2016.

[61] A. S. Gago, J. Bürkle, P. Lettenmeier, T. Morawietz, M. Handl, R. Hiesgen, F. Burggraf, P. A. V. Beltran, and K. A. Friedrich. Degradation of Proton Exchange Membrane (PEM) electrolysis: The influence of current density. *ECS Transactions*, 86:695–700, 2018.

[62] A. S. Gago, P. Lettenmeier, S. Stiber, A. S. Ansar, L. Wang, and K. A. Friedrich. Cost-effective PEM electrolysis: The quest to achieve superior efficiencies with reduced investment. *ECS Transactions*, 85:3–13, 2018.

[63] G. Gahleitner. Hydrogen from renewable electricity: An international review of power-to-gas pilot plants for stationary applications. *International Journal of Hydrogen Energy*, 38:2039–2061, 2013.

[64] A. Ganeshan, D. G. Holmes, L. Meegahapola, and B. P. McGrath. Enhanced control of a hydrogen energy storage system in a microgrid. In *2017 Australasian Universities Power Engineering Conference (AUPEC)*, pages 1–6, Nov 2017.

[65] J. Ganley. High temperature and pressure alkaline electrolysis. *International Journal of Hydrogen Energy*, 34:3604–3611, 2009.

[66] S. D. Ghadge, P. P. Patel, M. K. Datta, O. I. Velikokhatnyi, P. M. Shanthi, and P. N. Kumta. First report of vertically aligned (Sn, Ir)O_2: F solid solution nanotubes: highly efficient and robust oxygen evolution electrocatalysts for proton exchange membrane based water electrolysis. *Journal of Power Sources*, 392:139–149, 2018.

[67] S. Giddey, F. Ciacchi, and S. Badwal. Design, assembly and operation of polymer electrolyte membrane fuel cell stacks to 1 kwe capacity. *Journal of power sources*, 125(2):155–165, 2004.

[68] K. Glover. All optimal Hankel-norm approximations of linear multivariable systems and their L_∞ error bounds. *International Journal of Control*, 39(6):1115–1193, 1984.

[69] S. Y. Gómez and D. Hotza. Current developments in reversible solid oxide fuel cells. *Renewable and Sustainable Energy Reviews*, 61:155–174, 2016.

[70] J. Gorre, F. Ortloff, and C. van Leeuwen. Production costs for synthetic methane in 2030 and 2050 of an optimized power-to-gas plant with intermediate hydrogen storage. *Applied Energy*, 253:114594–114604, 2019.

[71] S. Grigoriev, M. Mamat, K. Dzhus, G. Walker, and P. Millet. Platinum and palladium nano-particles supported by graphitic nano-fibers as catalysts for pem water electrolysis. *International Journal of hydrogen energy*, 36(6):4143–4147, 2011.

[72] S. Grigoriev, P. Millet, and V. Fateev. Evaluation of carbon-supported Pt and Pd nanoparticles for the hydrogen evolution reaction in PEM water electrolysers. *Journal of Power Sources*, 177(2):281–285, 2008.

[73] S. Grigoriev, P. Millet, S. Korobtsev, V. Porembskiy, M. Pepic, C. Etievant, C. Puyenchet, and V. Fateev. Hydrogen safety aspects related to high-pressure polymer electrolyte membrane water electrolysis. *International Journal of Hydrogen Energy*, 34(14):5986–5991, 2009.

[74] H2A: Hydrogen Analysis Production Case Studies. *Current Central Hydrogen Production from Natural Gas without CO_2 Sequestration version 3.2018*, 2018. https://www.nrel.gov/hydrogen/h2a-production-case-studies.html.

[75] M. Hamdani, M. Pereira, J. Douch, A. Addi, Y. Berghoute, and M. Mendonca. Physicochemical and electrocatalytic properties of Li–Co_3O_4 anodes prepared by chemical spray pyrolysis for application in alkaline water electrolysis. *Electrochimica Acta*, 49:1555–1563, 2004.

[76] M. Hammoudi, C. Henao, K. Agbossou, Y. Dubé, and M. Doumbia. New multi-physics approach for modelling and design of alkaline electrolyzers. *International Journal of Hydrogen Energy*, 37:13895–13913, 2012.

[77] Q. Han, K. Liu, J. Chen, and X. Wei. Hydrogen evolution reaction on amorphous Ni–S–Co alloy in alkaline medium. *International Journal of Hydrogen Energy*, 28:1345–1352, 2003.

[78] C. Hao, H. Lv, C. Mi, Y. Song, and J. Ma. Investigation of mesoporous niobium-doped TiO_2 as an oxygen evolution catalyst support in an SPE water electrolyzer. *ACS Sustainable Chemistry & Engineering*, 4(3):746–756, 2016.

[79] P. Haug, M. Koj, and T. Turek. Influence of process conditions on gas purity in alkaline water electrolysis. *International Journal of Hydrogen Energy*, 42:9406–9418, 2017.

[80] P. Haug, B. Kreitz, M. Koj, and T. Turek. Process modelling of an alkaline water electrolyzer. *International Journal of Hydrogen Energy*, 42:15689–15707, 2017.

[81] K. Havre, P. Borg, and K. Tøysteinmmerberg. Modelling and control of pressurized electrolyzer for operation in stand alone photovoltaic hydrogen power systems. In *2nd nordic symposium on hydrogen and fuel cells for energy storage*, January 19-20 1995.

[82] B. Hinnemann, P. G. Moses, J. Bonde, K. P. Jørgensen, J. H. Nielsen, S. Horch, I. Chorkendorff, and J. K. Nørskov. Biomimetic hydrogen evolution: MoS_2 nanoparticles as catalyst for hydrogen evolution. *Journal of the American Chemical Society*, 127(15):5308–5309, 2005.

[83] J. Holladay, J. Hu, D. King, and Y. Wang. An overview of hydrogen production technologies. *Catalysis Today*, 139:244–260, 2009.

[84] W. B. Hooper. The 2-k method predicts head losses in pipe fittings. *Chemical Engineering*, 88:96–100, 1981.

[85] S. E. Hosseini and M. A. Wahid. Hydrogen production from renewable and sustainable energy resources: Promising green energy carrier for clean development. *Renewable and Sustainable Energy Reviews*, 57:850–866, 2016.

[86] J. Hu, H. Meng, J. Zhang, and C. Cao. Degradation mechanism of long service life Ti/IrO_2–Ta_2O_5 oxide anodes in sulphuric acid. *Corrosion Science*, 44(8):1655–1668, 2002.

[87] W. Hu. Electrocatalytic properties of new electrocatalysts for hydrogen evolution in alkaline water electrolysis. *International Journal of Hydrogen Energy*, 25:111–118, 2000.

[88] W. Hu and J. Lee. Electrocatalytic properties of Ti_2Ni/Ni–Mo composite electrodes for hydrogen evolution reaction. *International Journal of Hydrogen Energy*, 23:253–257, 1998.

[89] W. Hug, H. Bussmann, and A. Brinner. Highly efficient advanced alkaline electrolyzer for solar operation. *International Journal of Hydrogen Energy*, 17(9):699–705, 1992.

[90] W. Hug, J. Divisek, J. Mergel, W. Seeger, and H. Steeb. Intermittent operation and operation modelling of an alkaline electrolyzer. *International Journal of Hydrogen Energy*, 18(12):973–977, 1993.

[91] HyUnder. *Assessment of the potential, the actors and relevant business cases for large scale and long term storage of renewable electricity by H_2 underground storage in Europe - executive summary*, 2014.

[92] H. In Lee, D. T. Dung, J. Kim, J. H. Pak, S. k. Kim, H. S. Cho, W. C. Cho, and C. H. Kim. The synthesis of a zirfon-type porous separator with reduced gas crossover for alkaline electrolyzer. *International Journal of Energy Research*, 44(3):1875–1885, 2020.

[93] International Energy Agency, 9, rue de la Fédération, 75739 Paris Cedex 15, France. *Key world energy statistics 2020*, 2020.

[94] H. Ito, N. Kawaguchi, S. Someya, and T. Munakata. Pressurized operation of anion exchange membrane water electrolysis. *Electrochimica Acta*, 297:188–196, 2019.

[95] X. Ji, R. Zhang, X. Shi, A. M. Asiri, B. Zheng, and X. Sun. Fabrication of hierarchical CoP nanosheet microwire array via space-confined phosphidation toward high-efficiency water oxidation electrocatalysis under alkaline conditions. *Nanoscale*, 10:7941–7945, 2018.

[96] Y. Ji, L. Yang, X. Ren, G. Cui, X. Xiong, and X. Sun. Full water splitting electrocatalyzed by NiWO4 nanowire array. *ACS Publications*, 6:9555–9559, 2018.

[97] Y. Ji, L. Yang, X. Ren, G. Cui, X. Xiong, and X. Sun. Nanoporous CoP3 nanowire array: acid etching preparation and application as a highly active electrocatalyst for the hydrogen evolution reaction in alkaline solution. *ACS Sustainable Chemistry & Engineering*, 6:11186–11189, 2018.

[98] H. Ju, S. Giddey, and S. P. Badwal. The role of nanosized SnO_2 in Pt-based electrocatalysts for hydrogen production in methanol assisted water electrolysis. *Electrochimica Acta*, 229:39–47, 2017.

[99] J. Kerres, G. Eigenberger, S. Reichle, V. Schramm, K. Hetzel, W. Schnurnberger, and I. Seybold. Advanced alkaline electrolysis with porous polymeric diaphragms. *Desalination*, 104(1-2):47–57, 1996.

[100] K. Kovács, G. Maróti, and G. Rákhely. A novel approach for biohydrogen production. *International Journal of Hydrogen Energy*, 31:1460–1468, 2006.

[101] G. Kreysa and J. Kuhn. Modelling of gas evolving electrolysis cells. i. the gas voidage problem. *Journal of Applied Electrochemistry*, 15:517–526, 1985.

[102] S. S. Kumar, S. Ramakrishna, D. Bhagawan, and V. Himabindu. Preparation of $Ru_xPd_{1-x}O_2$ electrocatalysts for the oxygen evolution reaction (OER) in PEM water electrolysis. *Ionics*, 24(8):2411–2419, 2018.

[103] A. Kusoglu, A. M. Karlsson, M. H. Santare, S. Cleghorn, and W. B. Johnson. Mechanical behavior of fuel cell membranes under humidity cycles and effect of swelling anisotropy on the fatigue stresses. *Journal of Power Sources*, 170:345–358, 2007.

[104] S. Lædre, O. E. Kongstein, A. Oedegaard, H. Karoliussen, and F. Seland. Materials for proton exchange membrane water electrolyzer bipolar plates. *International Journal of Hydrogen Energy*, 42(5):2713–2723, 2017.

[105] M. Laguna-Bercero. Recent advances in high temperature electrolysis using solid oxide fuel cells: A review. *Journal of Power Sources*, 203:4–16, 2012.

[106] T. Laurinavichene, S. Kosourov, M. Ghirardi, M. Seibert, and A. Tsygankov. Prolongation of H_2 photoproduction by immovilized, sulfur-limited chlamydomonas reinhardtii cultures. *Journal of Biotechnology*, pages 275–277, 2008.

[107] M. J. Lavorante and J. I. Franco. Performance of stainless steel 316L electrodes with modified surface to be use in alkaline water electrolyzers. *International Journal of Hydrogen Energy*, 41:9731–9737, 2016.

[108] D.-Y. Lee, A. Elgowainy, and Q. Dai. Life cycle greenhouse gas emissions of hydrogen fuel production from chlor-alkali processes in the United States. *Applied Energy*, 217:467–479, 2018.

[109] J. Lee, A. Alam, and H. Ju. Multidimensional and transient modeling of an alkaline water electrolysis cell. *International Journal of Hydrogen Energy*, 46:13678–13690, 2021.

[110] L. Lema-Pérez, J. Garcia-Tirado, C. Builes-Montaño, and H. Alvarez. Phenomenological based model of human stomach and its role in glucose metabolism. *Journal of Theoretical Biology*, 460:88–100, 2019.

[111] Y. Leng, G. Chen, A. J. Mendoza, T. B. Tighe, M. A. Hickner, and C.-Y. Wang. Solid-state water electrolysis with an alkaline membrane. *Journal of the American Chemical Society*, 134:9054–9057, 2012.

[112] R. LeRoy, C. Bowen, and D. LeRoy. The thermodynamics of aqueous water electrolysis. *Journal of Electrochemical Society*, 127:1954–1962, 1980.

[113] P. Lettenmeier, R. Wang, R. Abouatallah, S. Helmly, T. Morawietz, R. Hiesgen, S. Kolb, F. Burggraf, J. Kallo, A. S. Gago, et al. Durable membrane electrode assemblies for proton exchange membrane electrolyzer systems operating at high current densities. *Electrochimica Acta*, 210:502–511, 2016.

[114] P. Lettenmeier, R. Wang, R. Abouatallah, B. Saruhan, O. Freitag, P. Gazdzicki, T. Morawietz, R. Hiesgen, A. Gago, and K. Friedrich. Low-cost and durable bipolar plates for proton exchange membrane electrolyzers. *Scientific reports*, 7(1):1–12, 2017.

[115] J. Levene, M. Mann, R. Margolis, and A. Milbrandt. An analysis of hydrogen production from renewable electricity sources. *Solar energy*, 84:773–780, 2007.

[116] K. Lewinski, F. Sun, S. Luopa, J. Park, and R. Masel. Operation of low-temp electrolyzers at very high current densities: a pipe dream or an opportunity. In *Presentation number 52 at the 1st international conference on electrolysis, Copenhagen, June 13–15*, 2017.

[117] K. A. Lewinski, D. van der Vliet, and S. M. Luopa. NSTF advances for PEM electrolysis - the effect of alloying on activity of NSTF electrolyzer catalysts and performance of NSTF based PEM electrolyzers. *ECS Transactions*, 69:893–917, 2015.

[118] A. Li, Y. Sun, T. Yao, and H. Han. Earth-abundant transition-metal-based electrocatalysts for water electrolysis to produce renewable hydrogen. *Chemistry European Journal*, 24:18334–18355, 2018.

[119] G. Li, H. Yu, W. Song, X. Wang, Y. Li, Z. Shao, and B. Yi. Zeolite-templated $Ir_xRu_{1-x}O_2$ electrocatalysts for oxygen evolution reaction in solid polymer electrolyte water electrolyzers. *international journal of hydrogen energy*, 37(22):16786–16794, 2012.

[120] T.-J. Li, M.-H. Yeh, W.-H. Chiang, Y.-S. Li, G.-L. Chen, Y.-A. Leu, T.-C. Tien, S.-C. Lo, L.-Y. Lin, J.-J. Lin, et al. Boron-doped carbon nanotubes with uniform boron doping and tunable dopant functionalities as an efficient electrocatalyst for dopamine oxidation reaction. *Sensors and Actuators B: Chemical*, 248:288–297, 2017.

[121] J. Y. Lim, G. Rahman, S. Y. Chae, K.-Y. Lee, C.-S. Kim, and O.-S. Joo. Highly stable RuO_2/SnO_2 nanocomposites as anode electrocatalysts in a PEM water electrolysis cell. *International journal of energy research*, 38(7):875–883, 2014.

[122] T. Liu, L. Xie, J. Yang, R. Kong, G. Du, A. M. Asiri, X. Sun, and L. Chen. Self-standing CoP nanosheets array: A three-dimensional bifunctional catalyst electrode for overall water splitting in both neutral and alkaline media. *ChemElectroChem*, 4:1840–1845, 2017.

[123] P. Los, A. Rami, and A. Lasia. Hydrogen evolution reaction on Ni–Al electrodes. *Journal of Applied Electrochemistry*, 23:135–140, 1993.

[124] B. Lux and B. Pfluger. A supply curve of electricity-based hydrogen in a decarbonized european energy system in 2050. *Applied Energy*, 269:115011–115030, 2020.

[125] H. Ma, C. Liu, J. Liao, Y. Su, X. Xue, and W. Xing. Study of ruthenium oxide catalyst for electrocatalytic performance in oxygen evolution. *Journal of Molecular Catalysis A: Chemical*, 247(1-2):7–13, 2006.

[126] T. Mahlia, T. Saktisahdan, A. Jannifar, M. Hasan, and H. Matseelar. A review of available methods and development on energy storage: technology update. *Renewable and Sustainable Energy Reviews*, 33:532–545, 2014.

[127] A. T. Marshall, S. Sunde, M. Tsypkin, and R. Tunold. Performance of a pem water electrolysis cell using irxruytazo2 electrocatalysts for the oxygen evolution electrode. *International Journal of Hydrogen Energy*, 32(13):2320–2324, 2007.

[128] A. Mauer, D. Kirk, and T. Steven. The role of iron in the prevention of nickel electrode deactivation in alkaline electrolysis. *Electrochimica Acta*, 52:3505–3509, 2007.

[129] K. Mazloomi and C. Gomes. Hydrogen as an energy carrier: Prospects and challenges. *Renewable and Sustainable Energy Reviews*, 16:3024–3033, 2012.

[130] K. Mazloomi, N. Sulaiman, S. A. Ahmad, and N. Yunus. Analysis of the frequency response of a water electrolysis cell. *International Journal of Electrochemical Science*, 8:3731–3739, 2013.

[131] S. Mazloomi and N. Sulaiman. Influencing factors of water electrolysis electrical efficiency. *Renewable and Sustainable Energy Reviews*, 16:4257–4263, 2012.

[132] M. A. McArthur, S. Jorge, L. Coulombe, and S. Omanovic. Synthesis and characterization of 3D Ni nanoparticle/carbon nanotube cathodes for hydrogen evolution in alkaline electrolyte. *Journal of Power Sources*, 266:365–373, 2014.

[133] K. McHugh. Hydrogen production methods. *MPR Associates Inc.*, page 41, 2005.

[134] S. Meyer, A. V. Nikiforov, I. M. Petrushina, K. Kohler, E. Christensen, J. O. Jensen, and N. J. Bjerrum. Transition metal carbides (WC, Mo2C, TaC, NbC) as potential electrocatalysts for the hydrogen evolution reaction (HER) at medium temperatures. *International Journal of Hydrogen Energy*, 40:2905–2911, 2015.

[135] J. Milewski, G. Guandalini, and S. Campanari. Modeling an alkaline electrolysis cell through reduced-order and loss-estimate approaches. *Journal of Power Sources*, 269:203–211, 2014.

[136] P. Millet, D. Dragoe, S. Grigoriev, V. Fateev, and C. Etievant. Genhypem: A research program on pem water electrolysis supported by the european commission. *International Journal of Hydrogen Energy*, 34(11):4974–4982, 2009.

[137] P. Millet, R. Ngameni, S. Grigoriev, N. Mbemba, F. Brisset, A. Ranjbari, and C. Etiévant. Pem water electrolyzers: From electrocatalysis to stack development. *International Journal of hydrogen energy*, 35(10):5043–5052, 2010.

[138] F. Mueller-Langer, E. Tzimas, M. Kaltschmitt, and S. Peteves. Techno-economic assessment of hydrogen production processes for the hydrogen economy for the short and medium term. *International Journal of Hydrogen Energy*, 32:3797–3810, 2007.

[139] Nationale Organisation Wasserstoff, Berlin, Germany. *Integration von Wind-Wasserstoff-Systemen in das Energiesystem*, 2014.

[140] S. K. Ngoh and D. Njomo. An overview of hydrogen gas production from solar energy. *Renewable and Sustainable Energy Reviews*, 16:6782–6792, 2012.

[141] P. Nikolaidis and A. Poullikkas. A comparative overview of hydrogen production processes. *Renewable and Sustainable Energy Reviews*, 67:597–611, 2017.

[142] N. A. of Science. *The Hydrogen Economy: Opportunities, Costs, Barriers, and R&D needs*. Nat'l. Academies Press, Washington DC, 2004.

[143] T. Ogawa, M. Takeuchi, and Y. Kajikawa. Analysis of trends and emerging technologies in water electrolysis research based on a computational method: A comparison with fuel cell research. *Sustainability*, 10:478–501, 2018.

[144] P. Olivier, C. Bourasseau, and P. B. Bouamama. Low-temperature electrolysis system modelling: A review. *Renewable and Sustainable Energy Reviews*, 78:280–300, 2017.

[145] K. Onda, T. Kyakuno, K. Hattori, and K. Ito. Prediction of production power for high-pressure hydrogen by high-pressure water electrolysis. *Journal of Power Sources*, 132:64–70, 2004.

[146] J. Otero, J. Sese, I. Michaus, M. Santa Maria, E. Guelbenzu, S. Irusta, I. Carrilero, and M. Arruebo. Sulphonated polyether ether ketone diaphragms used in commercial scale alkaline water electrolysis. *Journal of Power Sources*, 247:967–974, 2014.

[147] J. Parrondo, C. G. Arges, M. Niedzwiecki, E. B. Anderson, K. E. Ayersb, and V. Ramani. Degradation of anion exchange membranes used for hydrogen production by ultrapure water electrolysis. *Royal Society of Chemistry Advances*, 4:9875–9879, 2014.

[148] P. Parthasarathy and S. Narayanan. Hydrogen production from steam gasification of biomass: Influence of process parameters on hydrogen yield - a review. *Renewable Energy*, 66:570–579, 2014.

[149] T. Paulmier and L. Fulcheri. Use of non-thermal plasma for hydrocarbon reforming. *Chemical Engineering Journal*, 106:59–71, 2005.

[150] C. C. Pavel, F. Cecconi, C. Emiliani, S. Santiccioli, A. Scaffidi, S. Catanorchi, and M. Comotti. Highly efficient platinum group metal free based membrane-electrode assembly for anion exchange membrane water electrolysis. *Angewandte Chemie International Edition*, 53:1378–1381, 2014.

[151] B. Pierozynski, T. Mikolajczyk, and K. IM. Hydrogen evolution at catalytically modified nickel foam in alkaline solution. *Journal of Power Sources*, 271:231–238, 2014.

[152] I. Raj. Nickel-based, binary-composite electrocatalysts for the cathodes in the energy-efficient industrial-production of hydrogen from alkaline-water electrolytic cells. *Journal of Materials Science*, 28:4375–4382, 1993.

[153] K. Rajeshwar, R. McConnell, and S. Licht. *Solar Hydrogen Generation. Toward a renewable energy future.* Springer-Verlag, 2008.

[154] C. Rakousky, U. Reimer, K. Wippermann, M. Carmo, W. Lueke, and D. Stolten. An analysis of degradation phenomena in polymer electrolyte membrane water electrolysis. *Journal of Power Sources*, 326:120–128, 2016.

[155] C. Rakousky, U. Reimer, K. Wippermann, S. Kuhri, M. Carmo, W. Lueke, and D. Stolten. Polymer electrolyte membrane water electrolysis: Restraining degradation in the presence of fluctuating power. *Journal of Power Sources*, 342:38–47, 2017.

[156] S. Ramakrishna, D. S. Reddy, S. S. Kumar, and V. Himabindu. Nitrogen doped cnts supported palladium electrocatalyst for hydrogen evolution reaction in pem water electrolyser. *International Journal of Hydrogen Energy*, 41(45):20447–20454, 2016.

[157] A. Roy. *Dynamic and transient modelling of electrolysers powered by renewable energy sources and cost analysis of electrolytic hydrogen.* PhD thesis, Loughborough University, 2006.

[158] A. Roy, S. Watson, and D. Infield. Comparison of electrical energy efficiency of atmospheric and high-pressure electrolysers. *International Journal of Hydrogen Energy*, 31:1964–1979, 2006.

[159] B. Rozmiarek. Hydrogen generation from biomass-derived carbohydrates via aqueous phase reforming process. Technical report, U.S. Department of Energy, Washington DC, 2008.

[160] S. M. Saba, M. Müller, M. Robinius, and D. Stolten. The investment costs of electrolysis–a comparison of cost studies from the past 30 years. *International journal of hydrogen energy*, 43(3):1209–1223, 2018.

[161] M. Sánchez, E. Amores, D. Abad, L. Rodríguez, and C. Clemente-Jul. Aspen plus model of an alkaline electrolysis system for hydrogen production. *International Journal of Hydrogen Energy*, 45:3916–3929, 2020.

[162] M. Sánchez, E. Amores, L. Rodríguez, and C. Clemente-Jul. Semi-empirical model and experimental validation for the performance evaluation of a 15 kw alkaline water electrolyzer. *International Journal of Hydrogen Energy*, 43:20332–20345, 2018.

[163] R. Sánchez-Peña and M. Sznaier. *Robust System Theory and Applications.* Wiley & Sons, 1998.

[164] F. M. Sapountzi, J. M. Gracia, C. K.-J. Weststrate, H. O. Fredriksson, and J. H. Niemantsverdriet. Electrocatalysts for the generation of hydrogen, oxygen and synthesis gas. *Progress in Energy and Combustion Science*, 58:1–35, 2017.

[165] S. Sarkar and S. C. Peter. An overview on pd-based electrocatalysts for the hydrogen evolution reaction. *Inorganic Chemistry Frontiers*, 5(9):2060–2080, 2018.

[166] M. Sarno and E. Ponticorvo. High hydrogen production rate on RuS_2MoS_2 hybrid nanocatalyst by PEM electrolysis. *International Journal of Hydrogen Energy*, 44(9):4398–4405, 2019.

[167] SBC Energy Institute. *Electricity Storage FactBook, White paper*, 2013. http://energystorage.org/resources/sbc-energy-institute-electricity-storage-factbook.

[168] M. Schalenbach, M. Carmo, J. Fritz, David L.Mergel, and D. Stolten. Pressurized pem water electrolysis: Efficiency and gas crossover. *International Journal of Hydrogen Energy*, 38:14921– 14933, 2013.

[169] M. Schalenbach, W. Lueke, and D. Stolten. Hydrogen diffusivity and electrolyte permeability of the Zirfon PERL separator for alkaline water electrolysis. *Journal of Electrochemical Society*, 163:1480–1488, 2016.

[170] M. Schalenbach, W. Lueke, and D. Stolten. Hydrogen diffusivity and electrolyte permeability of the zirfon perl separator for alkaline water electrolysis. *Journal of the Electrochemical Society*, 14:1480–1488, 2016.

[171] M. Schalenbach, G. Tjarks, M. Carmo, W. Lueke, M. Mueller, and D. Stolten. Acidic or alkaline? towards a new perspective on the efficiency of water electrolysis. *Journal of the Electrochemical Society*, 11:3197–3208, 2016.

[172] M. Schalenbach, A. R. Zeradjanin, O. Kasian, S. Cherevko, and K. J. Mayrhofer. A perspective on low-temperature water electrolysis – challenges in alkaline and acidic technology. *International Journal of Electrochemical Science*, 13:1173–1226, 2018.

[173] S. Schiebahn, T. Grube, M. Robinius, V. Tietze, B. Kumar, and D. Stolten. Power to gas: Technological overview, systems analysis and economic assessment for a case study in Germany. *International Journal of Hydrogen Energy*, 40:4285–4294, 2015.

[174] O. Schmidt, A. Gambhir, I. Staffell, A. Hawkes, J. Nelson, and S. Few. Future cost and performance of water electrolysis: An expert elicitation study. *International Journal of Hydrogen Energy*, 42:30470–30492, 2017.

[175] C. A. Schug. Operational characteristics of high-pressure, high-efficiency water-hydrogen-electrolysis. *International Journal of Electrochemical Science*, 23:1113–1120, 1998.

[176] A. H. Shaaban. Pulsed DC and anode depolarization in water electrolysis for hydrogen generation. Technical report, Air Force Civil Engineering Support Agency, 1994.

[177] M. Shacham. An explicit equation for friction factor in pipe. *Industrial & Engineering Chemistry Fundamentals*, 19:228–229, 1980.

[178] S. Sharma and S. K. Ghoshal. Hydrogen the future transportation fuel: From production to applications. *Renewable and Sustainable Energy Reviews*, 43:1151–1158, 2015.

[179] G. Sheela, M. Pushpavanam, and S. Pushpavanam. Hydrogen evolution reaction on amorphous Ni–S–Co alloy in alkaline medium. *International Journal of Hydrogen Energy*, 27:627–633, 2002.

[180] S. Shibli, G. Harikrishnan, V. Anupama, K. Chinchu, and M. BN. Development of nano NiO incorporated nickel-phosphorus coatings for electrocatalytic applications. *Surface and Coatings Technology*, 262:48–55, 2015.

[181] N. Shimizu, S. Hotta, T. Sekiya, and O. Oda. A novel method of hydrogen generation by water electrolysis using an ultra-short-pulse power supply. *Journal of applied electrochemistry*, 36:419–423, 2006.

[182] S. Shiva Kumar and V. Himabindu. Hydrogen production by pem water electrolysis–a review. *Materials Science for Energy Technologies*, 2(3):442–454, 2019.

[183] S. Shiva Kumar, S. Ramakrishna, B. R. Devi, and V. Himabindu. Phosphorus-doped carbon nanoparticles supported palladium electrocatalyst for the hydrogen evolution reaction (her) in pem water electrolysis. *Ionics*, 24(10):3113–3121, 2018.

[184] S. Shiva Kumar, S. Ramakrishna, K. N. Mahesh, B. R. Devi, and V. Himabindu. Palladium supported on phosphorus–nitrogen dual-doped carbon nanoparticles as cathode for hydrogen evolution in PEM water electrolyser. *Ionics*, 25(6):2615–2625, 2019.

[185] S. Shiva Kumar, S. Ramakrishna, B. Rama Devi, and V. Himabindu. Phosphorus-doped graphene supported palladium (pd/pg) electrocatalyst for the hydrogen evolution reaction in pem water electrolysis. *International Journal of Green Energy*, 15(10):558–567, 2018.

[186] R. Singh, D. Mishra, Anindita, A. Sinha, and A. Singh. Novel electrocatalysts for generating oxygen from alkaline water electrolysis. *Electrochemistry Communications*, 9:1369–1373, 2007.

[187] S. Song, H. Zhang, X. Ma, Z. Shao, R. T. Baker, and B. Yi. Electrochemical investigation of electrocatalysts for the oxygen evolution reaction in pem water electrolyzers. *international journal of hydrogen energy*, 33(19):4955–4961, 2008.

[188] B. Sørensen. *Hydrogen and Fuel Cells Emerging Technologies and Applications*. Elsevier Academic Press, 2005.

[189] A. Steinfeld. Solar hydrogen production via a two-step water splitting thermochemical cycle based on zn/zno redox reactions. *International Journal of Hydrogen Energy*, 27:611–619, 2005.

[190] S. Sun, Z. Shao, H. Yu, G. Li, and B. Yi. Investigations on degradation of the long-term proton exchange membrane water electrolysis stack. *Journal of Power Sources*, 267:515–520, 2014.

[191] X. Tang, L. Xiao, C. Yang, J. Lu, and L. Zhuang. Noble fabrication of Ni-Mo cathode for alkaline water electrolysis and alkaline polymer electrolyte water electrolysis. *International Journal of Hydrogen Energy*, 39:3055–3060, 2014.

[192] A. J. Terezo, J. Bisquert, E. C. Pereira, and G. Garcia-Belmonte. Separation of transport, charge storage and reaction processes of porous electrocatalytic IrO_2 and IrO_2/Nb_2O_5 electrodes. *Journal of Electroanalytical Chemistry*, 508(1-2):59–69, 2001.

[193] S. Themsirimongko, N. Promsawan, and S. Saipanya. Noble metal and Mn_3O_4 supported carbon nanotubes: enhanced catalysts for ethanol electrooxidation. *Int J Electrochem Sci*, 11:967–982, 2016.

[194] J. Tian, Q. Liu, A. M. Asiri, and X. Sun. Self-supported nanoporous cobalt phosphide nanowire arrays: an efficient 3D hydrogen-evolving cathode over the wide range of pH 0–14. *Journal of the American Chemical Society*, 136:7857–7950, 2014.

[195] J. Turner, T. Deutsch, J. Head, and P. Vallett. Photoelectrochemical water systems for H_2 production. in: DOE Hydrogen Program Annual Merit Review, U.S. Department of Energy, Washington DC, 2007. http://www.hydrogen.energy.gov/pdfs/review07/pd_10_turner.pdf.

[196] J. Turner, G. Sverdrup, M. Mann, P.-C. Maness, B. Kroposki, M. Ghirardi, R. Evans, and D. Blake. Renewable hydrogen production. *International Journal of Hydrogen Energy*, 32:379–407, 2008.

[197] O. Ulleberg. Modeling of advanced alkaline electrolyzers: a system simulation approach. *International Journal of Hydrogen Energy*, 28:21–33, 2003.

[198] A. Ursúa. Hydrogen production from water electrolysis: Current status and future trends. *Proceedings of the IEEE*, 100:410–426, 2012.

[199] A. Ursúa and P. Sanchis. Static-dynamic modelling of the electrical behaviour of a commercial advanced alkaline water electrolyser. *International Journal of Hydrogen Energy*, 37:18598–18614, 2012.

[200] M. Vanags, J. Kleperis, and G. Bajars. Water electrolysis with inductive voltage pulses. In *Electrolysis*. InTech, 2012.

[201] H. Vandenborre, R. Leysen, and L. H. Baetsle. Alkaline inorganic-membrane-electrolyte (IME) water electrolysis. *International Journal of Hydrogen Energy*, 5:165–171, 1980.

[202] J. R. Varcoe and R. C. T. Slade. Prospects for alkaline anion-exchange membranes in low temperature fuel cells. *Fuel Cells*, 5:187–200, 2005.

[203] P. Vermeiren, W. Adriansens, J. P. Moreels, and R. Leysen. Evaluation of the Zirfon separator for use in alkaline water electrolysis and Ni-H_2 batteries. *International Journal of Hydrogen Energy*, 23:321–324, 1998.

[204] P. Vermeiren, R. Leysen, H. Beckers, J. Moreels, and A. Claes. The influence of manufacturing parameters on the properties of macroporous zirfon® separators. *Journal of Porous Materials*, 15(3):259–264, 2008.

[205] A. Villagra and P. Millet. An analysis of pem water electrolysis cells operating at elevated current densities. *International Journal of Hydrogen Energy*, 44(20):9708–9717, 2019.

[206] I. Vincent and D. Bessarabov. Low cost hydrogen production by anion exchange membrane electrolysis: A review. *Renewable and Sustainable Energy Reviews*, 81:1690–1704, 2018.

[207] F. Vivas, F. De las Heras, A.and Segura, and J. Andújar. A review of energy management strategies for renewable hybrid energy systems with hydrogen backup. *Renewable and Sustainable Energy Reviews*, 82:126–155, 2018.

[208] H. Vogt and R. Balzer. The bubble coverage of gas-evolving electrodes in stagnant electrolytes. *Electrochimica Acta*, 50:2073–2079, 2005.

[209] Y. Wang, W. Li, L. Ma, W. Li, and X. Liu. Degradation of solid oxide electrolysis cells: Phenomena, mechanisms, and emerging mitigation strategies—a review. *Journal of Materials Science & Technology*, 55:35–55, 2020.

[210] Z. Wang, X. Ren, Y. Luo, L. Wang, G. Cui, F. Xie, H. Wang, Y. Xie, and X. Sun. Ultrafine platinum–cobalt alloy decorated cobalt nanowire array with superb activity toward alkaline hydrogen evolution. *Nanoscale*, 10:12302–12307, 2018.

[211] Z. Wang, X. Ren, L. Wang, G. Cui, H. Wang, and X. Sun. A hierarchical CoTe 2–MnTe 2 hybrid nanowire array enables high activity for oxygen evolution reactions. *Chemical Communications*, 54:10993–10996, 2018.

[212] H. Wendt, H. Hofmann, and V. Plzak. Materials research and development of electrocatalysts for alkaline water electrolysis. *Materials Chemistry and Physics*, 22:27–49, 1989.

[213] L. Xiao, S. Zhang, J. Pan, C. Yang, M. He, L. Zhuang, and J. Lu. First implementation of alkaline polymer electrolyte water electrolysis working only with pure water. *Energy & Environmental Science*, 5:7869–7871, 2012.

[214] J. Xu, R. Miao, T. Zhao, J. Wu, and X. Wang. A novel catalyst layer with hydrophilic–hydrophobic meshwork and pore structure for solid polymer electrolyte water electrolysis. *Electrochemistry communications*, 13(5):437–439, 2011.

[215] J.-W. Yu, G.-b. Jung, Y.-J. Su, C.-C. Yeh, M.-Y. Kan, C.-Y. Lee, and C.-J. Lai. Proton exchange membrane water electrolysis system-membrane electrode assembly with additive. *International Journal of Hydrogen Energy*, 44(30):15721–15726, 2019.

[216] K. Zeng and D. Zhang. Recent progress in alkaline water electrolysis for hydrogen production and applications. *Progress in Energy and Combustion Science*, 36:307–326, 2010.

[217] F. Zhang, P. Zhao, M. Niu, and J. Maddy. The survey of key technologies in hydrogen energy storage. *International Journal of Hydrogen Energy*, 41:14535–14552, 2016.

[218] L. Zhang, K. Xiong, S. Chen, L. Li, and Z. D. Deng, Zihua Wei. In situ growth of ruthenium oxide-nickel oxide nanorod arrays on nickel foam as a binder-free integrated cathode for hydrogen evolution. *Journal of Power Sources*, 274:114–120, 2015.

[219] Y. Zhang and I. Angelidaki. Microbial electrolysis cells turning to be versatile technology: Recent advances and future challenges. *Water Research*, 56:11–25, 2014.

[220] Y. Zhang, C. Wang, N. Wan, Z. Liu, and Z. Mao. Study on a novel manufacturing process of membrane electrode assemblies for solid polymer electrolyte water electrolysis. *Electrochemistry communications*, 9(4):667–670, 2007.

[221] J. Zhao, X. Li, G. Cui, and X. Sun. Highly-active oxygen evolution electrocatalyzed by an Fe-doped NiCr 2 o 4 nanoparticle film. *Chemical Communications*, 54:5462–5465, 2018.

[222] Y. Zheng, J. Wang, B. Yu, W. Zhang, J. Chen, J. Qiao, and J. Zhang. A review of high temperature co-electrolysis of H_2O and CO_2 to produce sustainable fuels using solid oxide electrolysis cells (SOECs): advanced materials and technology. *Chemical Society Reviews*, 46(5):1427–1463, 2017.

[223] K. Zhou, J. C. Doyle, and K. Glover. *Robust and Optimal Control*. Prentice Hall, 1996.

[224] C. Ziems, D. Tannert, and H. J. Krautz. Project presentation: design and installation of advanced high pressure alkaline electrolyzer-prototypes. *Energy Procedia*, 29:744–753, 2012.